Universitat Autònoma de Barcelona

Departament de Bioquímica i Biologia Molecular
Institut de Biotecnologia i Biomedecina *Vicent Villar Palasí*

# Structural studies on Protein-Protein interactions: Analysis of the regulation of the DYNLL/LC8 binding to Nek9 and characterization of the enzymes composing the arginine deiminase pathway in *Mycoplasma penetrans.*

Doctoral thesis presented by Pablo Gallego Alonso for the degree of Ph.D in Biochemistry, Molecular Biology and Biomedicine, supervised by Dr. David Reverter Cendrós.

Pablo Gallego Alonso David Reverter Cendrós

Bellaterra, September 2014

*...*

*Allá muevan feroz guerra*

*ciegos reyes*

*por un palmo más de tierra;*

*que yo aquí tengo por mío*

*cuanto abarca el mar bravío,*

*a quien nadie impuso leyes.*

*...*

*Que es mi barco mi tesoro,*

*que es mi dios la libertad,*

*mi ley, la fuerza y el viento,*

*mi única patria, la mar.*

*La canción del pirata, José de Espronceda*

*A mi familia...*

# Summary

Protein-Protein Interactions (PPIs) are intentional physical contacts established between two or more proteins. These interactions form the large protein interaction network and are the core of the entire interatomic system of any living cell. Flaws in the interaction network by aberrant PPIs involve signal transduction fails, protein aggregation and a completely loss of cell's regulation. Indeed, missense PPIs are the basis of multiple diseases, such as Alzheimer's disease and cancer. The significance of the interatomic system makes worth to studying PPIs, their functions and structural properties, in different models.

In the present work X-ray crystallography is the main technique used, in addition to other methods to study Protein-Protein interactions. The study of protein-protein interactions is performed through two different experimental models: In the first model, we analyzed the role of phosphorylation in the interaction of a peptide derived from the mitotic kinase Nek9 with its binding partner LC8; in the second model, we decipher the structures of the three enzymes composing the arginine deiminase pathway in *Mycoplasma penetrans.*

The NIMA family protein kinase Nek9/Nercc1 plays a main role in the control of spindle. DYNLL/LC8 was originally described as a component of the dynein complex, but the recent discovery of multiple interaction partners for LC8 has proposed that it has a general role as a dimerization hub that organizes different protein partners. Recent experiments suggested that LC8 binding to Nek9 was regulated by Nek9 autophosphorylation. The present work sheds light into a novel phosphorylation regulatory mechanism that interferes with LC8 protein-protein complex formation.

The metabolism of arginine towards ATP synthesis has been considered a major source of energy for microorganisms such as *Mycoplasma penetrans* in anaerobic conditions. Additionally, this pathway has also been implicated in pathogenic and virulence mechanism of certain microorganisms, i.e. protection from acidic stress during infection. In this work we present the crystal structures of the three enzymes composing the gene cluster of the arginine deiminase pathway from *M.penetrans*: arginine deiminase (ADI), ornithine

carbamoyltransferase (OTC) and carbamate kinase (CK). *M.penetrans* ADI and CK structures disclose the structural conformation shifts upon the reaction mechanism of these proteins. In the case of *M.penetrans* OCT its dodecameric quaternary structure is compared with other organisms (including some thermophiles), revealing the formation common quaternary structure arranged interfaces with a low sequence homology.

The results collected in this thesis emphasize the important contribution of X-ray crystallography for studding PPIs properties. PPIs regulation, structural and functional differences depending on their association, posttranslational modifications and the environment adaptation thought evolution are some of the PPI properties and dependence factors studied in this thesis work.

# Contents

# List of publications

The present thesis is based on the following publications:

I. Gallego P, Velazquez-Campoy A, Regué L, Roig J, Reverter D. (2013) Structural analysis of the regulation of the DYNLL/LC8 binding to Nek9 by phosphorylation. J Biol Chem. 2013 Apr 26;288(17):12283-94.

II. Gallego P, Planell R, Benach J, Querol E, Perez-Pons JA, Reverter D. (2012) Structural characterization of the enzymes composing the arginine deiminase pathway in *Mycoplasma penetrans*. PLoS One. 2012;7(10):e47886.

# List of figures and tables

# Abbreviations

| Abbreviation | Meaning |
|---|---|
| ADI | Arginine deiminase |
| APC/C | Anaphase promoting complex/cyclosome |
| ATP | Adenosine triphosphate |
| CD | Circular dichroism spectroscopy |
| Cdcs or Cdks | Cyclin-dependent kinase |
| CK | Carbamate kinase |
| DIC | Dynein intermediate chains |
| DYNLL/LC8 | Dynein ligth chain 8 |
| IDPs | Intrinsically disordered proteins |
| ITC | Isothermal titration calorimetry |
| LUMIER | luminescence-based mammalian interactome mapping |
| MAD | Multiple Wavelength Anomalous Diffraction Method |
| MIR | Isomorphous Replacement Method |
| MR | Molecular replacement |
| MS | Mass Spectrometry |
| Neks | NIMA-related kinases |
| NIMA | Never in Mitosis, gene A |
| NLS | Nuclear localization signal |
| NMR | Nuclear magnetic resonance |
| OCT | Ornithine carbamoyltransferase |
| PEST region | Peptide sequence that is rich in proline (P), glutamic acid (E), serine (S), and threonine(T). |
| Plks | Polo-like kinases |
| PPIs | Protein-protein interactions |
| PSD | Postsynaptic density |
| PSD | Protruding subdomain |
| RCC1 | Regulator of Chromosome Condensation 1 protein |
| SAD | Single-Wavelength Anomalous Diffraction Method |

# **1.** Introduction.

## 1.1 Proteins.

Proteins are large biological molecules comprising in one or more amino acids residues chains. They constitute essential structural elements and are the main executors of a wide range of cellular functions, including catalyzing metabolic reactions, replicating DNA, responding to stimuli, and molecular transport. Their functional diversity and versatility are determined by sequence of amino acids, which is dictated by the nucleotide sequence of their genes and by the spatial conformation they can adopt due their folding, protein interactions, non-peptide groups attached, and several posttranscriptional modifications (Fig. 1.1).

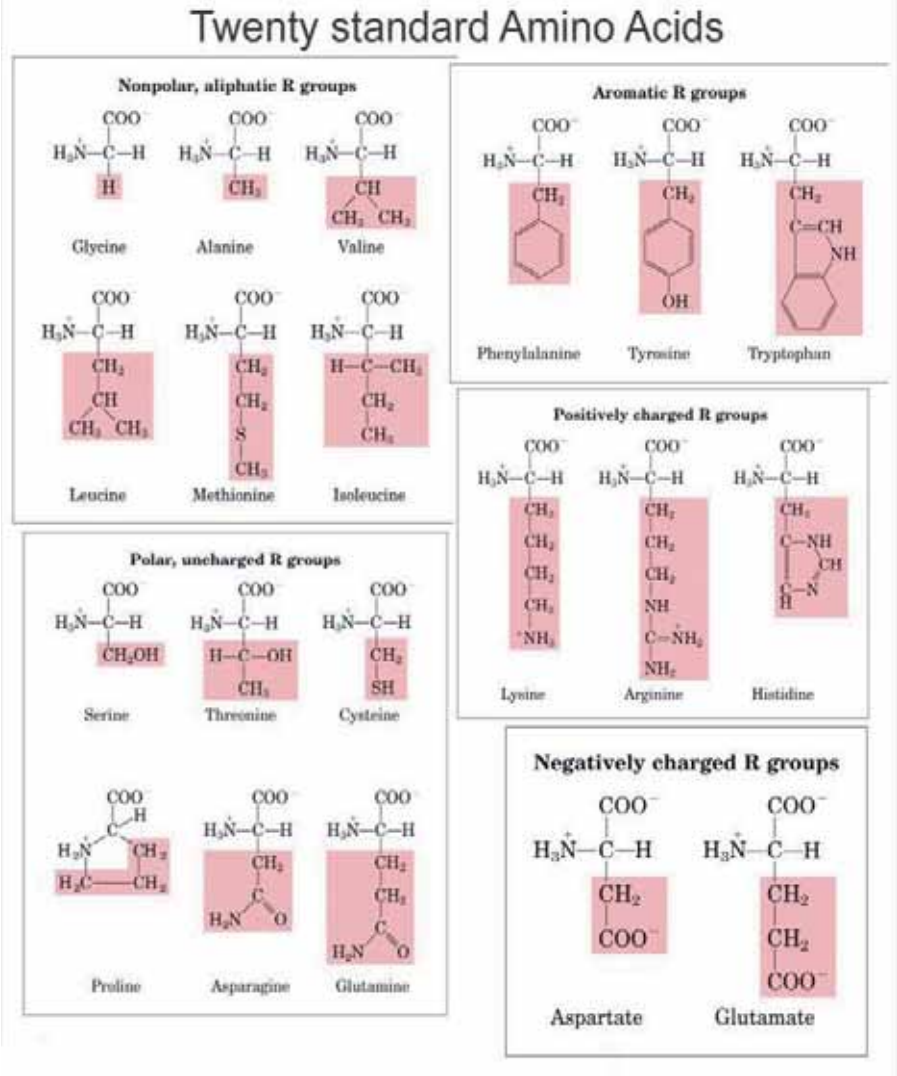


**Figure 1.1 List with the 20 natural amino acids.**

The different amino acid residues are classified depending on their physicochemical properties [1].

The amino acid residues chains or polypeptides are the basic component of a protein consisting in individual amino acids residues bonded to the adjacent amino acid residue by peptide bonds. The sequence of amino acid residues in a protein is defined by the sequence of a gene, which is encoded in the genetic code. The genetic code stipulate 20 amino acid residues, however certain organism the genetic code include different amino acids residues [1,2]. After synthesis of polypeptides the residues in a protein are often chemically modified by posttranslational modification, like phosphorylation, form complexes with other polypeptides and other macromolecules comprising protein complexes, or are attached to a prosthetic groups or cofactors. All these modifications can be stable or transient controlling the behavior of a protein and modifying their function or role in the cell [1].

### 1.1.1 Protein structure.

Most proteins fold into three-dimensional dimensional structures, the natural shape into which protein folds is known as native conformation. This fold can be spontaneous after synthesis however in other cases it must be helped by chaperones [3]. These chaperones are proteins which main function is to assist proteins to achieve their native conformation avoiding other conformational states. The specific intramolecular contacts like hydrogen bonds, hydrophobic and ionic interactions, and disulfide bridges depend on the primary sequence of amino acid residues and determine the spatial conformation of the protein [4]. Typically we refer to four distinct aspects of a protein's structure [1]:

#### 1.1.1.1 Primary structure.

The primary structure of a protein is the specification of its amino acids residues composition and the sequence connecting those amino acids residues to the adjacent for a typical un-modified uncross-linked polypeptide. The sequence is reported starting on the free N-terminal and ends in the free C-terminal end (Fig. 1.2) [1].

#### 1.1.1.2 Secondary structure.

In a polypeptide chain, local interactions form secondary structure elements

in a three-dimensional dimensional form. Secondary structure can be generally defined by the hydrogen bonds between backbone amino and carboxyl groups and may also based on the regular pattern of backbone dihedral angles in a particular region of the Ramachandran plot. Typically the secondary structure elements are regular structures as α-helix and β-sheet. There exist other minor secondary structures as 310-helix and π-helix, but are rarely observed. Tight and loose turns are other types of secondary structure, however, they are not always regular and sometimes the side-chain atoms participate forming some of the hydrogen bonds that define them (Fig. 1.2) [1,5].

#### 1.1.1.2.1 α-helix.

α-helix is a right-handed spiral conformation, in which every backbone amino group donates a hydrogen bond to the backbone carboxyl group of the amino acid four residues earlier.

#### 1.1.1.2.2 β-sheet.

β-sheet comprises several β-strands connected laterally by at least two or three hydrogen bonds, forming a generally twisted, pleated sheet. A β-strand is a stretch of polypeptide chain typically 3 to 10 amino acids residues long with backbone in an almost fully extended conformation. The orientation of the β-strands determines the parallel or antiparallel arrangement of the β-sheet.

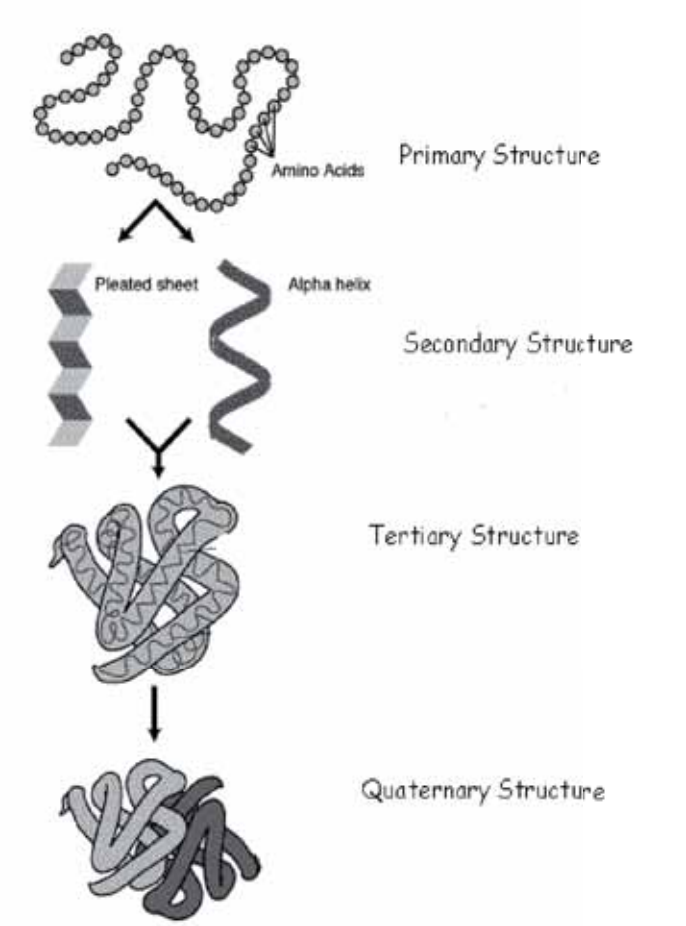


**Figure 1.2 Representation of the structural components of proteins.**

Primary, secondary (including α-helix and α-helix structures), tertiary and quaternary structure representation.
Adapted from: http://www.contexo.info

#### 1.1.1.2.3 Estimation of secondary structure content in a protein.

The rough secondary-structure content of a protein can often be estimated spectroscopically. A common method is far-ultraviolet circular dichroism (CD) where a double minimum at 208 and 222 nm indicate the presence of α-helical structure, whereas a single minimum at 204 nm reflects random-coil or 217 nm β-sheet structure. Another method is infrared spectroscopy (IR), which detects differences in the bond oscillations of amide groups due to hydrogen-bonding that depend on the secondary structure. Secondary-structure content may be estimated unambiguously using the chemical shifts of an unassigned NMR spectrum or resolving X-ray diffraction patterns of protein crystals.

#### 1.1.1.3 Tertiary structure.

The tertiary structure of a protein is its three-dimensional structure defined by the atomic coordinates. It is determined by a variety of bonding interactions between amino acid side chains and the spatial combination of the secondary structures (Fig. 1.2) [1,6]. Tertiary structure is generally stabilized by non-local interactions, the formation of a hydrophobic core, salt bridges, hydrogen bonds, and even posttranslational modifications. The tertiary structure controls the basic function of the protein and is also known by the term fold. Typically globular proteins or protein domains have a core of hydrophobic amino acid residues and a surface region of water-exposed, charged, hydrophilic residues.

##### 1.1.1.3.1 Protein Domain.

A protein domain is a conserved part of a given protein sequence and structure that can evolve, function, and exist independently of the rest of the protein chain, often it can be independently stable and folded. Proteins can have one or several domains.

##### 1.1.1.3.2 Tertiary structure determination.

X-ray crystallography and Nuclear magnetic resonance (NMR) are the two major techniques to determine the tertiary structure at atomic resolution. However, cryo-electron microscopy can determine the structure at low resolutions of some biological complexes such as viruses, small organelles, and macromolecular biological complexes around 200 kDa [7].

#### 1.1.1.4 Quaternary structure.

Quaternary structure is the arrangement of multiple protein molecules in a multi-subunit complex. Many proteins are assemblies of more than one polypeptide chain, which in the context of the larger assemblage are known as protein subunits (Fig. 1.2). These assemblies can be homogeneous if all the assemblies are the same polypeptide or heterogeneous if some assembles are different. Depending on the number of subunits the complex is described using Greco-Latinate names (e.g. two subunits dimer, three subunits trimer, twelve subunits dodecamer) [1]. These protein complexes can be stable and tight, transient or just weak interactions between proteins. In quaternary structure

underlies protein properties like cooperativity and allostery in multimeric enzymes. Many proteins undergo regulation and perform their physiological function through changes in quaternary structure that can occur by conformational changes within individual subunits, reorientation of the subunits relative to each other or addition or deduction of one or several subunits [1]. Also in quaternary structure relies the formation of fibrous or structural multimeric proteins such as collagen or keratin [8].

#### 1.1.1.5 Protein structures major classes.

Proteins can be informally divided into four main classes, which correlate with typical tertiary structures: globular proteins, fibrous proteins, membrane proteins and intrinsically disordered proteins (IDPs) [3,9]. Globular proteins are mainly soluble where the molecule's apolar (hydrophobic) amino acids are bound towards the molecule's interior whereas polar (hydrophilic) amino acids are bound outwards, allowing dipole-dipole interactions with the solvent [10].

Membrane proteins are attached to, or associated with the membrane of a cell or an organelle. Membrane proteins have several different topologies [11]. An integral membrane protein is a topology of membrane protein that is permanently attached to the biological membrane and is surrounded by lipids crossing the lipid bilayer. While peripheral membrane proteins are proteins that are adhered to the biological membrane. These molecules attach to integral membrane proteins, or penetrate the peripheral regions of the lipid bilayer.

Fibrous proteins form long protein filaments, which are shaped like rods or wires. They are structural proteins and the roles of such proteins include protection and support. Fibrous proteins are typically inert and water-insoluble [1,12].

IDPs are a large set of proteins displaying a disordered structure in physiological conditions. They are characterized by their inability to fold into a unique and stable conformation; rather they display a vast array of function-related structural organization. This concept is also applied to regions or domains of larger proteins [13]. IDPs have been under evolutionary pressure to increase their net charge and decrease their hydrophobicity, compared to globular proteins, in order to diminish their risk of aberrant assembly and keep being water-soluble. Their lack of defined structure together with their flexibility

provides conformational plasticity which is important for their functionality. These proteins can fold under a variety of conditions, including interactions with other proteins, membranes, small molecules or large biological complexes. Moreover, all this structural properties permit IDPs to interact with multiple partners, which is essential for organization, maintenance and control of complex protein-protein interaction networks [9,13].

Protein fold is not entirely a rigid structure. In addition to the structural properties, proteins structures may shift between several related functional rearrangements while they perform their functions. In the context of these tertiary or quaternary structures are usually referred to as conformations. The transitions between them are called conformational changes. Such changes are often induced by the binding of a substrate molecule, proteins posttranslational modifications, changes in the environment or changes in the protein-protein interaction network [14].

### 1.1.2 Cellular functions of proteins.

Proteins are the major actors within the cell, they carry out most of duties specified by the information encoded in genes. With the exception of certain types of RNA and some non-coding sequences of the genome, most other biological molecules are relatively inert elements upon which proteins act [15,16]. The set of proteins expressed in a particular cell or cell type is known as its proteome.

The ability to bind other molecules specifically, tightly, and transiently or permanently allow proteins to carry out the diverse set of functions. Generally, the structural region of the protein responsible of the interaction is the binding site and it is usually a depression, also known as binding pocket, on the molecular surface. This ability is often mediated by the tertiary structure of the protein which defines the binding site, and the chemical properties of the surrounding amino acids' side chains. This ability, being in line with the structural property of shifting their conformations through conformational changes, grants major proteins' functions. As a result proteins can bind to other proteins or macromolecules, as well as, to small-molecule substrates.

Protein-protein interactions regulate enzymatic activity, control progression

through the cell cycle, and allow the assembly of large protein complexes that carry out many related reactions with a common biological function. Particularly, for structural proteins this interaction consists in the formation of rigid fibers by the self-association of the polypeptide monomers. Moreover, protein binding ability also defines the protein localization at cell and allows the formation of quaternary structure, the enormously complex signaling network [14].

#### 1.1.2.1 Enzymes.

The best-known role of proteins in the cell is as enzymes, which catalyze thousands of metabolic processes that sustain life. The molecules at the beginning of the chemical reaction are called substrates and are converted into different molecules called products. Since enzymes are highly selective for their substrates and speed up only the required living chemical reaction, from among many possible substrate process, the set of enzymes of a particular cell or cell type determines which metabolic pathways occur in that cell [17]. Although enzyme processing, also known as activity, is principally affected by the presence of its substrates and its products it can be as well affected by other molecules and other environmental factors. Molecules that decrease enzyme activity are named inhibitors while molecules that increase activity are known as activators. pH, temperature, pressure and other chemical factors define the environment of the reaction which can affect the activity of the enzyme [18].

##### 1.1.2.1.1 Enzyme Kinetics.

Enzyme kinetics is the study of chemical reactions that are catalyzed by the enzymes. The substrate catalysis is ruled by two steps: the substrate binding and recognition by the enzyme and the catalytic step where the substrate is processed to from the product (Fig. 1.3). Although some enzymes process substrates to products irreversibly, most of them can catalyze the inverse reaction [1,19].

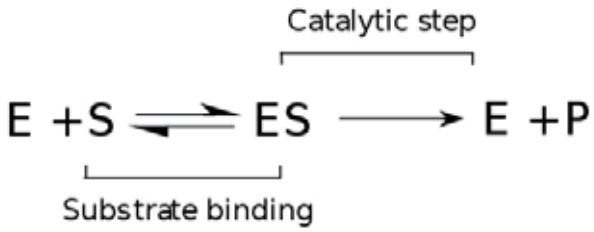


**Figure 1.3 Representation of the enzymatic steps**.

E represents the ezyme, S the substrate and P the product. Adapted from [1]

#### 1.1.2.2 Cell signaling.

Cell signaling is part of a complex system of communication that governs the cell activities and coordinates cells actions among them conforming the enormously complex signaling network. Some of these signaling molecules are extracellular proteins that transmit a signal from the cell in which they were synthesized to other cells in distance. Others signaling proteins act as receptors whose main function is to bind a signaling molecule. These signaling molecules induce a biochemical response in the cell, transduced by the signaling network, activating enzymatic activity or undergo a conformational change detected by other proteins within the cell (Fig. 1.4). Many receptors have exposed their signal binding site at the cell's surface, other are globular proteins that bind signaling molecules able to go through the cell or organelles' membrane [6].

##### 1.1.2.2.1 Signal transduction.

Signal transduction occurs when a signaling molecule, or ligand, activates a receptor altering intracellular molecules and creating a cellular response. Most of these responses go through a pathway of different proteins where the response is modulated in either steps of this pathway. Moreover, one signaling molecule may cause many responses on the same time. The signal can be amplified depending on the intracellular signaling network environment or either diminished [20].

Some pathways include a second step, in response to receptor or pathway activation, which carries out the overall or partial intracellular signal

transduction by a second ligand income at cell. In these cases signaling molecules that interact with the receptors are known as first messengers, while substances which increase at the cytoplasm or nucleoplasm and act within the cell to trigger a response are named second messengers [21].

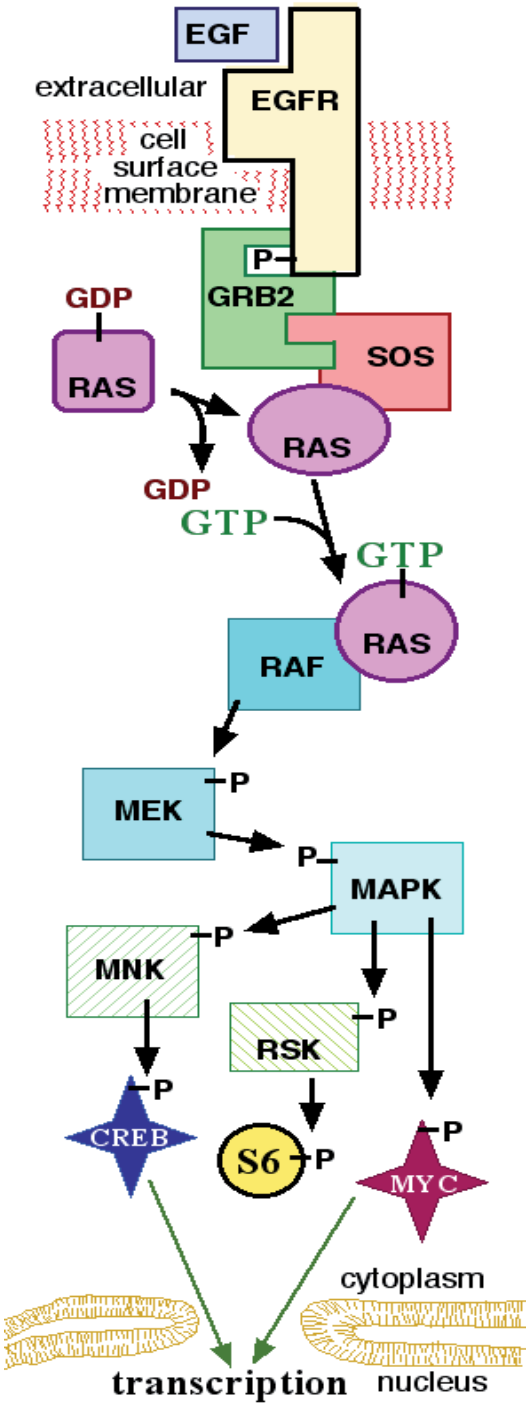


**Figure 1.4 Diagram showing key components of a signal transduction pathway.**

Representation of the MAPK signaling pathway. Starting at the activation of the receptor by the ligand inducing a signal transdcution process ending in a transcription response.
Adapted from: Schmidt, J. MAPK pathway. (2006). http://en.wikipedia.org/wiki/File:MAPKpathway.png

#### 1.1.2.2.2 Protein Kinase.

A protein kinase is an enzyme that modifies other proteins by chemically adding phosphate groups to them, this activity is also known as phosphorylation. Kinases are also known to participate in the majority of signal transduction pathways. The protein kinase transfers a phosphate group from a nucleoside triphosphate, usually ATP, covalently attaching it to specific amino acids residues with a free hydroxyl group, like serine, threonine and tyrosine in eukaryotic organisms (Fig. 1.5). Most protein kinases are able to phosphorylate both serine and threonine, or just tyrosine while a few number of kinases named dual-specific kinases act on all three amino acids residues [22]. Cell division, maturation or death, as well as, environmental responses, gene expression and other important cellular activities are mostly regulated by protein kinases. The cell regulates protein kinase activity by several ways: r conformational changes, intracellular location variations and activation/deactivation on them by phosphorylation and dephosphorylation, protein-protein or protein-ligand interactions and several posttranslationall modifications. Kinases are very often turned on or off by phosphorylation including autophosphorylation.

The catalytic domain of protein kinases is highly conserved. The N-terminal of the catalytic domain there is a glycine-rich stretch of residues near by a lysine amino acid, which is involved in ATP binding. In the central part of the catalytic domain, there is a conserved aspartic acid , which is essential for the catalytic activity of the enzyme [23].

##### 1.1.2.2.2.1 Autophosphorylation.

Autophosphorylation is defined as the phosphorylation of the kinase by itself. When the same molecule phosphorylate itself its known as cis-autophosphorylation, while trans-autophosphorylation happens when the kinase forms a dimer, or any other multimer, and one subunit phosphorylates the adjacent [24].

#### 1.1.2.2.3 Phosphatases.

A phosphatase is an enzyme that removes a phosphate group from its substrate by hydrolyzing phosphoric acid monoesters into a phosphate ion ($PO_4^{3-}$) and a molecule with free hydroxyl group (Fig. 1.5). In the case of protein phosphatases the free hydroxyl group belongs to an amino acid residue like serine, threonine and Tyrosine. This action is directly opposite to that of kinases, which attach phosphate groups to their substrates by using energetic molecules like ATP [1].

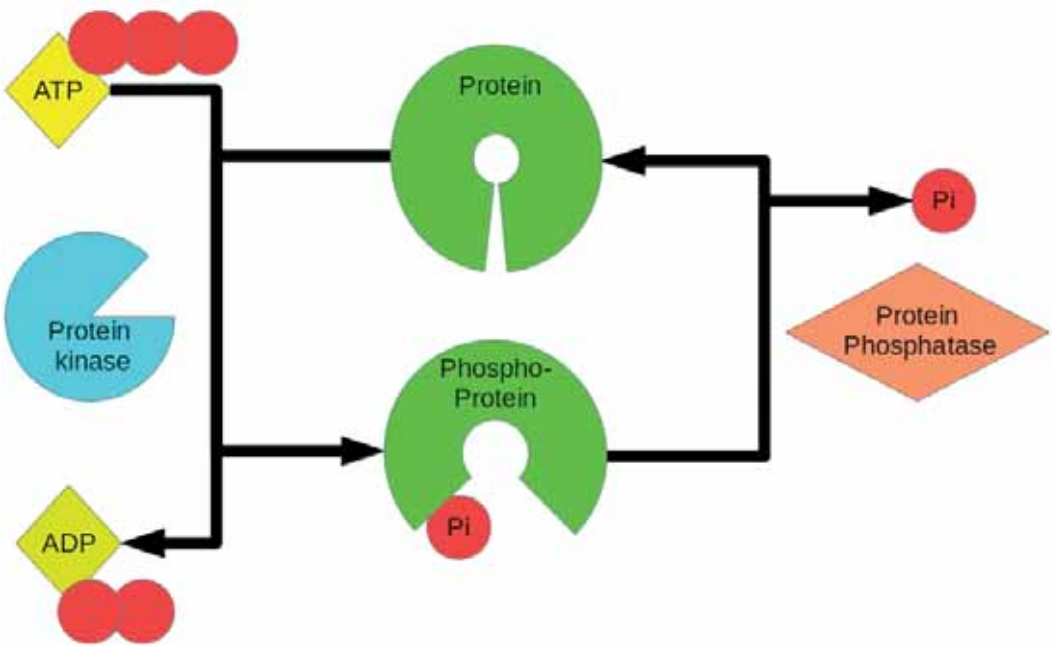


**Figure 1.5 Diagram showing kinase and phosphatase activity on a protein substrate.**

Representation of the phsophorylation of a protein by a Kinase using ATP and dephosphorylation by a Protein phosphatase.

### 1.1.3 Protein-Protein interactions.

Protein–protein interactions (PPIs) refer to intentional physical contacts established between two or more proteins. These interactions form the large protein interaction network and are the core of the entire interatomic system of any living cell. Flaws in the interaction network by aberrant PPIs involve signal transduction fails, protein aggregation and a completely loss of cell's regulation. Indeed, missense PPIs are the basis of multiple diseases, such as Alzheimer's disease and cancer [25,26].

#### 1.1.3.1 PPIs properties.

We can study PPIs by defining their different properties [27]:

##### 1.1.3.1.1 Homo/hetero-oligomerization.

Homo-oligomers are PPIs form by the same polypeptide subunit. Generally these complexes assemble is guided by non-covalent interactions spontaneously done. Several enzymes, carrier proteins, scaffolding proteins, carry out their functions as homo-oligomers. In hetero-oligomerization distinct protein subunits interact controlling several cellular functions. Generally the communication between heterologous proteins relays on scaffold domains within the proteins. The large variety of interactions types between these subunits relays on the importance of controlling their activity and consequences of the complex formation. Indeed, hetero-oligomers are heavily present in signal transduction, gene expression and a large variety of processes [27].

##### 1.1.3.1.2 Stable/transient interactions.

Stable interactions involve proteins that interact for a long time, taking part of permanent complexes, in order to carry out structural and functional roles which are permanently active in cell. This is the case for the most homo-oligomers, as well as, some enzyme hetero-oligomers. Protein complexes that may interact briefly and reversible in only certain cellular contexts, external factors or by the presence of other binding proteins are known as transient interactions. Indeed, this property is basic for signal transductions pathways [27].

##### 1.1.3.1.3 Covalent/non-covalent interactions.

PPI are normally established by non-covalent bonds, such as hydrogen bonds, ionic interactions, Van der Waals forces, or hydrophobic bonds. Covalent interactions are formed by covalent bonds such, pseudo-peptide bond, disulphide bond or electron sharing. Although being rare, these interactions are determinant in some posttranslational modifications, as ubiquitination and SUMOylation. Generally, these proteins don't have a binding

site between them, nevertheless, both or one of them have a recognition site or motif needed for the enzyme that rules this interaction [28,29].

#### 1.1.3.2 PPI's interface properties.

Molecular structure studies characterize the interface that enables the interaction between proteins. When characterizing PPI interfaces it is important to take into account the properties of the complex: size, shape, solvent-accessible surface area (SASA), complementary between surfaces, residue interface contacts, hydrophobicity, segmentation, and most importantly, secondary structure and conformational changes between the complex and isolated monomers. These changes provoke affects direly the complex activities and functions [27]. The great majority of PPI interfaces reflects the composition of protein surfaces, despite they are frequently enriched in hydrophobic residues [30]. PPI interfaces are dynamic and frequently planar, although they can be globular and protruding as well [31]. When the PPIs interface performs the interaction the surface area losses contacts with water indicating hydrophobicity as a major factor of stabilization of PPIs [32]. However, PPIs interfaces exhibit both shape and electrostatic complementarity. [27] Another interesting feature is that the more larger interaction interfaces are the more significant conformation changes are observed at least for one of the interaction partners [33].

#### 1.1.3.3 Major PPIs dependence factors.

##### 1.1.3.3.1 Subunit concentration.

Protein subunit's expression and degradation rates affect directly the protein concentration which in turn affects the complex assembly [27].

##### 1.1.3.3.2 Protein binding competition.

The protein affinity for binding different ligands, those compete between them, for forming a complex. The affinity and concentration of these competitors can directly affect the complex formation by assembling another one [27].

#### 1.1.3.3.3 Covalent modification or other posttranslational modification.

Phosphorylation, ubiquitination, SUMOylation, glicosilation, intracellular proteases activity and other posttranslational modifications can modify, block or deplete PPIs' interfaces changing its properties. Indeed, it can cause an alteration at the interaction network landscape, or even, an activation or deactivation of the binding ability for the modified subunit [27].

### 1.1.3.4 Methods for studding PPIs.

There are a multitude of methods to detect them [34] and study their molecular structure. [33].

The molecular structures of many protein complexes have been unlocked by the technique of X-ray crystallography [8]. Also nuclear magnetic resonance (NMR) is applied with the aim of unravelling the molecular structure of protein complexes and their flexibility [35]. Indeed, nuclear magnetic resonance is advantageous for characterizing weak PPIs [36].

The most conventional and widely used high-throughput methods for detecting PPIs are yeast two-hybrid screening and affinity purification coupled to mass spectrometry:

#### 1.1.3.4.1 Yeast two-hybrid screening (Y2H).

In this method yeast cells are transfected with two plasmids. One is the bait the protein under study fused with one domain of a yeast transcription factor. In the other hand, the prey a vector within a protein cDNA fragment linked to the other domain of the transcription factor. In a high-throughput study we use a cDNAs' library in this vector. Transcription of reporter genes does not occur unless bait and prey interact with each other and form the functional transcription factor. Thus, the interaction between proteins results in the reporter gene expression that the scientist can detect and then isolate the cDNA of the positive prey [29,37] (Fig. 1.6).

Despite its usefulness Y2H has some limitations. The specificity is relatively low because using yeast as host system can be a problem when studying proteins from other biological models. Moreover, the number of PPIs identified

is usually low because some transient PPIs are lost [37].

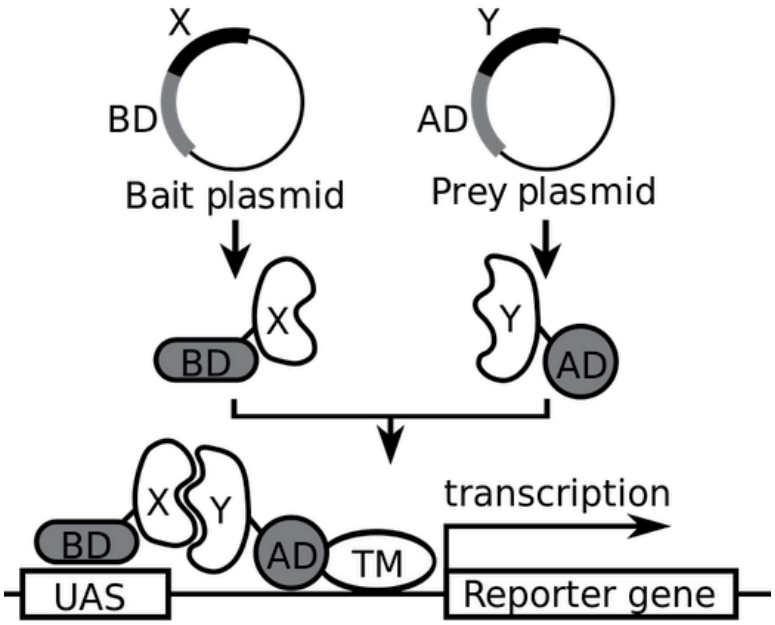


**Figure 1.6 Principles of yeast and mammalian two-hybrid systems.**

Schematic representation of the Y2H basic principles [38].

#### 1.1.3.4.2 Affinity purification coupled to mass spectrometry.

Affinity purification coupled to mass spectrometry detects stable interactions, thus better indicates functional in vivo PPIs. While Y2H uses a binary method (one to one), using this technique allows to report the overall complex subunits [39,40]. This method starts by purification of the tagged protein from a cell extract and its interacting proteins. One of the most advantageous and widely used methods to purify proteins with very low contaminating background is the tandem affinity purification (Fig. 1.7), where the bait protein is expressed with two different affinity tags in tandem. PPIs can be then identified and analyzed by mass spectrometry using different methods: chemical incorporation, biological or metabolic incorporation (SILAC), and label-free methods [27]. Mass spectrometry (MS) is an analytical technique that produces a singular spectrum of the accurate masses of molecules comprising a sample of material.

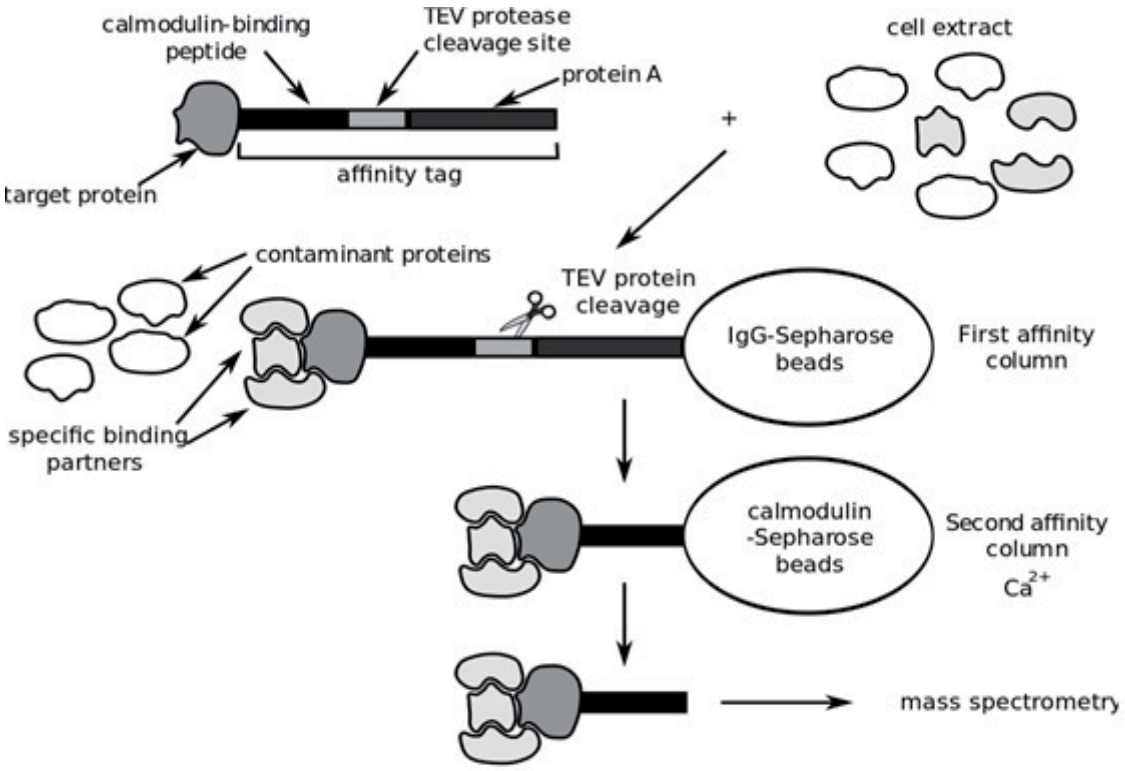


**Figure 1.7 Principle of Tandem Affinity Purification.**

Schematic representation of the Tandem Affinity Purification process [38].

#### 1.1.3.4.3 Circular dichroism spectroscopy.

Circular dichroism (CD) spectroscopy is a method to study protein-protein interactions in vitro in a soluble state. CD signal in the far ultraviolet spectra region (178–260 nm) arises from peptide bond and is sensitive to the secondary structure of the protein. Thus CD can determine whether there are secondary structure changes induced by PPIs (Fig. 1.8). CD bands in the near ultraviolet (350–260 nm) and visible regions arise from aromatic and prosthetic groups. Usually there are also changes in these regions when proteins bind to each other. Because CD is a quantitative technique, changes in CD spectra are directly proportional to the amount of the protein-protein complexes formed, and these changes can be used to estimate binding constants [41].

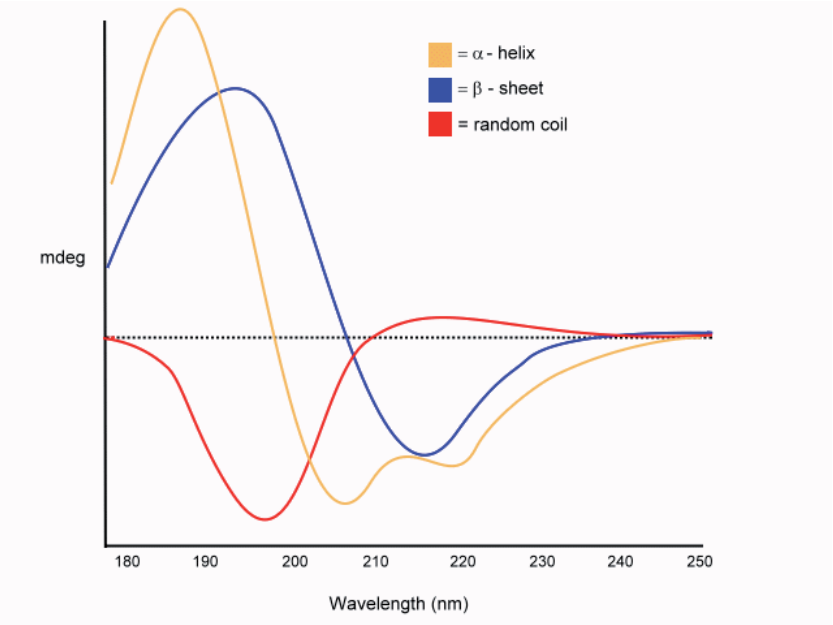


**Figure 1.8 Circular Dichroism spectra in the far ultraviolet spectra for different secondary structure elements.**

α-helix typical circular dichroism spectra is shown in orange, in blue β-sheet, and in red Random coil.
Adapted from: http://www.proteinchemist.com/cd/cdspec.html

#### 1.1.3.4.1 Isothermal titration calorimetry.

Isothermal titration calorimetry (ITC) studies both protein-ligand and protein-protein interactions. ITC is the only technique that determines directly the thermodynamic parameters of a given reaction. ITC is a quantitative technique that can determine the binding affinity (Ka), enthalpy changes (ΔH), and binding stoichiometry (n) of the interaction between two or more molecules in solution. From these initial measurements, Gibbs energy changes (ΔG) and entropy changes (ΔS) can be determined using the relationship: $\Delta G = -RT\ln Ka = \Delta H - T\Delta S$ [42].

#### 1.1.3.4.2 Other approaches to investigate PPIs.

A variety of techniques to identify or analyze PPIs has emerged recently. These include co-immunoprecipitation, protein microarrays, analytical ultracentrifugation, light scattering, fluorescence correlation spectroscopy, luminescence-based mammalian interactome mapping (LUMIER), resonance-energy transfer systems, mammalian protein-protein interaction trap, surface plasmon resonance and protein-fragment complementation assay [43].

#### 1.1.3.5 PPIs evolution in thermophilic organisms.

Proteins from thermophilic organisms adopt different strategies for stabilizing the native conformation of proteins at extreme temperatures, resulting from shorter loops linking secondary structure elements, or a decrease in both the number and size of internal cavities [44], a reduction in solvent accessible area [45], a reduced flexibility resulting from a higher proline content [46], a reinforced hydrophobic effect in the protein core or subunit-subunit interfaces [47], a stabilization via aromatic-aromatic interactions [48,49], the arrangement of several charged residues in ionic networks [50], an increased number of disulfide bonds [51], or mechanisms of oligomerization [52–54]. Moreover, not just the protein fold increases its stabilization; PPIs and oligomerization mechanisms also are over-stabilized. Indeed, PPIs interfaces imitate some of the strategies adopted for stabilization proteins fold, as the presence of ionic networks [55] or the use of a complex oligomeric state stabilized via an arrangement of hydrophobic clusters and ionic interactions not involved in extended networks [56].

## 1.2 PPIs studied in the present thesis.

We have studied PPIs in two different pathways: the NIMA-pathway and the ADI pathway involved in signal transduction and metabolic catalysis, respectively.

### 1.2.1 Nek9 - LC8 interaction.

Nek9 belongs to NIMA family protein kinases [57]. This family set up a signaling transduction module in early mitosis concerned in the spindle organization control [58–60]. In the other hand DYNLL/LC8, also known as dynein light chain 8, was originally described as a component of the dynein complex. Recently it is suggested that it has a general role as dimerization hub organizing different protein partners [61]. Recent studies report that DYNLL/LC8 is a Nek9 partner, and it has been proposed to participate in the regulation of the Nek9 Nek6/7 signaling module as a negative regulator of Nek6/7 binding and activation [62]. *In vivo* experiments suggest that phosphorylation, probably autophosphorylation, of Nek9 on Ser944 can regulate the interaction between DYNLL/LC8 and Nek9 [63,64]. In this thesis we measure this interaction *in vitro* by structural analysis of the complex between LC8 and the Nek9 binding region in the presence of a phosphate at position 944 or in the unmodified form. Together, different biophysical studies confirm the diminished LC8 binding to Nek9 upon phosphorylation [64]

#### 1.2.1.1 The NIMA pathway.

The protein kinase NIMA (Never in Mitosis, gene A) was identified in the 70's by Ronald Morris in a genetic screen for mutants that failed to progress through the cell cycle in the filamentous fungus *Aspergillus nidulans* [65].

NIMA is a mitotic protein kinase whose activity is necessary for the interfase-mitosis transition (G2 to M), mitosis progression and mitotic exit, moreover controls the organization nuclear envelope, chromosome condensation, bipolar spindle formation and cytokinesis [58,60].

As a key mitotic factor the kinase is tightly regulated by several processes, including transcription, phosphorylation, stabilization, oligomerization and subcellular localization [58,66,67]. NIMA overexpression promotes mitosis-

specific responses at any point in the cell cycle in *Aspergillus nidulans*, and also, chromosome condensation in yeast, amphibious and mammalian cells, suggesting the presence of NIMA-like pathway of mitotic regulation in these organisms[67].

NIMA homologues have been identified in all eukaryotes, but none of them can fulfill NIMA mitotic functions [67]. Fungi and yeasts have only a single NIMA-related kinase (Nek), although Nek family expanded in an ancestral ciliated cell to acquire new functions in regulating microtubules through centriole-based structures as well cilia and centrosomes. Indeed, there is a positive relationship between the ciliary structures complexity and the increment of the Nek's number of proteins in species [59,68].

NIMA has N-terminal catalytic domain and the C-terminal regulatory domain [58,66]. All Nek family members have an N-terminal kinase domain that shares 40-45% identity with the NIMA catalytic domain. Each member differs from NIMA or other family members in the C-terminal non-catalytic region [58,60].

In mammals, 11 different Nek proteins have been described, named Nek1 to Nek11 plus Nek2A, NEk2B and the Nek11L and Nek11S isoforms (Fig. 1.9) [58]. Neks can be phylogentically grouped in 5 clades: Nek1/3/5, Nek2, Nek6/7, Nek8/9 and Nek4/11; however this classification is not functionally relevant [68]. Nek2/6/7/9/11 kinases have been related to cell cycle progression [60,69], Nek1/8 are implicated in the cillia formation and maintenance [70,71], Nek3/ 4 participate in cell morphology and polarity control [72,73]. Recent studies related Nek1/2/6/10/11 to DNA damage response, suggesting another function for the NIMA kinase family [69,74–76].

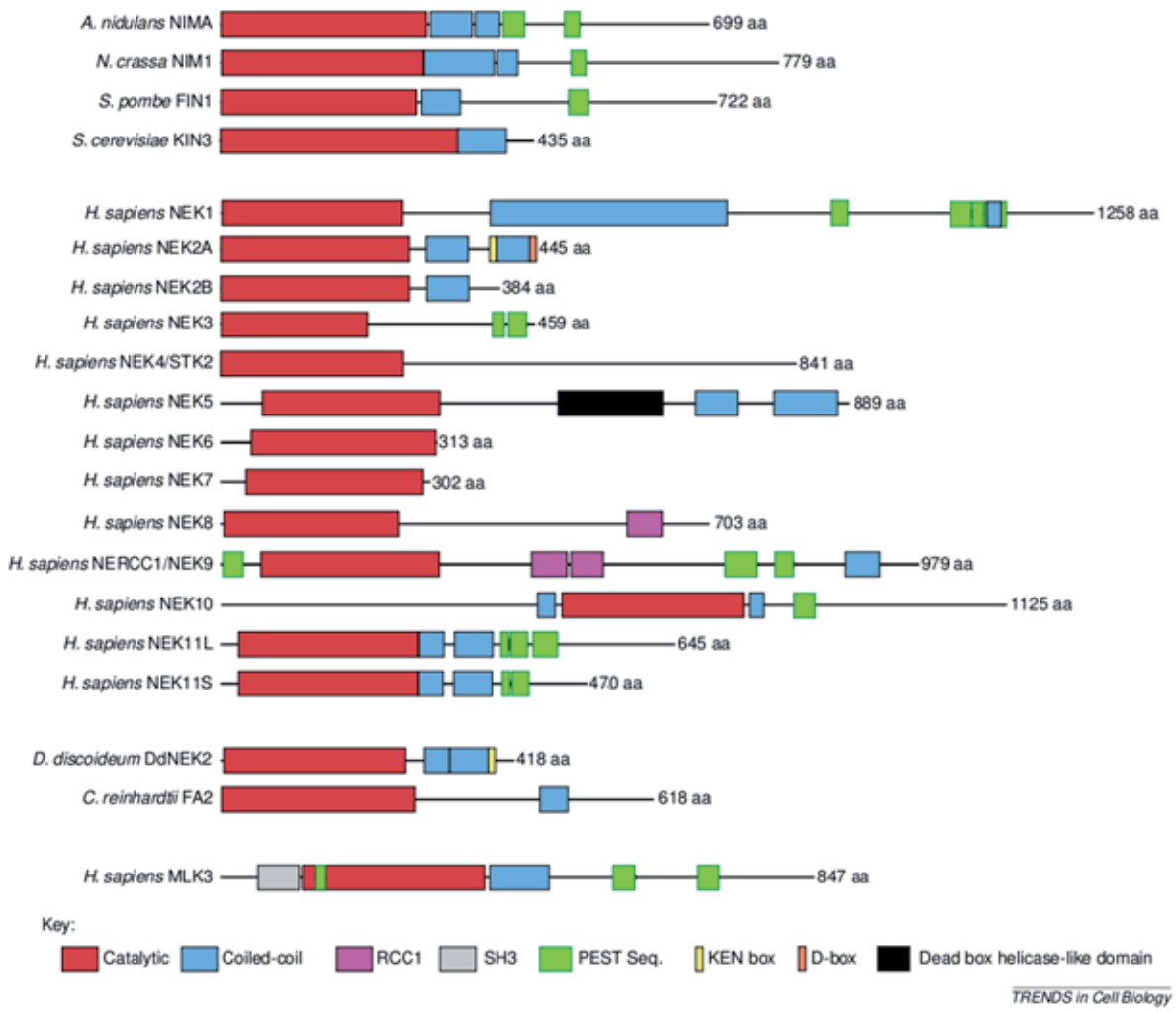


**Figure 1.9 The NIMA-related kinases family.**

Different NIMA-related proteins are shown indicating several domains and motifs which are conformed each one [58].

### 1.2.1.2 Mitosis.

Cell cycle is a series of events that take place in a cell guiding its division into two daughter cells which are exact genetic copies. Cell Cycle is divided in two phases: interfase and mitosis. During interfase the cell grows an duplicates its genetic information and centrosomes. In mitosis the cell divides its information and subcellular components to daughter cells which will be physically separated during the last mitotic step, cytokinesis [77] (Fig. 1.10).

The mitotic process can be subdivided into prophase, prometaphase, metaphase anaphase, telophase and cytokinesis. During these mitotic phases the cell performs several sequential steps, including chromosomes

condensation, nuclear envelope breakdown, centrosomes separation, spindle assembly, alignment and proper chromosomes segregation and nuclei reassembly [78]. At the final step, cytokinesis, cells form a contractile actine and myosin filaments ring to drive the constriction of the cellular's membrane [79].

Failure to complete any of the different mitotic steps properly may trigger apoptosis and cell death. Thus mitosis progression is tightly regulated by multiple independent regulatory steps. A major mechanism of regulation is irreversible protein degradation via ubiquitination through the anaphase promoting complex/cyclosome (APC/C) and reversible protein phosphorylation [80–82].

The regulation of mitosis via phosphorylation is performed by four main mitotic protein kinase families. The major control mechanism is the key cyclin-dependent kinase (Cdcs or Cdks), whose activity is modulated, localized and amplified by polo-like kinases (Plks), Aurora kinases and NIMA-related kinases (Neks) [81]. The phosphatases PP1 and PP2A, beside Cdc25 and Cdc14 phosphatase families counteract the kinase activity during the cell cycle, and are essential for achieving a tight cell cycle regulation [78].

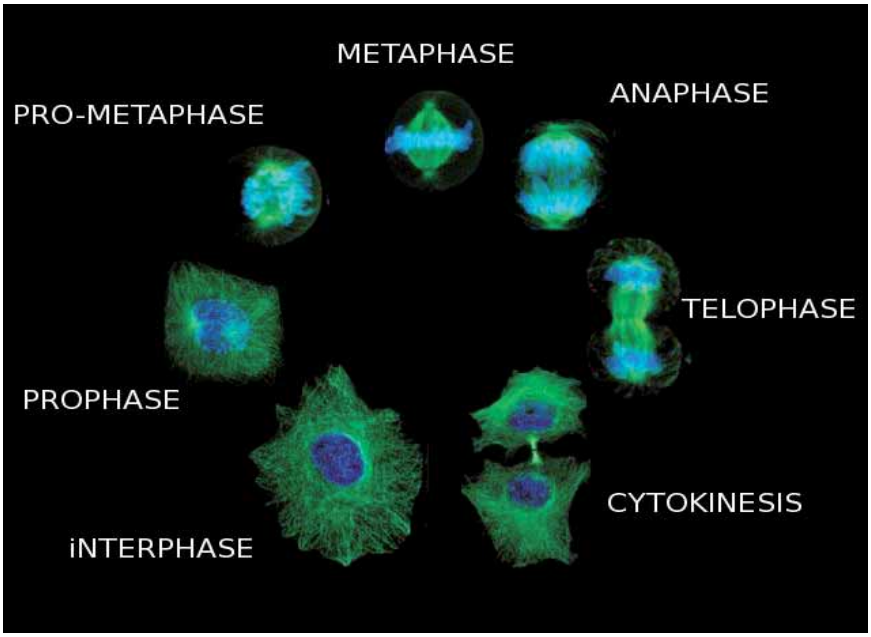


**Figure 1.10 Cell cycle progression.**
Cells are stained against β-tubulin and DNA. A representative image of each phase of the cell cycle is shown. Adapted from: www.cbp.pitt.edu

#### 1.2.1.3 The Nek9- Nek6/7 cassette.

Nek9/6/7 act together in a mitotic cascade where Nek9, the upstream kinase, upon activation at the centrosomes during mitosis onset, interacts with Nek6/7 phosphorylating and activating both of them [57,83].

##### 1.2.1.3.1 Nek9.

Nek9, also known as Nercc1, was originally identified as a Nek6 associated protein [57]. This kinase is a 120 Kda protein with 979 amino acid residues sequence encoded by 23 exons on human chromosome 14 [57,84]. Nek9 is highly conserved in mammals, birds and amphibian (82% similar) in fish and invertebrate animals Nek9 homologues are present, although they are shorter and only 20 to 50% similar to human Nek9 [68].

###### 1.2.1.3.1.1 Nek9 structure.

Three main domains can be identified in Nek9. The NIMA-related kinase domain is located at the N-terminal of the protein (residues 53-308), followed by an RCC1-like domain (residues 347-726) and a C-terminal tail with a coiled.coil domain (residues 891-940) necessary for Nek9 dimerization and activation [57,84] (Fig. 1.11).


**Figure 1.11 Schematic view of the Nek9 domains and motifs studied in this thesis.**

Nek9 has a kinase domain (yellow), a RCC1-like domain (orange), and a Coiled coil region (salmon) . Immediately after the LC8 binding motif is located (red).

Nek9 kinase domain shows all features of a Ser/thr protein kinase. Nek9 can be inactivated by mutations at the ATP-binding site (K81M) or at the proton acceptor residue in the catalytic site (D176A) [85]. Two nuclear localization motifs establish a nuclear localization signal (NLS). This NLS is localized between the kinase and the RCC1 domains (residues 306-313 and 325-330). Wild type Nek9 is confined at the cytoplasm in cell under mitotic-arrest or in

exponentially growing, while Nek9 K81M, a kinase dead mutant, shows a nuclear localization. Thus, suggest that NLS can be inactivated by autophosphorylation [57]. Moreover, Nek9 is phosphorylated throughout the cell cycle on Thr333, just after the NLS. On account of this phosphorylation is proposed that this modification can be implicated in keeping the NLS inaccessible.

The RCC1 domains were first characterized in the Regulator of Chromosome Condensation 1 protein. However is also present in several cytoplasmic proteins, like HERC3, that commonly held, a PPIs and protein localization participation [86]. As RCC1 protein Nek9's RCC1-like domain contain seven consecutive RCC repeats and can bind G-protein Ran. Whereas, RCC1 protein is a guanidine-exchange factor for Ran [86], Nek9 RCC1-like domain lacks some of the residues necessary for this activity [57].

A poly-glycine motif (residues 752-760) follows the RRC1-like domain, probably acts as a flexible hinge. The Nek9 C-Terminal tail contains the coiled-coil domain necessary for Nek9 dimerization. Gel-filtration analysis shows that the protein kinase exist in a high molecular mass complex of approximately 600 KDa, which correspond to a higher-order homoligomers and/or Nek9 dimers complexed with other proteins. Thus, suggest the importance of some motifs implicated in protein binding located between RCC1-like domain and the coiled-coil domain or the end of the protein. A PEST region (residues 734-779), two putative SH3-domain-binding motifs PXXP (residues 823-830 and 881-888) and a LC8-binding motif (K/R)XTQT (residues 945-949) are found after the RCC1-like domain [57,63,84].

#### 1.2.1.3.1.2 Nek9 localization.

Nek9 is expressed in all human and mouse tissues examined, but its expression is more abundant in brain, heart, liver, kidney, skeletal muscle and testis [57,84]. Nek9 protein levels are constant in cell, although is inactive during interphase and is activated when the cell enters in mitosis [57,85]. While inactive Nek9 localizes diffuse at the cytoplasm in interphase and mitotic cells, in prophase a small amount of Nek9 is activated by phosphorylation at the centrosomes and concentrates at spindle poles along prophase and

metaphase. At the beginning of the anaphase until telophase active Nek9 is slightly diminished at centrosomes and becomes associated with the chromosomes. During cytokinesis Nek9 activity is dramatically decreased at centrosomes and chromosomes while is increased at the midbody to finally disappear at the interphase beginning (G1) [85] (Fig. 1.12).

However Nek9 activity at the nucleus during interphase has been reported [87,88], suggesting a partial activation of Nek9 NLS during this phase of the cell cycle.

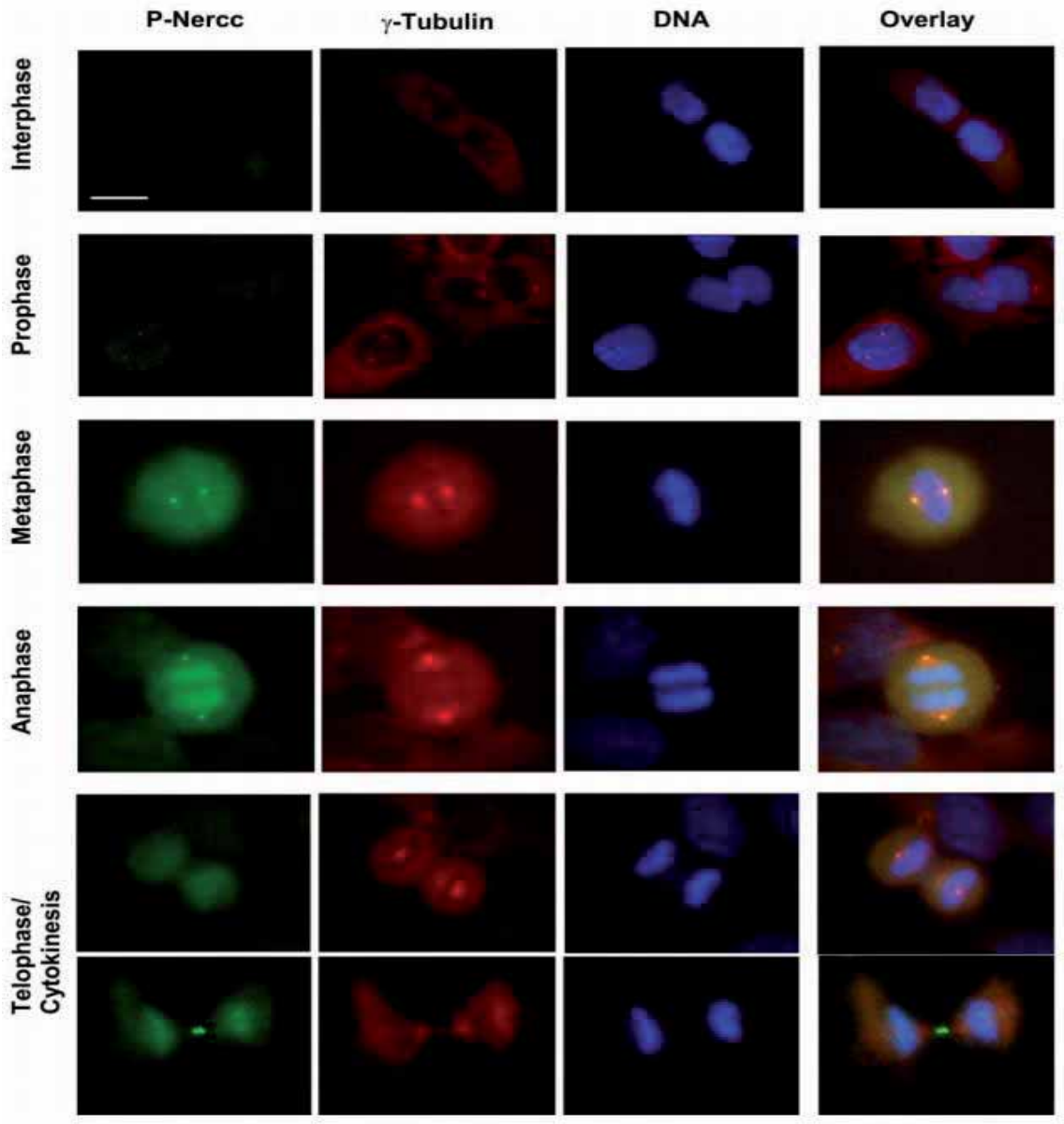


**Figure 1.12 Immunolocalization of active Nek9 during mitotic progression in U2OS cells.**

Active Nek9 (P-Nek9) is shown in green, γ-tubulin in red and DNA in blue [85].

#### 1.2.1.3.1.3 Nek9 activation.

Nek9 kinase activation is achieved by phosphorylation at Thr210 in the activation loop. Nek9 is also regulated by both dimerization and binding to RCC1-like domain, which inhibits the Nek9 kinase activity. Recombinant Nek9 lacking the coiled coil domain cannot be activated while just lacking the RCC1-like domain Nek9 is naturally active [57]. Nek9 activation is regulated by a sequential phosphorylation by Cdk1 and Plk1, this process implies a Cdk1 phosphorylation on Nek9 necessary for priming Plk1 binding and phosphorylation on Nek9 Thr210 [89]. Besides the phosphorylation, it is suggested additional inhibitory mechanisms for the kinase, such as phosphatase activity or the binding of an undescribed regulator that impairs Nek9 autophosphorylation [57,85,87].

#### 1.2.1.3.1.4 Nek9 function.

Overexpression of kinase-dead Nek9 mutant interferes the cell cycle progression and results in apoptosis [57]. Endogenous Nek9 inhibition by antibody microinjection in interphase cells prevents mitosis. In prophase cells Nek9 inhibition by antibody microinjection disrupts normal mitotic spindle formation, inducing promethaphase arrest or abnormal chromosomal segregation resulting in mitotic catastrophe [57]. Nek9 depletion by iRNA impairs centrosome separation out coming in a unseparated or less separate centrosomes in prophase cells [89]. In *Xenopus* egg extracts xNek9 immunodepletion impairs spindle assembly, RAN-GTP-induced aster formation and correct chromosome alignment [85]. All these data indicate that Nek9 is a mitotic regulator involved in mitotic spindle regulation.

Spindle formation requires microtubule nucleation performed by γ-tubulin ring complex [90], also requires the correct orientation of microtubules and centrosome separation performed by molecular motors as dynein or Eg5 [91,92]. Nek9 interacts with the γ-TuRC [85] and can phosphorylate the dynein motor complex associated protein BicD2 [84,93]. Then Nek9 substrates Nek6 and Nek7 [83] interact and regulates the mitotic kinesin Eg5 and its function in centrosome separation at the beginning of mitosis [62,89]. Except for Eg5, the functional relevance of these interactions remains unknown.

Recently a new function for Nek9 has been described in autophagy. Nek9 depletion impairs this process inhibiting the cargo recruitment to vesicles and its regulation [94].

#### 1.2.1.4 LC8/DYNLL

Originally, dynein light chains are described as accessory subunits of the large dynein motor complexes [95]. The LC8 family of light chains, DYNLL1 and DYNLL2 in vertebrates, in association with Tctex and LC7 light chains families binds as homodimers to the dimeric dynein intermediate chains (DIC) which are scaffold subunits for cargo binding to the motor complex [96–98]. LC8 genes are present in all sequenced eukaryotic genomes [98]. LC8 is an extremely conserved 10 Kda protein LC8 orthologs share more than 90% identity. The two mammalian paralogs DYNLL1 and 2 differ in 6 of the 89 amino acid residues. Embryonically lethal or severe pleiotropic phenotypes are found when LC8 gene is knocked down or out in Drosophila and *C. elegans*. Based on these genetic studies LC8 is an essential protein for metazoans [99,100].

##### 1.2.1.4.1 LC8 structure.

LC8 has a unique fold: two-five-stranded, antiparallel β-sheet responsible of the dimerization; each β-sheet contains 4 strands four strands from one monomer, the fifth strand belongs the other monomer. These β-sheets are flanked by two pairs of α-helices at the opposite face of the dimer [101,102]. Crystal structure of LC8 in apo form [103–107] and in complex with peptides from binding partners have been determined (Fig. 1.13) [103,106,108–111]. The bound ligands of LC8 lie in two identical parallel grooves formed at the two edges of the dimerization interface. These peptides from an extra antiparallel β-strant, consequently, increasing the central β-sheets [103–107]. Although LC8 constitute an homodimer, phosphorylation on Ser88 dissociates LC8 to stable monomers [112,113].

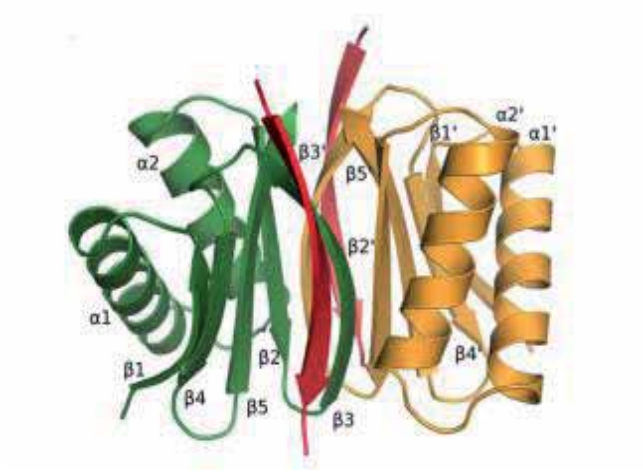


**Figure 1.13 Crystal structures of LC8 with LC8 binding motif of Nek9.**

Schematic representation of the LC8Nek9 peptide structure. α-Helices andβ-strands of each LC8 subunit are labeled. The two Nek9 peptides binding the homodimer are depicted in red [64].

### 1.2.1.4.2 LC8 binding motif.

LC8 binding motifs were originally divided in two clases: (K/R)XTQTX motif and XG(I/V)QVD motif [103,114,115] (Fig. 1.14). In both cases Q is the central position and caps the N-terminal end of the second α-helix, while the side-chains of some other amino acids residues interact with the binding groove. However, a few LC8 partners don't show this canonical binding, but the peptide topology is similar [106,116–118]

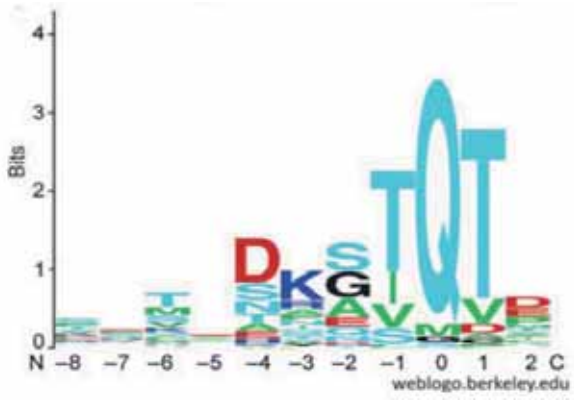


**Figure 1.14 Sequence logo of the binding motif of all hitherto determined and verified LC8 binding Motifs.**

Similar colors indicate similar chemical properties [119].

The conformation of the binding groove is very dynamic allowing this promiscuously interaction even being a highly conserved binding site [104]. The affinity of LC8 to the monomeric peptides is moderately weak, however most of the LC8 partners are dimeric which can form a dimer-dimer complexes acting as a bivalent ligands, whose binding affinity is increased [120].

#### 1.2.1.4.3 LC8 structural function.

Firstly LC8 was identified as a tail-binding light chain of dyneins (DYC) and myosin 5a [98,121]. Also it was found to interact with many proteins that were shown to be transported either on microtubules or on actin filaments. Thus, it was assumed that LC8 function as a cargo adapter [103,114,122–124]. However, recent studies defy this hypothesis arguing that LC8 improbably can bridge the cargo to either motor complex because the two identical binding sites of LC8 in addition to the homodimeric nature of DIC and myosin 5a probably induce dimer-dimer complexes in a bivalent interaction [125–127]. Supporting this hypothesis it is shown that LC8 interacts with other proteins that are not associated to intracellular transport, and also the devoid of dynein motors in plants, in which LC8 is present [96]. Moreover, last studies shown that the short linear LC8 binding motifs are located in intrinsically disordered segments [116,128]. Furthermore, the LC8 binding motif is usually located close to coiled-coil or other dimerization domains of the interacting partners. The current view is that LC8 acts as an essential hub protein promoting dimerization, structural stabilization of IDPs and could hence allosteric regulation in its binding partners in diverse complexes and networks [128].

Structurally consequences of LC8 binding to target coiled-coil containing proteins are characterized by increasing the α-helix content and stabilizing the coiled-coil region, providing additional binding platforms in various complexes (Fig. 1.15) [116,117]. Structural stabilization of intrinsically disordered or coiled coil regions does not necessarily induce structural stabilization of the overall target protein. LC8 binding causes spatial constrains in the target and they could lead dissociation of preexisting interactions between dimeric domains, destabilization of binding platforms or inhibiting activities of the associated protein partners. However LC8-induced dissociation of binding platform has not

been described yet [111].

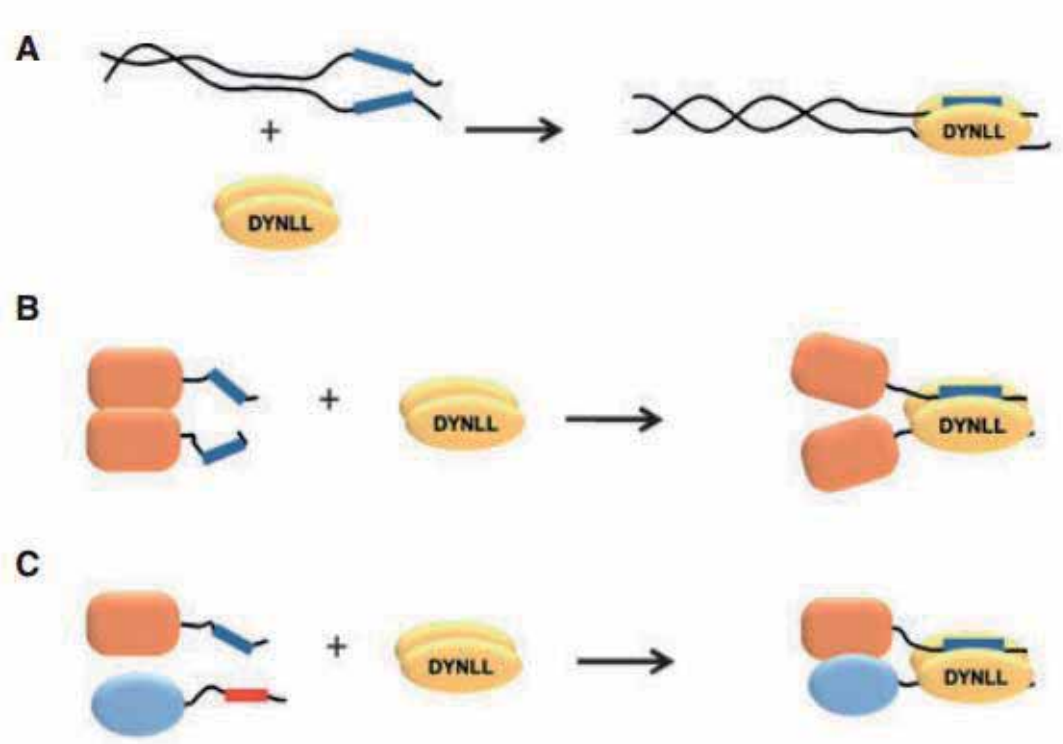


**Figure 1.15 Schematic representation of different scenarios where LC8 acts as a hub protein.**

A) Interaction of LC8 with a partner that contains a potential or preformed coiled-coil domain near the LC8 motif could lead to homodimerization or coiled-coil stabilization. The newly formed structure could act as a platform for further interactions. B) If the LC8 binding motif is localized near interacting globular domains, LC8 binding could pry apart the domains by steric constraints and might destroy further interaction sites or inhibit other activities. C) Heterodimerization of two targets could occur if two LC8 binding motifs are located near two weakly interacting domains. Adapted from: [61].

#### 1.2.1.4.4 LC8 as a hub protein.

LC8 is involved in a wide variety of functions through its partners [61]. In the following paragraphs few examples are shown.

##### 1.2.1.4.4.1 Intracellular transport.

Syntaphilin is targeted to axonal mitocondria and to microtubules as well. A model was proposed in which LC8 serves as stabilizator of coiled-coil structure in syntaphilin to facilitate its docking to mitochondrial receptor. This physical coupling between LC8 and syntaphilin may control mitochondrial mobility and

density in axons [129] .

Drosophila Dazl is an RNA-binding protein essential for gametogenesis. Its proposed that Dazl travels along microtubule network in association with the dynein complex controlling a subcellular distribution of specific mRNAs [122].
Basoon is an LC8 partner that links to the retrograde transport of Golgi-derived vesicles in neurons. It was convincingly shown that Basoon and LC8 are co-transported by the dynein motor complex [130].

#### 1.2.1.4.4.2 Nuclear transport.

The Yeast ortholog Dyn2 dimerizes and stabilizes the Nup82-Nsp1-Nup159complex, a module of the nuclear pore filaments. Dyn2 binds to five tandem motifs located between a disordered Phe-Gly repeat and coiled-coil domain of Nup159 forming a rigid structure facilitating nucleocytoplasmatic transport [131].

LC8 interacts with the replication factor Ciz1. In a proposed model LC8 brings Ciz1 to the nucleus, where it binds Cdk2 and p21. These complexes play a regulatory role in cell cycle progression [132].

#### 1.2.1.4.4.3 Mitosis.

Nek9 is a regulator of the mitotic progression. It is known that LC8 interacts at the C-terminal of Nek9 when is inactivated. This interaction is regulated by phosphorylation on Nek9 residue Ser944. It is proposed that the LC8 interaction interferes with the interaction of Nek9 with its downstream partner Nek6 as well as with Nek6 activation [60,63,64]. The nucleoporin Tpr functions during mitosis as a spatiotemporal regulator of spindle checkpoints and it is involved in recruitment of checkpoint proteins to dynein [133].

#### 1.2.1.4.4.4 Apoptosis and autophagy.

BimL and Bmf are BH3-only pro-apoptotic proteins thought to be normally sequestered to dynein and MYO5A motor complexes via DYNLL1 and DYNLL2, respectively [124,134]. Specific apoptotic stimuli liberate them from the cytoskeleton, in complex with LC8, helping them to translocate to Bcl-2 proteins thereby activating apoptosis.AMBRA1 is a component of a multiprotein

complex that regulates autophagy and development of the nervous system in mammals [135]. Binding of DYNLL1 inhibits TNFα-induced NFκβ activation by interacting with IκBα, thereby preventing its phosphorylation by IκBα kinase, its nuclear translocation and its regulatory role in apoptosis [136,137]. This interaction is redox regulated: TNFα induces the production of reactive oxygen species, which in turn oxidize DYNLL1, on Cys2 which is an isoform-specific residue, resulting in the dissociation of the complex and NFκβ activation. A novel disulfide reductase, TRP14, contributes to the NFκβ inhibitory activity by maintaining LC8 in its reduced state [137].

#### 1.2.1.4.4.5 Postsynaptic density (PSD).

PSD is a dynamic complex crucial for receptor immobilization at both excitatory and inhibitory synapses. Gephyrin is a scaffold protein critical for glycine- and GABA-receptor clustering. LC8 binds to a disordered linker domain between two globular dimerization⁄oligomerization domains [138,139]. It was shown that the gephyrin–LC8 complex together with the Gly-receptor is involved in transport processes by the dynein complex [140].

#### 1.2.1.4.4.6 Transcription regulation.

BS69 is a multifunctional scaffold protein involved in transcription repression in association with various transcription factors in cellular senescence through the p53–p21 and JNK pathways [141]. LC8 interacts with the transcription factor TRPS1 and suppresses its transcriptional repression activity [142].

LC8 binds to the N-terminal disordered domain of ERα and facilitates its nuclear accumulation. In the nucleus the recruitment of the LC8–ERα complex to the chromatin of estrogen-receptor-targeted genes is assisted by the LC8–KIBRA–histone H3 complex [143,144].

#### 1.2.1.4.4.7 Dynein motor complex.

Originally it was proposed that LC8 acts as a cargo adapter that links the cargo to the motor complex [101,102,108]. However, based on recent results LC8 together with the other two classes of light chains is involved in regulating

dynein complex assembly and hence indirectly affecting cargo binding [145,146]. Current speculations about the cargo binding to the dynein motor complex suggest that cargo binds directly or indirectly to the genuine adaptor dyactin or dynein subunit (dynamitin, intermediates or DIC). Moreover, LC8 is not a cargo adapter and the co-localization of LC8-partner pairs, LC8-DIC (Dynein Intermediate Chain) and LC8-cargo in complex is merely coincidental [61].

### 1.2.2 The Arginine Deiminase Pathway in *Mycoplasma penetrans*.

Arginine Deiminase Pathway rules the metabolism of arginine towards ATP synthesis [147]. This pathway is considered a major source of energy for microorganisms such as *Mycoplasma penetrans,* among other pathogenic organism*,* in anaerobic conditions, and also is probably implicated in pathogenic and virulence, protecting the mollicutes from acidic stress during infection [148–153].

In the present thesis we present the crystal structures of the three enzymes composing the gene cluster of the arginine deiminase pathway from *M. penetrans*: arginine deiminase (ADI), ornithine carbamoyltransferase (OTC) and carbamate kinase (CK). All three enzymes present an homo-oligomeric assemble. Ornithine carbamoyltransferase (OTC) displays a dodecameric structure with a 23-point symmetry. The dodecameric structure of OTC represents the highest level of organization in this protein family and in *M.penetrans* it is constituted by a novel interface between the four catalytic homotrimers [154]. OCT proteins have a wide range of quaternary structures, the most common is an homotrimer [155]. However, dodecameric assembly has only been observed in *P.aeruginosa* [156], and hyperthermophilic *Pyrococcus furiosus* [157]. It is suggested that dodecameric assemblies of OCT's are involved in thermophilic resistance or in allosteric enzyme regulation by coooperativity [156,158]. Arginine deiminase (ADI) and Carbamate kinase (CK) show the common dimeric organization known in other orthologs. The arginine deiminase (ADI) structure displays its apo-form in an open conformation of the active site of the enzyme. The active site pocket of ADI is empty, with some of the catalytic and binding residues far from their active

positions. Comparing with other known ADI structures in bibliography [159] we suggest the major conformational changes upon substrate binding. Carbamate kinase (CK) structure is characterized by the presence of two ion sulfates in the active site, one in the carbamoyl phosphate binding site and the other in the β-phosphate ADP binding pocket of the enzyme. The CK structure also shows variations in some of the elements that regulate the catalytic activity of the enzyme. The relatively low number of metabolic pathways and the relevance in human pathogenesis of *Mycoplasma penetrans* places the arginine deiminase pathway enzymes as potential targets to design specific inhibitors against this human parasite [153,154]

#### 1.2.2.1 Mollicutes.

The Mollicutes are a class of bacteria distinguished by the absence of a cell wall. They are obligated parasites of various animals and plants, living on or in the host's cells. Interestingly, they are only 0.2–0.3 μm in size and more importantly, have a very small genome size known for a living cell. Only the genus *Ureplasma* and *Mycoplasma* are able to infect human or animal cells [160]. Their genome is a circular double strand helix with low GC percentage between 23-30%. Interestingly, the UGA codon codes for a Trytophan instead for a stop codon [161].

#### 1.2.2.2 Minimal genome.

The Mollicutes have the smallest sequenced genome. For *Mycoplasma*, the genome size range swings between 0.580 Mb for *Mycoplasma genitalium* [162] and 1.358 Mb for *Mycoplasma penetrans* [163]. This incredible feature is originated by the degenerative evolution their ancestors underwent, losing genome complexity [164]. In fact, Mycoplasma are obligated parasites and their living environments are quite stable and rich in macromolecules, in consequence, their adaptive, and also, anabolic capacity is reduced [165]. In addition to the limited adaptive capacity or regulation, reduced anabolism and the lack of genome redundancy Mycoplasma are close to be the minimum bacteria cell with the minimal genome. Moreover, their simple genome and proteome makes them a fascinating model for studying the simplest living

system containing only the essential genes for living.

#### 1.2.2.3 Energetic metabolism and ADI pathway in *M.penetrans*.

All mollicutes lack of tricarboxylic acids cycle (TCA cycle) and cytochroms, consequently, a oxidative phosphorylation mechanism is rejected as an energy source [147]. Indeed, the energy springs from substrate-level phosphorylation. This metabolic reaction has low efficiency ATP production although produces high amounts of secondary metabolites, often toxic for the host. ADI pathway is one of the metabolic reactions producing energy by substrate-level phosphorylation in bacteria.

The ADI pathway is performed by three catalytic enzymes: arginine deiminase (ADI, EC 3.5.3.6), ornithine carbamoyltransferase (OTC, EC 2.1.3.3) and carbamate kinase (CK, EC 2.7.2.2). This pathway metabolizes arginine producing ornithine, ammonia, CO2 and ATP, generating one mole of ATP (energy) and 2 mole of ammonia per mole of arginine (Fig. 1.16).

ADI pathway is essential for some bacterial metabolism or pathogenicity mechanism, like that of *S. pyrogenes* [166] among others [167]. Indeed, for some species ADI pathway is not essential for they growth but it is for they survival in their natural environment acting as a protection mechanism, i.e. protection from acidic stress during the infection [168,169]. Thus, the scientific community has spent efforts in ADI inhibitors synthesis [170,171].

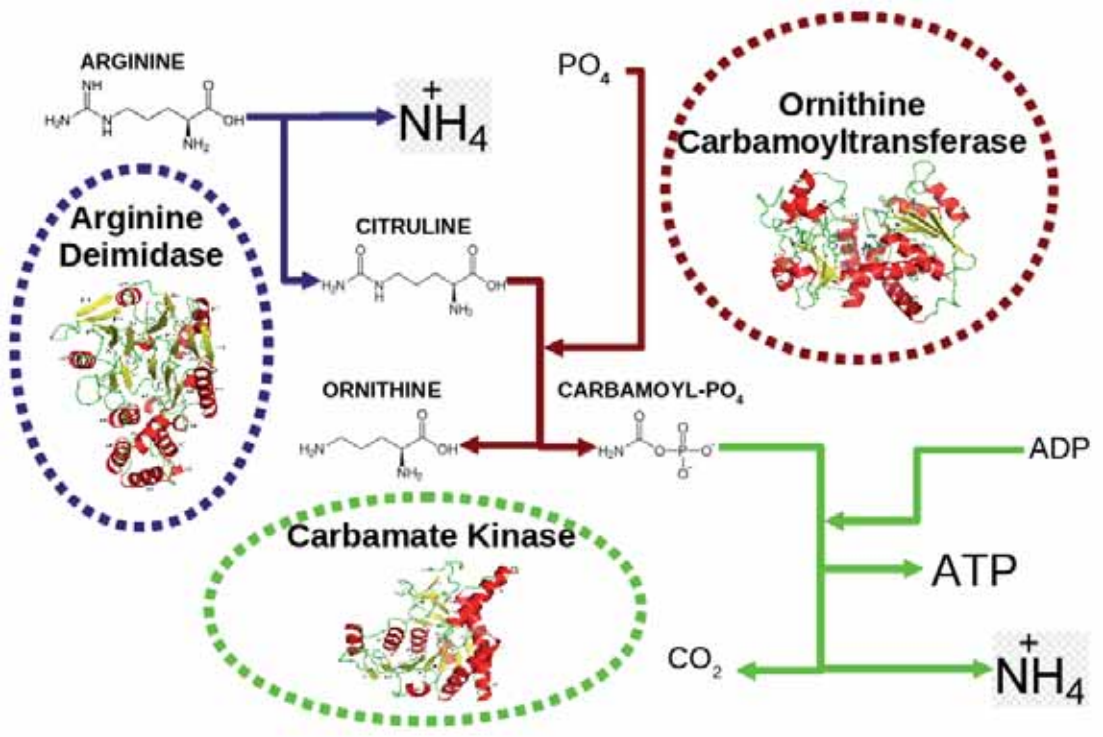


**Figure 1.16 Schematic representation of the ADI pathway in *M. penetrans*.**

Arginine Deimidase reaction is labeled in blue, in red for Ornithine Carbbamoyltransferase and in green for Carbamate Kinase. The monomer structure of these proteins for *M. penetrans* are shown.

#### 1.2.2.3.1 Arginine deiminase (ADI).

In the first step of the ADI pathway, ADI catalyzes the deimination of arginine, and it is the first step of the argininine degradation pathway (Fig. 1.16). This reacction performs the conversion of arginine to citrulline and ammonium. The absence of the Arginine deiminase gene in the human genome, and it importance in pathogenenicity [148–153] make ADI an attractive therapeutic target for some parasitic and bacterial infection. ADI structures and reaction mechanisms have been described in *P.aeruginosa* [170,172] and *Mycoplasma arginini* [159]. In the present work the apo form of *M.penetrans* ADI is shown and compared with previous substrate-bound structures revealing structural rearrangements in the active site (Fig. 1.17).

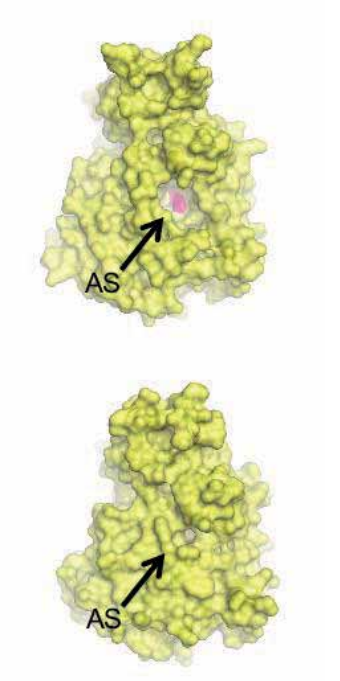


**Figure 1.17 ADI structure.**

A) Surface representation of ADI from M.penetrans. AS indicates the active site pocket (colored in magenta). B) Surface representation of ADI from M.arginini in complex with arginine in the active site. Adapted from: [154]

Based in crystal structure and gel-filtration chromatography, the biological unit of ADI is a dimer. The ADI catalytic domain is composed by a characteristic repeated motif forming five ββαβ modules in a cyclical arrangement. This fold is also characteristic of other arginine-catabolizing enzymes [173–175]. In the case of ADI it contains an additional 85-residue α-helical domain. The role of this domain is still not clear, but has been speculated that can participate in the apoptotic activation [159].

#### 1.2.2.3.2 Ornithine carbamoyltransferase (OTC).

The citruline obtained by ADI is processed by OTC and uptakes inorganic phosphate to generate ornithine and carbamoyl phosphate (Fig. 1.16). OTC enzymes can also be anabolic catalyzing the reverse reaction. In this sense, some organisms, such as *Pseudomonas aeruginosa,* encode different OTCs genes dedicated to either the ADI pathway or to the arginine biosynthetic pathways [176–178]. The anabolic reaction is also related to the arginine biosynthesis in plants and to the urea cycle in the mitochondria in mammals [179,180].

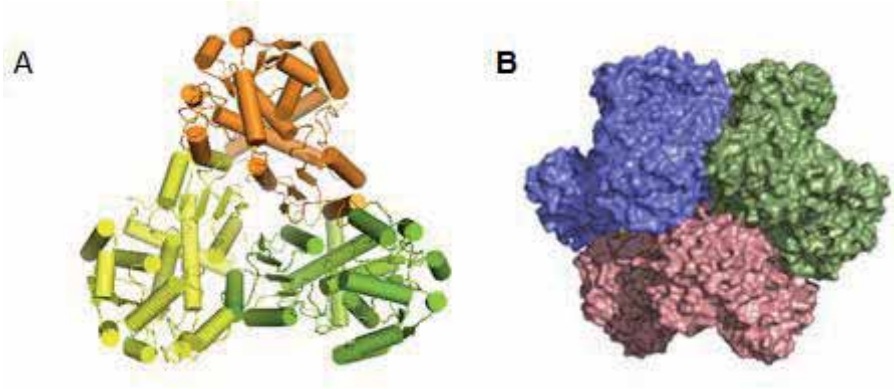


**Figure 1.18 OTC Trimer and dodecamer conformations.**

A) Ribbon representation of the OTC homotrimer structure. B) Surface view of the M. penetrans OTC dodecamer. Each homotrimer is shown with a different color. Adapted from: [154].

All carbamoyltransferases share the same basic overall protein fold which contains two domains: a CP-binding domain (carbamoyl phosphate binding domain) and an amino acid binding domain. The basic quaternary structure organization is a homotrimer, with the active site located at the interface between monomers [156,181] However, a dodecameric assembly containing four homotrimers has been observed in the catabolic OTC of *Pseudomonas aeruginosa* and in the hyperthermophilic *Pyrococcus furiosus.* Dodecameric assemblies of OTCs have been suggested to be involved in thermophilic resistance or in allosteric enzyme regulation by cooperativity [56,156–158]. The crystal structure of OTC from *Mycoplasma penetrans* described in this thesis possess a quaternary dodecameric assembly, which is unique to *Mycoplasma penetrans. A*t the interface between the catalytic homotrimers contains particular interactions (Fig. 1.18). In this work we compare the interface differences between dodecameric OTC assemblies from *M.penetrans* and *P.aeruginosa* as mesophillic organisms and from *P.furiosus* and *Thermotoga .maritima* as thermophilic organisms.

#### 1.2.2.3.3 Carbamate kinase (CK).

In the last step of the ADI pathway, CK catalyzes the hydrolysis of the carbamoyl phosphate to CO2 and ammonia, while the phosphate group is used to phophorylate ADP to generate ATP (Fig. 1.16). Similarly to OTCs, in some organisms such as *Pyrococcus furiosus,* CK can catalyze the opposite reaction

synthesizing carbamoyl phosphate from carbamate and ATP. The absence of this protein in animals and its importance in generating energy in some pathogenic microorganisms like *Giardia intestinalis* or *Trichomonas vaginalis* makes CK an attractive therapeutic target [182,183]. Structures of CK bound to ADP and to sulfate ions have already been described in two different organisms, *Enterococcus faecalis* and *Pyrococcus furiosus* [184–186]. As previously described CK organizes as a dimer, and it is performed by three domains, with a large crevice in the middle that creates the binding sites for the two substrates, carbamoyl phosphate (CP) and ADP. The N-terminal domain (residues Met1 to Ala222), and the mobile PSD domain ("protruding subdomain", from Lys126 to Val159), which is involved in the catalytic reaction by an overall "rigid body" movement upon substrate binding, and the C-terminal domain (residues Asp223 to Ala309). Whereas the binding residues for carbamoyl phosphate basically emanate from the N-terminal domain, the C-terminal domain is responsible for the binding of ADP. Interestingly, the structure present in this work of CK from *M.penetrans* differs from the previous structures by the presence of two sulfate ions, one in the carbamoyl phosphate pocket and another in the β-phosphate ADP binding pocket. Particularly interesting, in the *M.penetrans* CK structure described here, is the "open" and non-catalytic conformation of the PSD subdomain, despite the presence of a sulfate ion in the carbamoyl phosphate-binding pocket (Fig. 1.19). More importantly, the "open" orientation of the PSD domain with a sulfate ion occupying the CP binding site has not been observed, and might represent a structural snapshot of the binding of CP before the enzymatic reaction occurs. However, it could also be an example of the product complex before the release of the CP from the active site in the anabolic reaction of synthesis of the carbamoyl phosphate from carbamate [184].

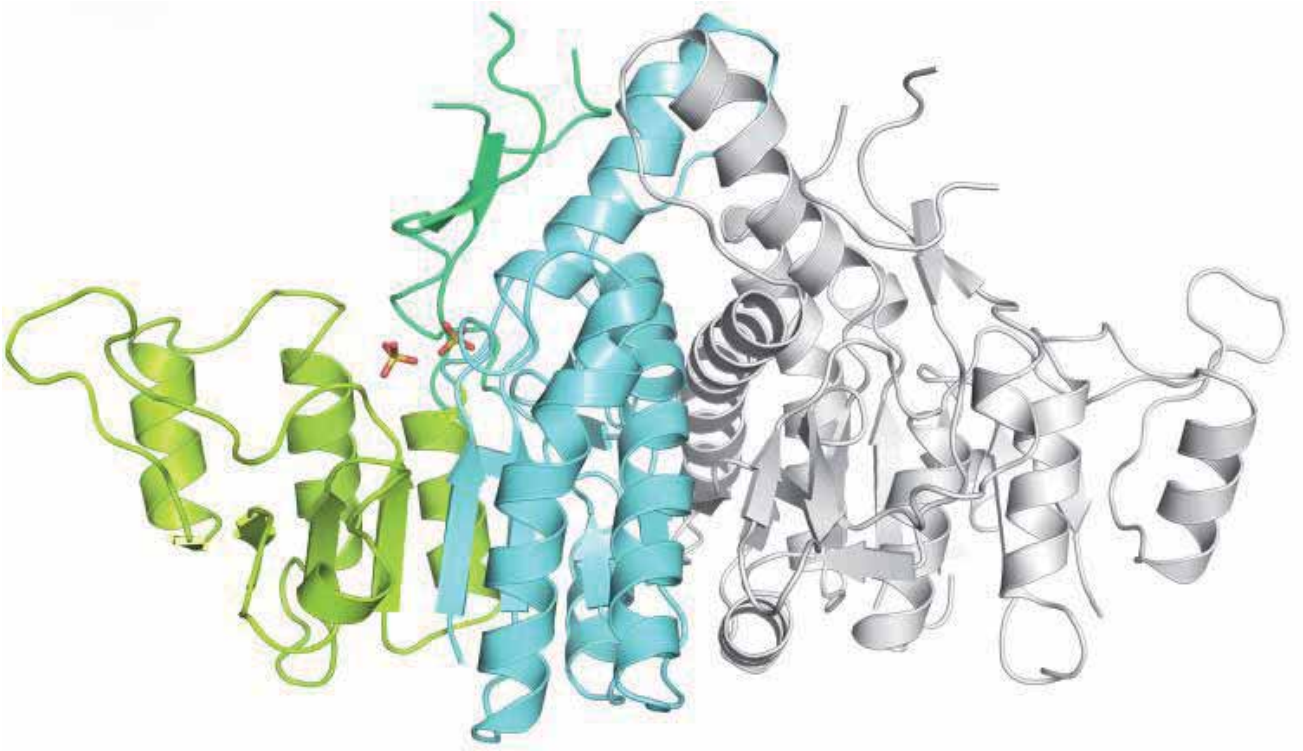

**Figure 1.19 Dimer structure of CK.**

Ribbon representation of the dimer of CK. In one of the monomers, the N-terminal domain is in colored in light blue, the C-terminal domain in forest green and the PSD domain in lime green. The two sulfate ions are shown in stick representation. Adapted from: [154].

#### 1.2.2.3.4 Interactions in the ADI pathway.

Despite our efforts it was not possible to obtain crystal structures for the complex between OTC and CK. However previous data shown evidences of the OTC-CK complex for *P.furiosus*. The first evidences for biologically significant interaction were provided by isotopic competition experiments with cell-free extracts of *P. furiosus*; showed a marked preference of ornithine carbamoyltransferase (OTC) for CP synthesized by carbamate kinase (CK) rather than for CP added to the reaction mixture [187] and by affinity electrophoresis and co-immunoprecipitation in combination with cross-linking [188,189]. In order to obtain evidences of an interaction between OTC and CK a Y2H, ITC and Hummel-Dreyer chromatography experiments were performed, obtaining significant information of the biological formation of the complex [190].

## 1.3 Protein crystallization and structural determination by X-Ray diffraction.

X-ray crystallography is a technique used for determining the atomic and molecular structure of a crystal, in which the organized atoms cause a beam of X-rays to diffract into many specific directions (Fig. 1.20). By measuring the angles and intensities of these diffracted beams, can be produced a three-dimensional map of the density of electrons within the crystal. From this electron density, the mean positions of the atoms in the crystal can be determined, as well as their chemical bonds and various other information.

Two procedures rule this high complexity-level technique: In one hand, protein crystallization is needed due to the use of protein crystals diffraction to magnify the signal by reason of a single molecule diffraction would be too weak to be measurable. In the other hand, the X-ray diffraction is consequence of the electromagnetic waves used by crystallographers are approximately 0.5 to 1.5 angstroms long, which are just the right size to measure the distance between atoms in a molecule, and these wavelengths are X-Rays

### 1.3.1 Protein crystallization.

Protein crystallization is indeed an ordered soluble protein precipitation which all the protein atoms are orientated in a fixed way with respect to one another while still maintaining their biologically active conformations. Several critical steps must be achieved in order to crystallize a protein. First protein sample must be purified around 95%. Then the protein solubility must decrease usually mixing the protein in a buffer which excludes water from the protein surface. Finally, the protein solution has to be brought to supersaturation where the protein is condensed from the rest of the solvent, allowing the protein to form a highly organized crystal. Usually this is done by increasing the precipitant compound at the protein solution buffer by methods that include batch crystallization, liquid-liquid crystallization, vapor diffusion, and dialysis [191].

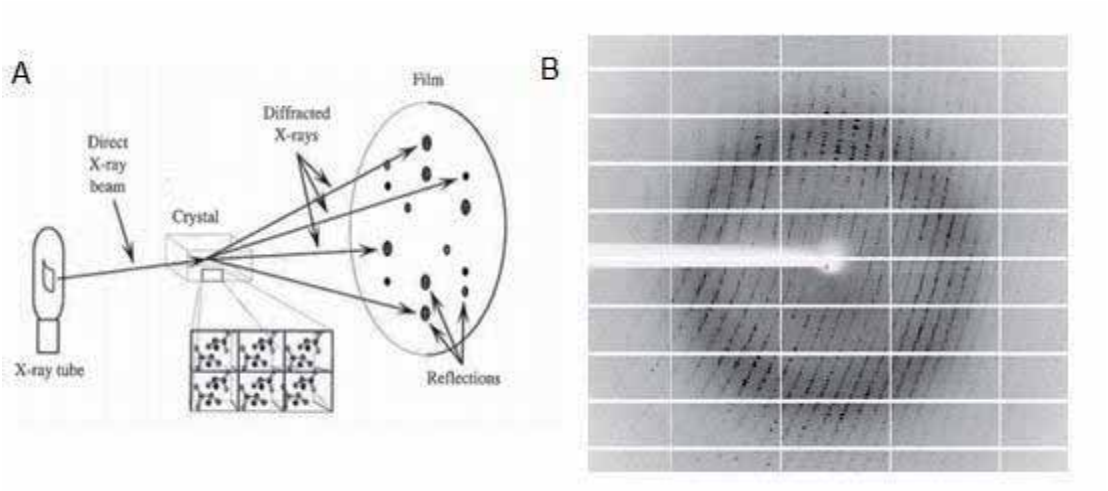


**Figure 1.20 X-ray diffraction and data collection**

A) The crystal diffracts the source beam into many discrete beams producing distinct reflections on the film. Adapted from: [191]. G. B) Diffraction pattern from a crystal of LC8.

#### 1.3.1.1 Vapor Diffusion.

Vapor diffusion is the most commonly employed method of protein crystallization. In this method, the purified protein is mixed with a precipitant buffer, the resulting mixture is enclosed with a larger reservoir containing the same precipitants in higher concentrations and in a significative larger volume than the mixture. Initially the mixture of protein solution contains comparatively low precipitant and protein concentrations but, as the protein mixture buffer and reservoir buffer equilibrate, the precipitant and protein concentrations increase in the drop over the time. If the appropriate crystallization solutions are used for a given protein, crystal growth will occur in the drop (Fig. 1.21). This method is used because it allows for gentle and gradual changes in concentration of protein and precipitant, which aid in the growth of large and well-ordered crystals [191].

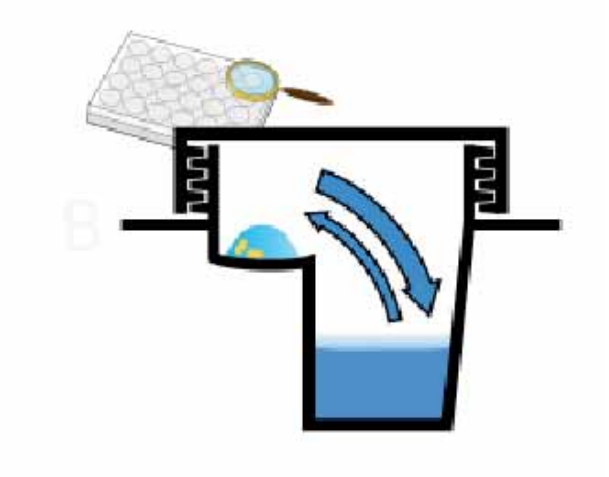

**Figure 1.21 Vapor diffusion technique representation.**

Vapor diffusion flows are shown as arrows. Note that the wither arrow marks a higher amount of vapor exchange resulting on the sample drying.
Adapted from: http://en.wikipedia.org/wiki/File:CrystalDrops.svg. This is original work created for Wikipedia

### 1.3.2 X-Ray diffraction.

The x-rays are shot at the protein crystal resulting in some of the x-rays passed through the crystal and the rest being scattered in various directions being recorded by a detector. The scattering of x-rays is also known as x-ray diffraction. Such scattering results from the interaction of electric and magnetic fields of the radiation with the electrons in the atoms of the crystal. The patterns are a result of interference between the diffracted x-rays governed by Bragg's Law: $2d\sin\theta=n\lambda$, if the diffracted x-rays interfere constructively. In Bragg's Law: d is the distance between two regions of electron density, θ is the angle of angle of diffraction, λ is the wavelength of the diffracted x-ray and n is an integer.

Constructive interference indicates that the diffracted x-rays are in phase or lined up with each other, while destructive interference indicates that the x-rays are not exactly in phase with each other. The result is that the measured intensity of the x-rays increases and decreases as a function of angle and distance between the detector and the crystal. The crystal is rotated so that the x-rays are able to hit the protein from all sides and angles.

Several basic physical principles underlying this technique are: The amplitude of the diffracted x-ray is directly proportional to the number of electrons in the atom that scatters x-rays. Then the scattered waves recombine,

thus, the beams reinforce one another at the detector if they are in phase or cancel one another out if they are out of phase. Note that every atom contributes to a scattered beam. Finally, three-dimensional atomic arrangement determines how the beams recombine. So, the intensities of the spots and their positions are thus the basic experimental data of the analysis.

A Fourier Transform can be applied to the intensities on the diffraction data to reconstruct the electron density distribution of the crystal. The Fourier Transform takes the reciprocal spatial frequency in the form of the diffraction pattern and gives out the spatial arrangement of the electron density. Through the Fourier Transform, the electron density distribution is illustrated as a terrain map. The mapping gives a three-dimensional representation of the electron densities observed through the x-ray crystallography. The interaction of X-rays with the electrons in a crystal gives rise to a diffraction pattern, which mathematically is the Fourier transform of the electron density distribution. The detectors used to measure the X-rays, however, can only measure the amplitude of the diffracted x-rays. The phase shifts, which are required to use the Fourier Transform and find the electron density distribution, cannot be measurable directly. This is known in the physics community as the “Phase Problem”. The problem can be simplified by finding specific atoms, which are usually a heavy metal, using the Patterson Synthesis and then using those atoms positions to estimate the initial phases and calculate an initial electron density map, which can further help in the modeling of the position of other atoms and improve the phase estimation. The commonly used methods are: Molecular Replacement (MR), the Isomorphous Replacement method (MIR), the Multiple-wavelength Anomalous Diffraction method (MAD) and the Single-wavelength Anomalous Diffraction method (SAD) [191].

#### 1.3.2.1 Isomorphous Replacement Method (MIR).

This method compares the x-ray diffraction patterns between a protein crystal and the same type of crystal with an addition of at least one atom with high atomic number, usually a heavy atom. The only difference that the crystal and its derivative have in a perfect isomorphism is the intensity differences due to the addition of heavy atoms on the derivative. These differences can be

identified by a Patterson search procedure, and such information is important as to determine the protein phase angles. The commonly used method for adding heavy atoms to the crystal derivatives is to soak the protein crystal in a solution that is composed identically to the mother liquor, but with a slight increase of precipitant concentration.

#### 1.3.2.2 Multiple Wavelength Anomalous Diffraction Method (MAD) and Single-Wavelength Anomalous Diffraction Method (SAD).

In MAD or SAD as in isomorphous replacement, the complexity of the phase problem is reduced by determining the position of a few heavy atoms with direct methods. If the wavelength of the X-ray corresponds to a transition between different electron shells of the atom, there will be a modification of the phase. This anomalous scattering results in effects in the diffraction pattern that can be distinguished from the rest. Requirements for using this method to determine the phases the protein must include atoms that cause significant scattering from X-rays, notably sulfur or metal ions from metalloproteins. Since selenium can replace naturally sulfur, it is more commonly used. In comparison to multi-wavelength anomalous diffraction (MAD), single-wavelength anomalous diffraction (SAD) uses a single set of data from a single wavelength. The main beneficial difference between MAD and SAD is that the crystal spends less time in the x-ray beam with SAD, which reduces potential radiation damage to the molecule. Also, since SAD uses only one wavelength, it is more time-efficient than MAD. A particle accelerator, called synchrotron, is also required for the method, due to the need of tunable wavelength.

#### 1.3.2.3 Molecular replacement (MR).

MR is nowadays the most common method to solve phase problems in x-ray crystallography. MR locates the orientation and position of a protein structure with its unit cell, whose protein structure is homologous to the unknown protein structure that needs to be determined. The obtained phases can help generate electron density maps and help produce calculated intensities of the position of the protein structure model to the observed structures from the x-ray crystallography experiment. MR relies upon the

existence of a previously solved protein structure which is homologous, 20% identity at least, to our unknown structure from which the diffraction data is derived. For that purpose a Patterson map is calculated from the experimental intensities and compared to a theoretical Patterson map of the homologous structure coordinates. In Patterson maps all phases are set to 0 which results in a density that corresponds where the peaks correspond to distance vectors between individual atoms. By rotating and then translating the Patterson maps relative to each other the position of the molecules can be found and initial phases determined (Fig. 1.22).

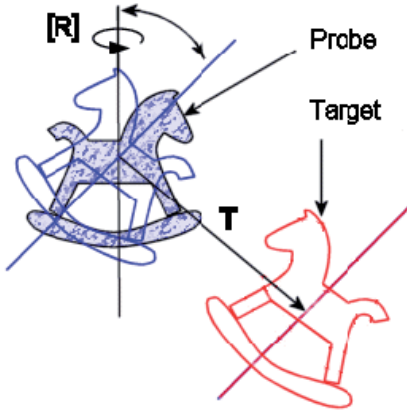


**Figure 1.22 Molecular replacement schematic representation of translation and rotation functions.**

MR tries to find the model which fits best experimental intensities among known structures. Adapted: http://my.yetnet.ch/dergutemensch/crystallography/molecularreplacement.htm

In the rotation function, our unknown Patterson map is compared to Patterson maps derived from our known homologue structure in different orientations. To score the rotation function modern programs use maximum likelihood-based algorithms. The highest correlation is obtained when the two structures are in similar orientation. In the translation function, the now correctly oriented known model can be correctly positioned by translating it to the correct co-ordinates within the asymmetric unit. This is accomplished by moving the model, calculating a new Patterson map, and comparing it to the unknown-derived Patterson map. This brute-force search is computationally expensive and fast translation functions are now more commonly used. Positions with high correlations are output in Cartesian coordinates.

# 2. Aims.

The basic objective of this thesis is the study of protein-protein interactions, which we applied in two different experimental models. In the first model we analyzed the role of phosphorylation in the interaction of a peptide derived from the mitotic kinase NEK9 with its binding partner LC8 [64]. In the second model we decipher the structures of the three enzymes composing the arginine deiminase pathway: arginine deiminase (ADI), ornithine carbamoyl transferase (OTC) and carbamate kinase (CK) [154].

The specific aims of the thesis can be summarized in the following items:

**2.1 Structural analysis of the regulation of the DYNLL/LC8 binding to Nek9 by phosphorylation**:

2.1.1 Determine the influence of the Nek9 phosphorylation on Ser944 in the LC8 binding.

2.1.2 Analyze the structural changes produced on LC8-Nek9 interaction upon phosphorylation on Ser944.

2.1.3 Study and compare the conformational changes of the Nek9-LC8 binding motif upon the interaction with LC8.

**2.2 Structural characterization of the enzymes composing the arginine deiminase pathway in *Mycoplasma penetrans:***

2.2.1 Determine the crystal structures of the enzymes composing the ADI pathway in *M.penetrans*.

2.2.2 Define the mobile regions of the arginine deiminase enzyme upon substrate binding.

2.2.3 Analyze and compare the dodecameric structure of ornithine carbamoyl transferase from *M.penetrans* with the few known dodecameric OTC structures, and particulary from thermophylic organisms.

2.2.4 Shed light about the carbamate kinase conformational changes of domains upon the interaction with substrates.

# 3. Publications.

## 3.1 Publication I:

**Structural analysis of the regulation of the DYNLL/LC8 binding to Nek9 by phosphorylation.**

Gallego P, Velazquez-Campoy A, Regué L, Roig J, Reverter D.

J Biol Chem. 2013 Apr 26;288(17):12283-94.

THE JOURNAL OF BIOLOGICAL CHEMISTRY VOL. 288, NO. 17, pp. 12283–12294, April 26, 2013


# Structural Analysis of the Regulation of the DYNLL/LC8 Binding to Nek9 by Phosphorylation*

Received for publication, February 5, 2013, and in revised form, March 8, 2013 Published, JBC Papers in Press, March 12, 2013, DOI 10.1074/jbc.M113.459149

**Pablo Gallego**[‡1], **Adrian Velazquez-Campoy**[§], **Laura Regué**[¶2], **Joan Roig**[¶3], **and David Reverter**[‡4]

*From the* [‡]*Structural Biology Unit, Institut de Biotecnologia i Biomedicina, Universitat Autònoma de Barcelona, 08193 Bellaterra, Spain, the* [§]*Department of Biochemistry and Molecular and Cell Biology and Institute of Biocomputation and Physics of Complex Systems (BIFI), Joint Unit IQFR, Consejo Superior de Investigaciones Científicas-BIFI, Universidad de Zaragoza, Spain, and Fundacion ARAID, 500018 Government of Aragon, Spain, and the* [¶]*Institute for Research in Biomedicine, 08028 Barcelona, Spain*

**Background:** Phosphorylation regulates binding of the mitotic kinase Nek9 to LC8, controlling signal transduction through the Nek9/Nek6/7 module.
**Results:** Crystal structures reveal the basis for the reduced interaction of LC8 for Nek9 upon phosphorylation on Nek9(Ser$^{944}$).
**Conclusion:** The reduced binding affinity of Nek9 for LC8 is due to diminished enthalpic interactions.
**Significance:** Disclosing phosphorylation as a novel mechanism that directly regulates LC8 protein-protein interactions.

**The NIMA family protein kinases Nek9/Nercc1, Nek6, and Nek7 constitute a signaling module activated in early mitosis involved in the control of spindle organization. DYNLL/LC8 (dynein light chain 8) was originally described as a component of the dynein complex, but the recent discovery of multiple interaction partners for LC8 has suggested that it has a general role as a dimerization hub that organizes different protein partners. Recent experiments suggested that LC8 binding to Nek9 was regulated by Nek9 autophosphorylation on Ser$^{944}$, a residue immediately located N-terminal to the LC8 conserved (K/R)*x*-TQT binding motif, and that this was crucial for the control of signal transduction through the Nek/Nek6/7 module. In the present work, we present two crystal structures of LC8 with a peptide corresponding to the Nek9 binding region with and without a phosphorylation on Ser$^{944}$. Structural analysis of LC8 with both Nek9 peptides, together with different biophysical experiments, explains the observed diminished binding affinity of Nek9 to LC8 upon phosphorylation on Ser$^{944}$ within the Nek9 sequence, thus shedding light into a novel phosphorylation regulatory mechanism that interferes with LC8 protein·protein complex formation.**

Nek9 (also known as Nercc1) belongs to the mammalian NIMA family of protein kinases, named after the *Aspergillus nidulans* NIMA kinase (1). Mammals contain 11 members of the NIMA family or *Neks*, some of which are modular proteins with different protein domains, whereas some others only contain the kinase domain that has a sequence identity of ~40% for all members of the family (2). Mammalian *Nek* members seem to be specialized in functions related to the control of the microtubule and cilliary machineries (3). Nek6 and Nek7, together with Nek9, constitute a signaling module activated early in mitosis and involved in the regulation of the mitotic spindle (4). Nek9 (also called Nercc1) is a 120-kDa modular protein composed of an N-terminal kinase domain, with a strong sequence identity to the other members of the *Nek* family, followed by a domain homologous to RCC1 (the exchange factor for the small G protein Ran) and a C-terminal domain that contains a coiled-coil motif involved in dimerization (1). Nek9 is inactive during interphase and is activated at centrosomes and spindle poles during mitosis through a two-step mechanism involving CDK1 and Plk1 (1, 5, 6). In mitosis, Nek9 specifically interacts with the highly similar Nek6/7 (2, 7) and is able to directly phosphorylate and activate these two kinases (8). Thus, Nek9, together with Nek6 and Nek7, form a phosphorylation signaling module that is activated in mitosis and has been shown to be essential for correct mitotic progression, controlling spindle formation and different aspects of the centrosomal cycle during early mitosis (1, 4, 7, 9–11).

A recent report using two-hybrid experiments uncovered DYNLL/LC8 as a protein partner of Nek9 (12). LC8 was shown to interact with the C-terminal tail of Nek9, immediately after the coiled-coil region, in a conserved consensus motif (12). DYNLL/LC8 is a highly conserved ubiquitous eukaryotic protein with many protein partners involved in a great variety of cellular functions (13). Partners of LC8 include, among other proteins, dynein, myosin V, neuronal nitric oxide synthase, the proapoptotic protein BimL, and transcription factors Swallow and Trps1 (14–20). Although DYNLL/LC8 was initially proposed to be a cargo adapter for the molecular motor dynein and myosin V, the existence of multiple protein partners revealed LC8 as a regulatory hub protein that interacts with a linear consensus binding motif normally located in intrinsically disordered protein regions (21).

* This work was supported by "Ministerio de Ciencia e Innovacion" of Spain Grants BFU2012-37116 (to D. R.), BFU2010-19451 (to A. V. C.), and BFU2011-25855 (to J. R.) and European Community Grant MIRG-CT-2007-200346 (to D. R.).

*The atomic coordinates and structure factors (codes 3ZKE and 3ZKF) have been deposited in the Protein Data Bank (http://wwpdb.org/).*

[1] Supported by the Formación Personal Investigador fellowship from the "Ministerio de Ciencia e Innovacion" of Spain.

[2] Present address: Dept. of Molecular Biology and Medical Services, MA General Hospital and Dept. of Medicine, Harvard Medical School, Boston, MA 02115.

[3] Supported by the I3 program from the "Ministerio de Ciencia e Innovacion" of Spain.

[4] Supported by the Ramon y Cajal program from the "Ministerio de Ciencia e Innovacion" of Spain. To whom the correspondence should be addressed: Universitat Autonoma de Barcelona, 08193 Bellaterra, Barcelona, Spain. Tel.: 93-5868955; Fax: 93-5812011; E-mail: david.reverter@uab.cat.

Binding of LC8 normally promotes dimerization and a gain of structure of the protein partner, in some examples by facilitating the formation of coiled-coil structures immediately N-terminal to the LC8 binding region.

LC8 is a homodimeric structure that contains two hydrophobic binging grooves for linear peptides located in opposite sites of the central β-sheet interface (22). As shown by crystal structures of LC8 complexes, two peptides can interact simultaneously with the two hydrophobic grooves forming each one an extra β-strand to the central β-sheet of LC8 homodimer (23–25). Structural and functional data indicate that the homodimer structure of LC8 is essential for the interaction with protein partners, which are normally formed by dimeric structures (26, 27). Signaling inputs such as LC8 phosphorylation, pH variations, or the cellular redox state have been shown to regulate LC8 function by controlling its dimerization (28–30). Interestingly, it has been recently shown that phosphorylation of $Ser^{88}$ in LC8, which promotes the disruption of the LC8 homodimer, can regulate the binding of protein partners such as dynein intermediate chain (27, 31).

Two different protein sequence motifs in target proteins can be recognized by LC8: (K/R)*X*TQT and G(I/V)QVD (where *X* is any amino acid) (32, 33). In addition to these short sequences, the binding region of the peptide can be extended at the N terminus, thus completing a total of nine residues forming the extra β-strand of the interface. Only a few LC8 partners contain non-canonical binding motifs lacking the most conserved Gln residue (25). The binding affinity of LC8 to monomeric peptides is moderately weak ($K_d$ between 0.1 and 40 μM) (13); however, bivalent peptides linking two consensus motifs have been shown to increase significantly the binding affinity for LC8 (34), indicating the importance of the dimer-dimer interaction in the complex of LC8 with protein partners. Despite the strong conservation in the LC8 binding region, recent biophysical data indicates an inherent plasticity that allows the interaction with these different consensus motifs (24).

LC8 has been proposed to participate in the regulation of the Nek9/Nek6/Nek7 kinase signaling module as a negative regulator of Nek6/7 binding and activation (12). LC8 binding to the C-terminal region of Nek9 interferes with the interaction of Nek9 with Nek6 and Nek7, thus impeding Nek9 activation of Nek6/7. *In vivo* experiments suggest that autophosphorylation of Nek9 can regulate this process by regulating the binding of Nek9 to LC8. $Ser^{944}$, which is immediately located N-terminal to the LC8 consensus motif, has been proposed to be phosphorylated upon Nek9 activation and directly promote the LC8 dissociation from Nek9 *in vivo*, although such direct effect of $Ser^{944}$ phosphorylation on LC8 binding has never been measured. The conservation in this position of a serine residue and the presence of other Ser/Thr residues in LC8 consensus motifs of many protein partners might indicate that phosphorylation could represent a general manner of regulation for the LC8 binding. To gain insights in this regulation, we have crystallized LC8 in complex with a Nek9 peptide corresponding to the LC8 binding region and with a similar phosphopeptide modified on the equivalent of Nek9($Ser^{944}$). Comparison of both crystal structures sheds light into the diminished LC8 binding of Nek9 upon phosphorylation on $Ser^{944}$. Additionally, *in vitro* LC8 binding experiments using different biophysical methods demonstrate that phosphorylation on $Ser^{944}$ reduces the affinity to form a complex with LC8, thus directly confirming that phosphorylation of the partner could be a general way to regulate interactions with LC8.

## EXPERIMENTAL PROCEDURES

*Protein Expression and Purification*—The cDNAs encoding full-length LC8 and the Nek9-CC[5] constructs (Nek9, residues 893 to 974) were cloned into a pET28b vector with the fusion protein Smt3 tagged with six histidines at the N-terminal. Constructions were expressed in *Escherichia coli* BL21(DE3) for 4 h at 37 °C after induction with 1 mM isopropyl 1-thio-β-D-galactopyranoside, and recombinant proteins were purified by nickel-nitrilotriacetic acid agarose resin (Qiagen) and dialyzed against 20 mM Tris-HCl (pH 8.0), 250 mM NaCl, and 1 mM β-mercaptoethanol in the presence of SENP2 SUMO protease overnight at 4 °C. After protease cleavage, LC8 and Nek9-CC were purified by ion exchange chromatography using a Resource Q (GE Healthcare) column and by gel filtration using a Superdex75 column (GE Healthcare).

Single point mutants of NEK9-CC, including Q948A and S944E, were constructed using the QuikChange site-directed mutagenesis kit (Stratagene) according to the manufacturer's instructions. All sequences were sequenced after generation. Nek9-CC mutants were produced and purified as the wild-type form.

*Peptide Design*—The Nek9 peptide contains the amino acids between the Nek9 positions 940 to 950 resulting in the sequence VGMHSKGTQTA. In case of the Nek9 P-peptide, with a phosphate group on $Ser^{944}$, the resulting phosphopeptide contains the sequence VGMH(pS)KGTQTA. Both peptides were provided by the company Pepnome Limited.

*Circular Dichroism*—CD spectra were measured in a Jasco-715 spectropolarimeter thermostatted at 25 °C. Spectra were recorded from 260 to 200 nm at 0.5-nm intervals, 1-nm bandwidth, and scan speed of 10 nm/min. Ten accumulations were done for each spectrum. LC8 concentration for each scan is 11.2 μM buffered with 100 mM NaCl, 10 mM sodium phosphate, pH 7.5, and 1 mM β-mercaptoethanol. In each spectrum, we vary the Nek9 peptide or the Nek9 P-peptide concentration ranged between 0 and 26.6 μM.

In the case of LC8 binding to Nek9-CC (Nek9 residues from 893 to 974) wild-type and point mutants, LC8 and Nek9-CC concentrations were 10 μM and 6.66 μM, respectively, buffered as mentioned above. Same concentrations were used for the spectra of the LC8·Nek9-CC complexes. Data were normalized to $[\theta]$ (molar ellipticity) using the formula shown in Equation 1,

$$[\theta] = \theta \frac{1}{10 \cdot M \cdot N_e \cdot l} \qquad \text{(Eq. 1)}$$

where $[\theta]$ means molar ellipticity, $\theta$ indicates measured ellipticity, $M$ represents molarity of the sample, $N_e$ indicates the number of peptide bonds, and $l$ indicates the cuvette path length in cm.

[5] The abbreviations used are: CC, coiled coil; SASA, solvent-accessible surface area.

*Determination of the Interaction Constants ($K_a$) by Circular Dichroism*—To determine the interaction constants between LC8 and the peptides, we measured the ellipticity at 220 nm in every spectrum. Because the interaction of LC8 with the peptides is characterized by moderate-to-high affinity and the concentrations are comparable with the expected dissociation constant, no approximation for the free ligand concentration can be made. The total concentration of ligand is expressed as follows:

$$[PL] = [P]_T \frac{K_A[L]}{1 + K_a[L]} \quad \text{(Eq. 2)}$$

where $[L]_T$ and $[P]_T$ are the total concentration of the peptide and LC8, respectively, $K_a$ is the association constant, and $[L]$ is the concentration of the free ligand. Solving this equation for the unknown $[L]$ will allow calculating the concentration of the LC8·peptide complex, $[PL]$, for each experimental point,

$$[PL] = [P]_T \frac{K_a[L]}{1 + K_a[L]} \quad \text{(Eq. 3)}$$

from which the change in circular dichroism signal can be calculated in Equation 4,

$$Y = A_0 + A[PL] \quad \text{(Eq. 4)}$$

where $A_0$ is the circular dichroism signal at zero peptide concentration, and $A$ accounts for the maximal change of the signal at high peptide concentration.

*Thermal Denaturation of LC8 and LC8·Peptide Complexes*—Thermal transition curves of LC8 and LC8·Nek9-peptide complexes were obtained in a spectrofluorometer (Cary Eclipse) at a heating rate of 0.2 °C/min following changes of intrinsic fluorescence at 338 nm while excited at 280 nm. The LC8 concentration was 11.2 $\mu$M in a buffer containing 100 mM NaCl, 10 mM sodium phosphate, pH 7.5, and 1 mM $\beta$-mercaptoethanol. To obtain the thermal denaturation curves for the LC8 in the presence of the two peptides, the experiments were performed in the presence of 11.2 $\mu$M concentration of the Nek9 peptide and P-peptide.

*Thermodynamic Parameters from Thermal Unfolding*—The thermal transition curves were fitted to obtain the unfolding thermodynamic parameters using Equation 5,

$$Y = (b_j + m_jT) + (b_u + m_uT)\frac{e^{((-\Delta H_m(1 - T/T_m))/RT)}}{1 + e^{((-\Delta H_m(1 - T/T_m))/RT)}} \quad \text{(Eq. 5)}$$

where $m_j$ and $b_j$ are the slope and the intercept with $y$ axis in the pretransition region, $m_u$ and $b_u$ are the slope and the intercept with $y$ axis in the post-transition region, $\Delta H_m$ is the unfolding enthalpy, $T$ is the absolute temperature, $T_m$ is the temperature at the melting point, and $R$ is the universal gas constant.

*Thermodynamic Binding Profile by Isothermal Titration Calorimetry*—Binding interaction between LC8 and both peptides was assessed by high-sensitivity isothermal titration microcalorimeter AutoITC200 (MicroCal, GE Healthcare). Protein and peptide samples were properly degassed and carefully loaded into the cells to avoid bubble formation during stirring. Experiments were performed in 100 mM NaCl, 10 mM sodium phosphate, or Tris-HCl, pH 7.5, and 1 mM $\beta$-mercaptoethanol. Experiments were carried out titrating 20 $\mu$M LC8 in the calorimetric cell with 200–300 $\mu$M peptide in the injection syringe. The heat evolved after each ligand injection was obtained from the integral of the calorimetric signal. The heat due to the binding reaction was obtained as the difference between the reaction heat and the corresponding heat of dilution, and the latter was estimated as a constant heat throughout the experiment and included as an adjustable parameter in the analysis. The association constant ($K_a$) and the enthalpy change ($\Delta H$) were obtained through non-linear regression of experimental data to a model for a protein with a single binding site. Data were analyzed using software developed in our laboratory implemented in Origin (version 7, OriginLab). The dissociation constant ($K_d$), the free energy change ($\Delta G$), and the entropic change ($\Delta S$) were obtained from basic thermodynamic relationships. Experiments performed in two buffers with different ionization enthalpies (0.86 kcal/mol phosphate, 11.4 kcal/mol Tris) allowed eliminating the contribution of proton exchange processes to the binding interaction and determining buffer-independent thermodynamic interaction parameters (enthalpy and entropy) (35, 36). Experiments performed at two temperatures, at 15 and 25 °C, allowed estimating the change in heat capacity upon binding, which is a binding parameter associated with changes in solvent accessible (polar and non-polar) surface area and, therefore, provides fundamental information on the binding interaction and possible conformational changes coupled to the complex formation.

*Crystallization and Data Collection*—Crystals of DYNLL/LC8 (dynein light chain 1) in complex with Nek9 peptide were obtained at 18 °C by sitting drop vapor diffusion methods. The reservoir solution contained 35% PEG 1500, 0.1 M MIB buffer (malonate, imidazole, and boric acid 2:3:3), pH 4. Crystals of LC8 in complex with Nek9 P-peptide were obtained at 18 °C by sitting drop vapor diffusion methods. The reservoir solution contained 30% PEG 1500, 0.1 M MIB buffer, pH 4.5. Single crystals appeared after 1 week from equal volumes of protein solution (12 mg/ml in 5 mM Tris, pH 8.0, 50 mM NaCl) and reservoir solution. All crystals were cryo-protected in reservoir buffer containing 15% glycerol and flash-frozen in liquid nitrogen prior to diffraction analysis. Diffraction data were recorded from cryo-cooled crystals (100 K) at the ALBA synchrotron in Barcelona (BL13-XALOC beamline). Data were integrated and merged using XDS (37) and scaled, reduced, and further analyzed using CCP4 (Table 1) (38).

*Structure Determination and Refinement*—The structure of LC8 in complex with Nek9 peptide and P-peptide were determined from the x-ray data by molecular replacement using a previous LC8 structure (Protein Data Bank code 2P1K) as a model. The initial electron density maps produced from molecular replacement programs were manually improved to build up complete models for LC8 and peptides using the program COOT (39). Model refinement was performed with Refmac (38) and Phenix (40). LC8 in complex with Nek9 P-peptide contained six LC8 molecules assembling three homodimers in the asymmetric unit, and the Ramachandran analysis shows 91.06%

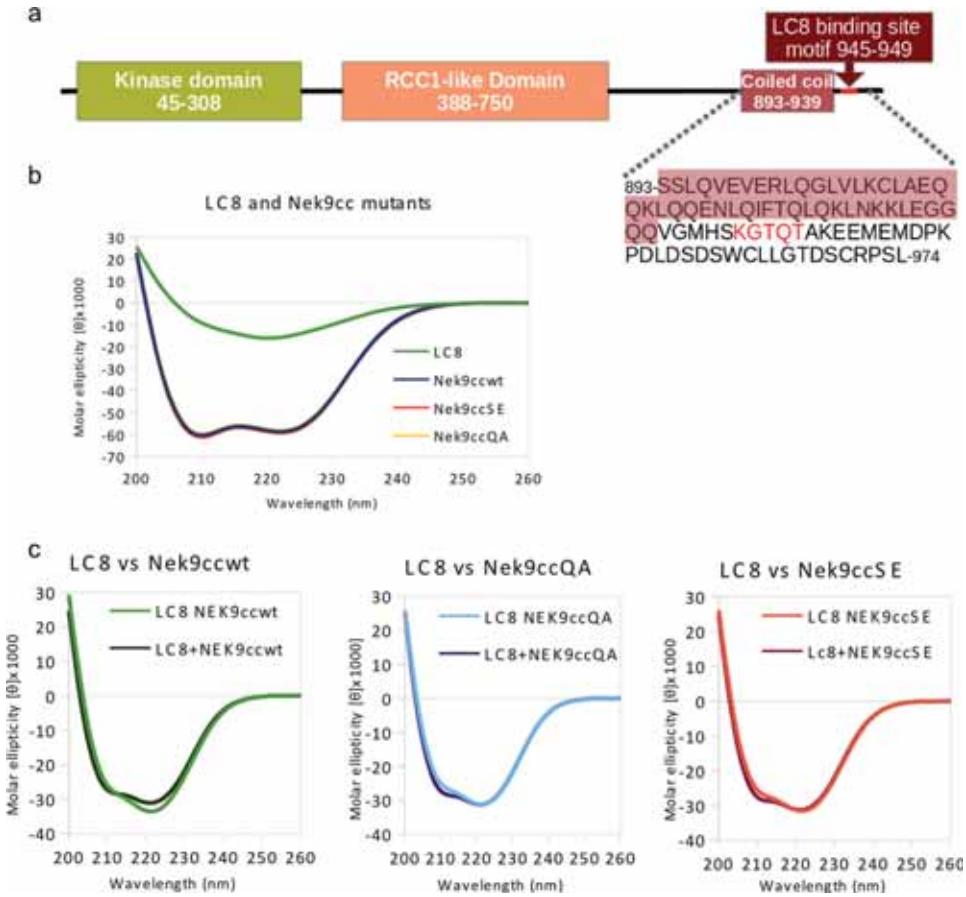


FIGURE 1. **Circular dichroism analysis of LC8 binding to the Nek9 C-terminal region.** *a*, schematic representation of the Nek9 protein. Amino acid sequence for the Nek9-CC construct is shown in one letter code. *b*, circular dichroism spectra of LC8 and Nek9-CC wild-type and single point mutants. *c*, circular dichroism spectra of the mixture of LC8 in complex with Nek9-CC and of the spectral sum of LC8 and Nek9-CC, for the Nek9-CC wild-type form and the Nek9-CC point mutants.

of residues (499 residues) are in preferred regions, 7.12% of residues (39) are in allowed regions, and 1.82% of residues (10) are in outlier regions. LC8 in complex with Nek9 peptide also contained six LC8 molecules assembled in three homodimers in the asymmetric unit, and the Ramachandran analysis shows 96.91% of residues (534 residues) are in preferred regions, 1.81% of residues (10) are in allowed regions, and 1.27% of residues (7) are in outlier regions. Refinement and data statistics are provided in Table 1. Structural representations were prepared with PyMOL (41).

*Accession Codes*—Coordinates and structure factors from the two structures were deposited in the Protein Data Bank with accession codes 3ZKE and 3ZKF.

## RESULTS

*Circular Dichroism Experiments on LC8 Binding to the Nek9 C-terminal Region*—Dimerization of Nek9 has been proposed to occur by means of the predicted C-terminal coiled-coil region (residues 891–939), which is located immediately upstream of the LC8 consensus binding region (residues 940–950). In addition to Nek9 dimerization through its C-terminal coiled-coil region, LC8 has been suggested to contribute to Nek9 oligomerization as it does for other proteins (12). To analyze *in vitro* the interaction between LC8 and Nek9, CD experiments were carried out with LC8 and a fragment of the C-terminal region of Nek9, which includes the consensus LC8 binding region and the predicted coiled-coil region (Nek9-CC, residues 893–939) (Fig. 1). The concentrations of LC8 and Nek9-CC used in the CD experiments were 10 $\mu$M and 6.7 $\mu$M, respectively. CD spectra of the individual proteins show an expected $\alpha$-$\beta$ profile for LC8, and interestingly, a rich $\alpha$-helix profile for the Nek9-CC fragment, which could be indicative of the presence of a coiled-coil structure. This is supported by the higher ordered multimeric structures that appear during the gel filtration purification of the recombinant Nek9-CC protein (12).

Remarkably, differences can be observed after comparison of the CD spectra of a mixture of the two proteins, LC8 and Nek9-CC, and the sum of their individual spectra (Fig. 1*C*). These changes in the ellipticity values between 200 and 240 nm suggest variations in the composition of secondary structure elements; in particular, the increase in ellipticity ~222 nm may indicate changes in the $\beta/\alpha$ structure. These results are in agreement with the previously reported binding between Nek9 and LC8 (12), and with crystal structures of LC8·peptide complexes, that indicated the formation of an extra $\beta$-strand (22).

To analyze the binding between LC8 and Nek9, we produced two Nek9-CC point mutant constructs. Nek9-CC Q948A can destabilize the binding by perturbing the highly conserved

Gln948 interaction with the LC8 dimer; and Nek9-CC S944E, a phosphomimetic that can destabilize the complex by mimicking phosphorylation on Ser$^{944}$, as it has been recently shown *in vivo* (12). Individual CD spectra of both Nek9-CC point mutants show similar profiles as the Nek9-CC wild-type form, probably indicating the formation of a coiled-coil structure (Fig. 1*B*). However, using the same protein concentrations as the wild-type form, the CD spectra of the mixture of LC8 with both Nek9-CC point mutants show differences in the CD profile compared with Nek9-CC wild-type, in particular in the region ~222 nm. This reduction in the ellipticity at 222 nm could indicate a decrease in the affinity of LC8 for both Nek9 mutant constructs under these experimental conditions. Thus, the destabilization of the binding with LC8 can occur either by the mutation on the conserved Gln$^{947}$ residue, which has already been established to play an important role in LC8 binding, or by a mutation on Ser$^{944}$, a site proposed to regulate LC8 binding to Nek9 upon phosphorylation.

*Crystal Structures of LC8 in Complex with Nek9 Peptide and Nek9 P-peptide*—To gain insight at the atomic level into the Nek9 binding to LC8, we synthesized two different peptides corresponding to the Nek9 binding consensus region, with one of them carrying a phosphoserine modification at position 5 corresponding to position Ser$^{944}$ in the Nek9 sequence, $^{940}$VGMHSKGTQTA$^{950}$. Both peptides displayed good solubility properties and could be dissolved in aqueous buffers at relatively high concentrations. LC8 was also produced at milligrams level amounts, as reported previously (12). Purification of recombinant LC8 by gel filtration chromatography indicated unequivocally the presence of a homodimer organization in the quaternary structure of the protein.

Crystals of LC8 with both Nek9 peptides were produced in a similar reservoir condition but with different crystallographic space groups. Orthogonal protein crystals of LC8 with the unmodified Nek9 peptide diffracted beyond 2.2 Å resolution, whereas hexagonal protein crystals of LC8 with Nek9 P-peptide (phosphopeptide) diffracted at 2.6 Å resolution (see Table 1 for details). In both crystal forms, the asymmetric unit contained three homodimers, with each LC8 molecule bound to a Nek9 peptide (a total number of 12 distinct molecules form the asymmetric unit). Both Nek9 peptides could be completely traced in the electron density maps in the three homodimers and only in some cases lacked the flexible terminal residue.

Both crystal forms display a similar LC8 homodimeric structure, which constitutes the biological unit and has been well established in the recent years by different structures, either in the apo form or in complex with peptides (13, 22–25). Basically, the LC8 structure is composed by two monomers with a characteristic fold formed by five five-stranded antiparallel β-sheets at the center of the homodimer, swapping four strands from one monomer with a fifth strand from the other monomer (Fig. 2*A*). Additionally, each LC8 monomer contains a pair of α-helices flanking the central β-sheet region at opposite faces of the homodimer. The peptide-binding region is located in identical opposite grooves at the two edges of the dimerization interface. As observed in other LC8 complex structures, the bound peptide interacts in an extended orientation and forms an extra β-strand with LC8, increasing the total number of strands of the central β-sheet. The parallel orientation of the two Nek9 peptides in the LC8 homodimer would be compatible with the presence of the coiled-coil structure immediately before the LC8 binding region (Fig. 2*A*).

**TABLE 1**
**Data collection and refinement statistics**
Statistic for highest resolution shell is shown in parentheses.

| | LC8·Nek9 peptide | LC8·Nek9 P-peptide |
|---|---|---|
| **Data collection** | | |
| Space group | $P2_12_12_1$ | $P6_3$ |
| *a*, *b*, *c* (Å) | 39.98, 105.12, 133.89 | 154.86, 154.86, 47.72 |
| α, β, γ | 90.00°, 90.00°, 90.00° | 90.00°, 90.00°, 120.00° |
| Resolution (Å) | 44.63–2.20 (2.32–2.20) | 47.73–2.50 (2.63–2.50) |
| Rmerge[a] | 0.080 (0.53) | 0.100 (0.95) |
| $I/\sigma I$ | 8.0 (2.7) | 7.6 (1.5) |
| Completeness (%) | 97.6 (95.4) | 99.2 (95.6) |
| Redundancy | 3.2 (3.1) | 3.4 (3.3) |
| **Refinement** | | |
| Resolution (Å) | 82–2.2 | 45–2.6 |
| No. of reflections | 27,276 | 19,327 |
| $R_{work}/R_{free}$[b] | 19.73/22.76 | 21.96/26.86 |
| No. of atoms | 4726 | 4671 |
| Protein | 4619 | 4650 |
| Water | 107 | 19 |
| r.m.s. bond lengths (Å)[c] | 0.02 | 0.01 |
| r.m.s. bond angles | 1.92° | 1.19° |

[a] $R_{merge} = \Sigma|I_i - \langle I\rangle|/\Sigma I_i$, where $I_i$ is the *i*th measurement of the intensity of an individual reflection or its symmetry-equivalent reflections and ⟨I⟩ is the average intensity of that reflection and its symmetry-equivalent reflections.
[b] $R_{work} = \Sigma||F_o| - |F_c||/\Sigma|F_o|$ for all reflections and $R_{free} = \Sigma||F_o| - |F_c||/\Sigma|F_o|$, calculated based on the 5% of data excluded from refinement.
[c] r.m.s., root mean square deviation.

As observed in previous LC8·peptide complexes, the Nek9 peptide and Nek9 P-peptide interact extensively with the central β-sheet of the LC8 homodimer (Figs. 2 and 3), establishing several backbone hydrogen bonds and side chain interactions with the β3 strand of one of the LC8 subunit. The only interaction of the peptide with the opposite subunit of the LC8 homodimer is mainly established by Gln$^{947}$ from the highly conserved K*X*TQT*X* motif, with its side chain buried in a hydrophobic pocket formed by Ile$^{34}$, Glu$^{35}$, and Lys$^{36}$ from the α2 helix.

Most of the interactions are basically conserved between in both complex structures, although two hydrogen bonds are disrupted in the Nek9 P-peptide structure. In particular, the backbone hydrogen bond of the carbonyl group of Gly$^{941}$ is not formed in some of P-peptide molecules found in the asymmetric unit. A second disrupted interaction is the hydrogen bond between Ser$^{944}$ and Thr$^{67}$ (at 2.69 Å in the case of the Nek9 peptide structure), which is in all cases disrupted by the presence of the phosphate group at Ser$^{944}$. The phosphate group of Ser$^{944}$ is located at the homodimer interface, in contact with the side chain of Tyr$^{65}$, from the β3 strand, and next to the side chains of Lys$^{43}$ and Lys$^{44}$ from the opposite LC8 subunit (Fig. 2).

Interestingly, structural superposition of the six different peptides found in the asymmetric unit show that the Nek9 P-peptides display a high degree of flexibility when compared with the unmodified Nek9 peptides, which displays an almost identical superposition of peptides (Fig. 3). This increase of flexibility displayed by the Nek9 P-peptide is more prominent at the N-terminal part of the P-peptide (from Val$^{940}$ to His$^{943}$), compared with the K*X*TQT*X* C-terminal part (from Lys$^{945}$ to Thr$^{949}$). These results suggest that phosphorylation on Ser$^{944}$,

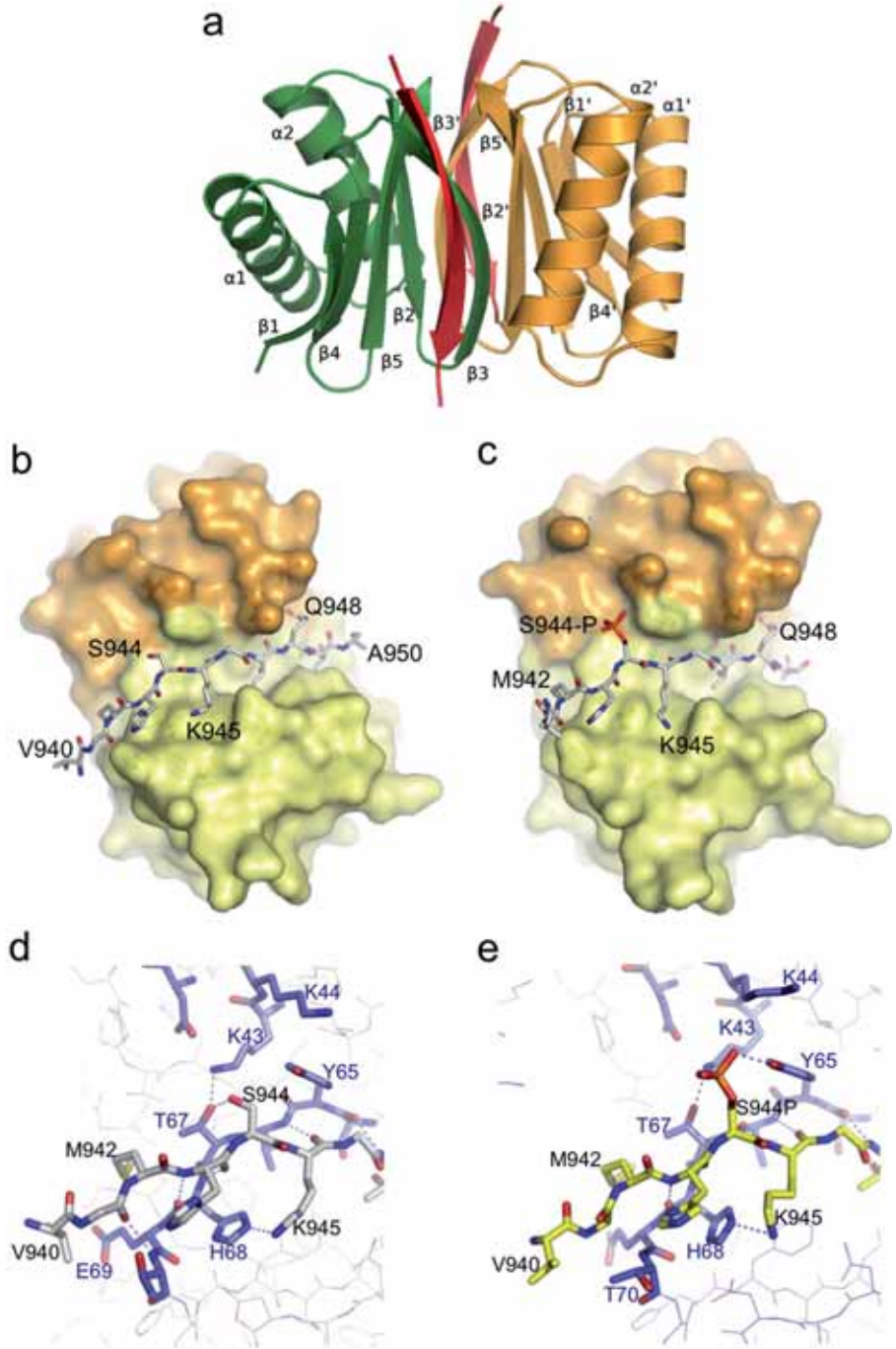


FIGURE 2. **Crystal structures of LC8 with Nek9 peptide and Nek9 P-peptide.** *a*, schematic representation of the LC8·Nek9 peptide structure. α-Helices and β-strands of each LC8 subunit are labeled. The two Nek9 peptides binding the homodimer are depicted in *red*. *b*, surface representation of the LC8 homodimer (*yellow* and *orange*) in complex with the Nek9 peptide, which is labeled and shown in stick representation. *c*, surface representation of the LC8 homodimer (*yellow* and *orange*) in complex with the Nek9 P-peptide, which is labeled and shown in stick representation. *d*, detailed stick representation of the interaction between the N-terminal regions of the Nek9 peptide (*gray*) with LC8 (*blue*). *e*, detailed stick representation of the interaction between the N-terminal region of the Nek9 P-peptide (*yellow*) with LC8 (*blue*). The figure was prepared with PyMOL (43).

which is located four positions N-terminal to the central $Gln^{948}$, affects the interaction of the Nek9 peptide to LC8 by producing a destabilization of the complex. Our detailed structural analysis supports the hypothesis that phosphorylation on $Ser^{944}$ can modulate and weaken the binding of LC8 to Nek9 in the cellular context, in which protein concentrations are much lower than in crystal structures and the phosphorylation outcome may be more evident.

Another remarkable difference found after comparison of both crystal structures is a shift produced in the LC8 homodimer structure upon binding to the Nek9 P-peptide, in particular in one of the LC8 monomers with respect to the other monomer (Fig. 3*C*). This shift might be attributed to the presence of a phosphate group at $Ser^{944}$, in which its negative charge might somehow interfere in the dimer interface. It is possible that the lysine residues from the opposite subunit next to the phosphate group are affected by the

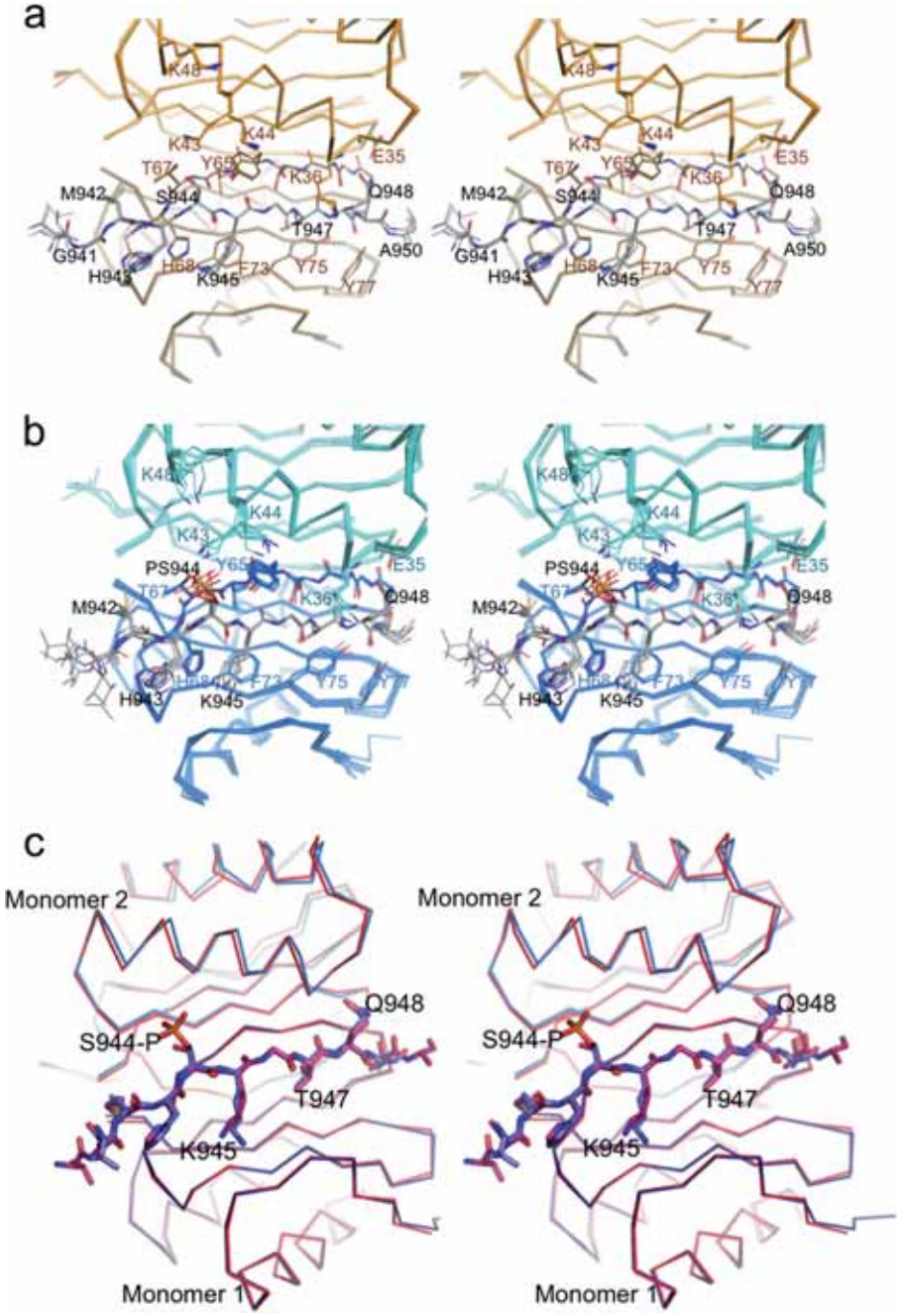


FIGURE 3. **Comparison of the interaction of LC8 with Nek9 peptide and Nek9 P-peptide.** *a*, stereo representation of the superposition of the six Nek9 peptides from the asymmetric unit. Nek9 peptide and interacting LC8 residues are labeled and shown in stick representation. *b*, stereo representation of the superposition of the six Nek9 P-peptides from the asymmetric unit. Nek9 P-peptide and interacting LC8 residues are labeled and shown in stick representation. *c*, stereo representation of the ribbon superposition of the LC8·Nek9 peptide and LC8·Nek9 P-peptide structures. Both Nek9 peptides are labeled and shown in stick representation. The two LC8 subunits of the homodimer are labeled monomers 1 and 2.

negative charge of the phosphate group. In contrast to the structural comparison between LC8· neuronal nitric oxid synthase and LC8·Swa complexes (42) and despite the aforementioned LC8 subunit shift, we have not observed an enlargement of the peptide-binding cleft in the Nek9 P-peptide complex. This movement in the homodimer quaternary structure upon $Ser^{944}$ phosphorylation could be significant to perturb the binding and stability of the Nek9 peptide to LC8.

*Circular Dichroism Experiments of the Binding of LC8 to Nek9 Peptides*—Because the binding partners increase the $\beta$-sheet signal by adding an extra strand to the central five-stranded $\beta$-sheet of LC8, CD represents an appropriate method to calculate the binding affinity in titration experiments. The CD spectrum of LC8 shows a characteristic curve for a $\alpha/\beta$-rich protein, displaying a maximal negative ellipticity value ~220 nm (Figs. 1*B* and 4). Using fixed LC8 concentrations, titration experiments were conducted by measuring the CD spectra of increasing concentrations of the unmodified Nek9 peptide (Fig. 4*A*). The observed augment of the ellipticity ~220 nm, which signals changes in the $\alpha/\beta$-secondary structure, might indicate an increase of $\beta$-structure produced by the binding of the Nek9 peptide. CD spectra comparisons indicate a major increase of

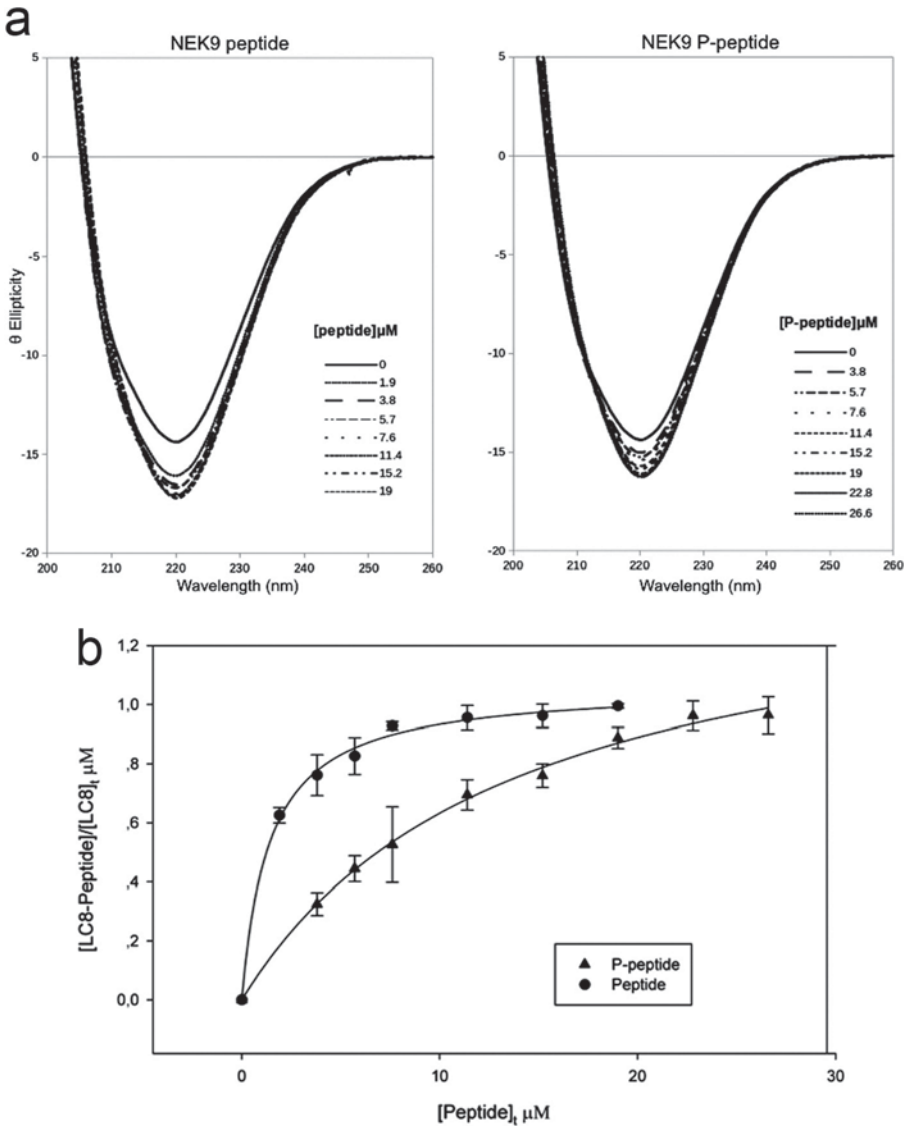


FIGURE 4. **Circular dichroism analysis of LC8 binding to Nek9 peptide and Nek9 P-peptide.** *a*, *right*: circular dichroism spectra of the titration of LC8 with an increasing concentration of the Nek9 peptide. *Left*: circular dichroism spectra of the titration of LC8 with an increasing concentration of the Nek9 P-peptide. *b*, plot of the variation of the ellipticity values from the CD spectra of *a* and *b* at 220 nm, which follows the change of β-secondary structure. *Circles*, Nek9 peptide; *squares*, Nek9 P-peptide.

the β-signal between 0 and 1.9 μM peptide concentration (Fig. 4*A*).

When identical CD titration experiments were carried out with the Nek9 P-peptide, a smaller increase in β-signal was observed, in contrast to the unmodified Nek9 peptide (Fig. 4*A*). The LC8 titration with the Nek9 P-peptide shows a smoother increase at 220 nm and, unlike the unmodified Nek9 peptide, the signal is not saturated ~1.9 μM. The β-signal of the Nek9 P-peptide spectra seems to increase more gradually, probably indicating a reduced binding affinity of the Nek9 peptide upon phosphorylation.

To calculate the different binding capabilities between the two peptides, the change in ellipticity at 220 nm has been represented as a function of the increase of peptide concentration (phospho- and unmodified Nek9 peptide) (Fig. 4*B*). The two curves were analyzed considering that the concentrations of protein and peptide are comparable (see "Experimental Procedures"), and the dissociation constant ($K_d$) for each peptide was determined. Using this approach, we have estimated $K_d$ values ~ 0.2 and 3.7 μM for the unmodified and the Nek9 P-peptide, respectively, thus confirming our hypothesis that the unmodified peptide binds tightly to LC8. These $K_d$ values are in the range of reported LC8-peptide interactions (13) and suggest that phosphorylation of the Nek9 peptide results in a 18-fold reduction of binding to LC8, thus supporting conclusions drawn from crystal structures.

*Thermal Denaturation of the LC8·peptide Complex*—Protein stability of the LC8·peptide and LC8·P-peptide complexes was analyzed by changes of the intrinsic fluorescence during thermal denaturation. Based on our CD experiments, fixed concentrations of Nek9 peptides (11 μM) were chosen to form a complex with LC8. At this concentration, CD analysis showed a partial binding of the Nek9 P-peptide to LC8 in comparison with the Nek9 peptide at 20 °C. The transition curves of the heat-induced fluorescence emission changes of LC8 complexes are shown in Fig. 5. These curves include LC8 alone,

and LC8·peptide and LC8·P-peptide complexes. Single cooperative transition curves were observed, and the data were fitted to a two-state temperature-induced protein-unfolding model (all curves with $R > 0.999$). As shown in Table 2, the transition temperatures of unfolding obtained for the three curves are quite similar ($T_m$ ~333 K), indicating minor changes produced in the context of a global denaturation. However, the different extracted thermodynamic enthalpies support the existence of significant differences for both Nek9 peptides (Table 2).

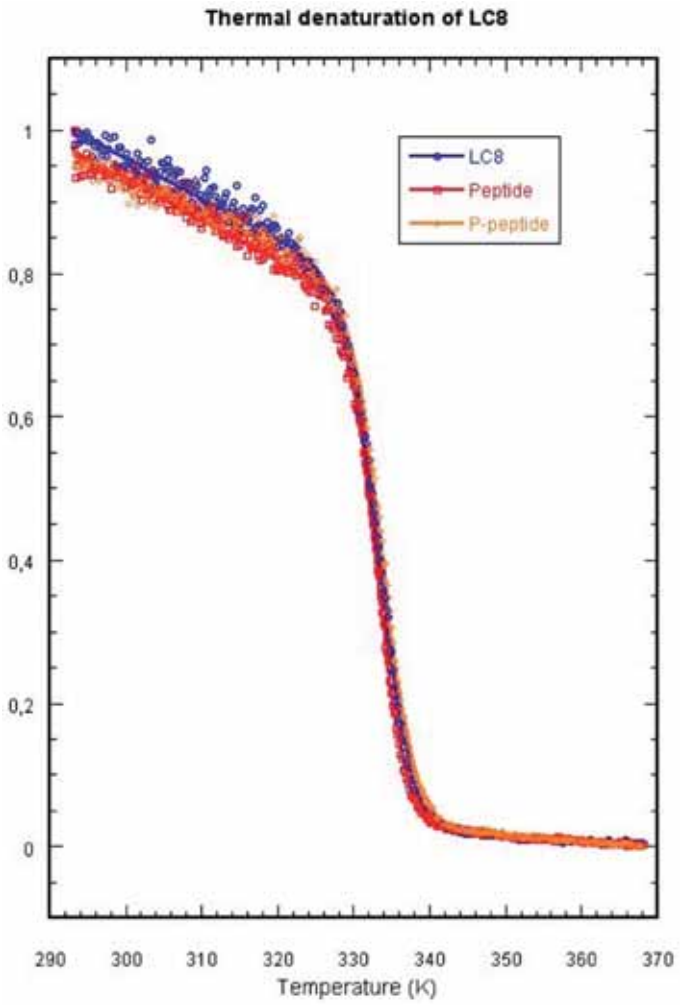


FIGURE 5. **Thermal unfolding of LC8 followed by intrinsic fluorescence.** *Blue circles* indicate the thermal unfolding kinetic of LC8 *Red squares* indicate the thermal unfolding kinetic of LC8 in the presence of 11 $\mu$M Nek9 peptide. *Orange diamonds* indicate the thermal unfolding kinetic of LC8 in the presence of 11 $\mu$M Nek9 P-peptide.

**TABLE 2**

**Parameters from the thermal unfolding of the LC8·Nek9 peptide complexes**

| | LC8 | LC8·Nek9 peptide | LC8·Nek9 P-peptide |
|---|---|---|---|
| $T_m$ (K) | 333.4 ± 0.1 | 333.1 ± 0.1 | 333.8 ± 0.1 |
| $\Delta H_m$ (kcal/mol) | 158 ± 2 | 174 ± 2 | 156 ± 2 |

In the case of LC8 alone and LC8·Nek9 P-peptide complex, the enthalpies for the thermal denaturation unfolding experiments are comparable, ~156.8 and 155.8 kcal/mol for each, respectively. However, these similar values are in contrast with the higher enthalpy value (~174.2 kcal/mol) shown for the LC8·Nek9 peptide complex. This higher enthalpy value could be an indication of a large number of disrupted bonds during the denaturation experiment, thus suggesting the formation of a tighter complex between LC8 and Nek9 peptide that would support our previous observations.

*Thermodynamic Profile of the LC8 Complex Formation*—Thermodynamic binding parameters for LC8 in complex with the two Nek9 peptides were determined by isothermal titration calorimetry. Experiments performed in two buffers with different ionization enthalpies indicated that the binding of the peptides is coupled to a minor proton uptake process. (The number of exchanged protons, $n_H$, is small and positive (Table 3).). Titration experiments of both Nek9 peptides on LC8 showed that the affinity of the Nek9 P-peptide for LC8 is reduced by ~6-fold in the dissociation constant ($K_d$ is 0.16 and 0.96 $\mu$M, for both Nek9 peptide and P-peptide, respectively) (Fig. 6). This decrease of the $K_d$ in the Nek9 P-peptide is due to a reduction of the enthalpy in the complex with LC8 (Table 3), probably by a reduced number of bonds formed between LC8 and Nek9 peptide.

Thus, the decrease of the affinity for LC8 for the Nek9 P-peptide is basically caused by less favorable enthalpic interactions ($\Delta\Delta H$ = 1.7 kcal/mol) combined by a partial compensation from more favorable entropic interactions ($-T\Delta\Delta S$ = −0.6 kcal/mol) (Table 3). These two factors produce a global reduction of the affinity, as observed in the difference of the binding Gibbs energy value ($\Delta\Delta G$ = 1.1 kcal/mol), producing the aforementioned 6-fold decrease of the dissociation constant. The estimated heat capacities ($\Delta C_P$) of the complex formation for both peptides are quite similar, −0.21 and −0.22 kcal/K·mol for the unmodified and the Nek9 P-peptide, respectively. These values are in good agreement with the binding heat capacities estimated from the change in solvent-accessible surface area (SASA), −0.27 and −0.26 kcal/K·mol for the unmodified and

**TABLE 3**

**Thermodynamic parameters for the binding of Nek9 peptides to LC8 (pH 7.5 and 25 °C)**

Relative errors were 10% for $K_a$ and $K_d$, 2% for $\Delta G$, 5% for $\Delta H$ and $-T\Delta S$, and 10% for $n_H$.

| | $K_a$ | $K_d$[a] | $\Delta G$[b] | $\Delta H$[c] | $-T\Delta S$[d] | $n_H$[c] |
|---|---|---|---|---|---|---|
| | $\times 10^6\ M^{-1}$ | $\mu M$ | *kcal/mol* | *kcal/mol* | *kcal/mol* | |
| Nek9 peptide | 6.2 | 0.16 | −9.3 | −11.2 | 1.9 | 0.16 |
| Nek9 P-peptide | 1.0 | 0.96 | −8.2 | −9.5 | 1.3 | 0.26 |

[a] $K_d = 1/K_a$.
[b] $\Delta G = -RT(\ln K_a)$.
[c] $\Delta H$ is the buffer-independent binding enthalpy, and $n_H$ is the net number of exchanged protons between the complex and the bulk solvent upon ligand binding. These two parameters are estimated by linear regression from the observed binding enthalpies, $\Delta H_{obs}$, in experiments performed using buffers with different ionization enthalpies, $\Delta H_{B(ion)}$, using this relationship: $\Delta H_{obs} = \Delta H + n_H \Delta H_{B(ion)}$.
[d] $-T\Delta S = \Delta G - \Delta H$.

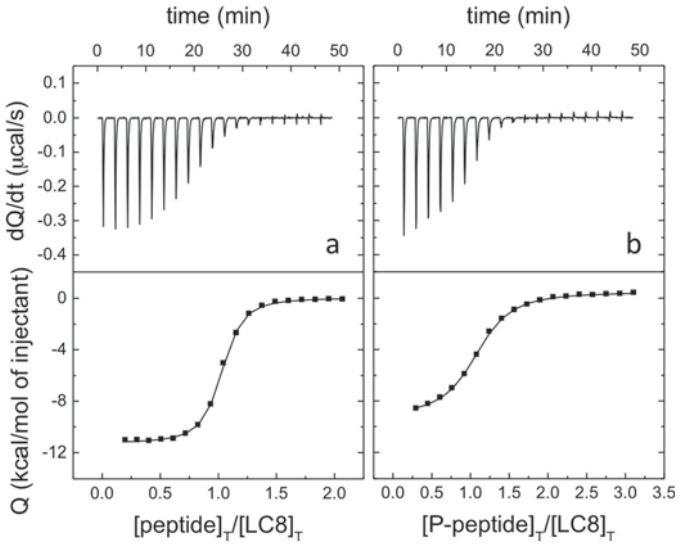


FIGURE 6. **Calorimetric titrations (isothermal titration calorimetry) for the LC8 binding to Nek9 peptides and Nek9 P-peptide.** Shown are calorimetric thermograms (*upper panels*, thermal power *versus* time) and binding isotherms (*lower panels*, normalized heat *versus* molar ratio) for the titration of LC8 10 $\mu$M with 200 $\mu$M Nek9 peptide (*a*) and 300 $\mu$M Nek9 P-peptide (*b*), in 100 mM NaCl, 10 mM sodium phosphate, 7.5 and 1 mM $\beta$-mercaptoethanol, at 25 °C.

the Nek9 P-peptide, respectively, employing a well known structural parameterization of the binding energetics in proteins ($\Delta C_P = 0.45 \times \Delta SASA_{nonpolar} - 0.26 \times \Delta SASA_{polar}$) (43) and the crystallographic structures of the complexes and apoLC8. These values indicate that there are not substantial conformational changes in LC8 upon binding of the peptides.

## DISCUSSION

Post-translational modification of proteins by phosphorylation is one the most, if not the most, important manner of regulating protein-protein interactions and many signaling pathways inside of the cell (44). DYNLL/LC8 has been recently postulated to be a dimerization hub that can control the function of other proteins by regulating their oligomerization state, normally by inducing higher oligomerization states (13, 21). This might be the case for the protein kinase Nek9, which is involved in the control of early events of mitosis, and it has been shown to interact with LC8 through a canonical consensus region located in a partially disordered region of the C-terminal tail. In addition, LC8 negatively controls the binding of Nek9 to the related kinases Nek6/7 and thus their activation (12), suggesting that LC8 binding may have additional functions in the context of specific complexes besides regulating oligomerization. Thus, the regulation of LC8 binding might represent an important event to control the function of the target protein, in this case Nek9 and the formation of the mitotic spindle. In a recent work, we showed that Nek9 autophosphorylation on $Ser^{944}$ may impair the interaction with LC8 *in vivo*, thus supporting the view that phosphorylation of LC8 binding partners can have a major effect in regulating the LC8 interaction (12). A similar LC8-mediated regulation was described for the proapoptotic Bim, which is sequestered to the LC8·dynein motor complexes but can be released upon phosphorylation by JNK kinase on the LC8 binding consensus motif. In this case, phosphorylation occurs on threonines adjacent to the central glutamine residue of the LC8 binding motif (45).

Examples describing the interaction of different partners to LC8 such as Dynein intermediate chain and Swallow (46, 47), indicate that LC8 seems to facilitate the folding and increase the $\alpha$-helical content by stabilization of coiled-coil structures in those proteins. This "chaperone-like activity" of LC8 normally occurs in proteins with coiled-coil regions next to the LC8 binding consensus motif; those regions are normally intrinsically or partially disordered. In those examples, binding of LC8 can thus facilitate the formation of coiled-coil structures and thus dimerization of protein targets. In the case of dynein, in which LC8 was first described to act as a cargo adapter, this chaperone-like activity effect of LC8, which indirectly affects the cargo binding, has also been described (46, 48). In this case, the dynein intermediate chain is partially disordered and gains structure upon binding to LC8. In Nek9, our CD experiments show a high content of $\alpha$-helical structure at the C-terminal region (Nek9-CC constructs, Fig. 1), probably indicating the presence of the predicted coiled-coil structure (1). In our LC8/Nek9-CC binding experiments with two point mutants for the LC8 consensus-binding motif, we observed different CD spectra when compared with the wild-type Nek9-CC construct. It might be that LC8 binding to Nek9 produces changes in the stability of the predicted Nek9 coiled-coil, thus affecting the Nek9 oligomerization state, as suggested in previous experiments (12).

We have analyzed the LC8-Nek9 interaction by using different biophysical methods. CD is an optimal approach to determinate directly the interaction of the peptide to LC8 by the measurement of changes in the $\beta$-signal, which is the type of secondary structure formed upon binding of the peptide (22). The ~18-fold reduction in the $K_d$ extracted from the CD experiments with the Nek9 P-peptide is a direct indication of the perturbation of the interaction produced by the presence of the phosphate group. In the thermal denaturation unfolding of LC8 complexes, chased by intrinsic fluorescence, the major enthalpy of the complex between LC8 and the unmodified Nek9 peptide indicates a major energy released for the disruption of the complex in comparison with the Nek9 P-peptide. Finally, the thermodynamic values extracted from isothermal titration calorimetry experiments also show a 6-fold decrease of the dissociation constant ($K_d$) for the Nek9 P-peptide, due basically to less favorable enthalpic interactions, probably indicating a reduction in the number of bonds formed in the complex. All three methods point to a direct perturbation of the complex between LC8 and Nek9 upon phosphorylation on $Ser^{944}$.

The crystal structures of LC8 with both Nek9 peptides shed light to the binding differences observed in the biophysical experiments. The interaction of both Nek9 peptides to LC8 is carried out by a similar $\beta$-like antiparallel strand, which starts seven N-terminal positions to $Gln^{948}$, namely from $Gly^{941}$ to $Thr^{949}$, forming a total number of eight backbone $\beta$-sheet hydrogen bonds between the Nek9 peptide and $\beta$3 strand of LC8 (see Fig. 2). However, comparisons between the six LC8 monomers in the asymmetric unit indicate that the phosphate negative charge on $Ser^{944}$ perturbs the interaction with LC8, displaying a high degree of flexibility that affects mainly the

binding of the first half of the peptide, from positions −7 to −4 ($Gly^{941}$ to $Ser^{944}$). The position of $Ser^{944}$ in the LC8 binding motif of Nek9 is located four positions N-terminal to the central $Gln^{948}$ and varies from Asp, Ser, Asn and Thr in the consensus sequence analysis for LC8 binding partners (13). Interestingly, some of them are either residues susceptible of being phosphorylated or residues with an inherent negative charge.

Despite the lower affinity for the Nek9 P-peptide and the important binding differences described *in vivo* (12), the high protein concentration in crystals favors the formation of fairly similar LC8·Nek9 complex structures. However, such high concentration of proteins are difficult to occur in the cellular context, and the reported $K_d$ values strongly suggest that the differences between the unmodified and the Nek9 P-peptide are sufficient to perturb binding *in vivo*. The slight shift observed in the LC8 homodimer interface, the two disrupted hydrogen bonds in the Nek9 P-peptide complex and the higher flexibility of the Nek9 P-peptides produces a binding reduction on LC8 upon $Ser^{944}$ phosphorylation.

We thus provide for the first time *in vitro* experimental data directly indicating that phosphorylation can regulate the binding of LC8 to a particular protein partner, in this instance, Nek9. Regulation of protein-protein interaction by phosphorylation is one of the most common ways to regulate many cellular signaling pathways. In the case of the mitotic Nek9/Nek6/Nek7 signaling module, LC8 seems to interfere in this pathway by a direct binding competition with the downstream kinases Nek6 and Nek7, regulation that can be reversed by direct phosphorylation on the interface between the two proteins. The fact that LC8 has multiple binding partners, that it is ubiquitously present, and that many of its protein partners contain Ser/Thr residues in the consensus binding motif, suggest that phosphorylation on this motif might be a general mechanism of controlling LC8 interaction in different cellular contexts.

*Acknowledgments—We acknowledge Salvador Ventura for suggestions and stimulating discussions. We acknowledge Jordi Benach and Jordi Juanhuix from the XALOC beamline (BL13) at the ALBA synchrotron for help in data collection.*

## REFERENCES


1. Roig, J., Mikhailov, A., Belham, C., and Avruch, J. (2002) Nercc1, a mammalian NIMA-family kinase, binds the Ran GTPase and regulates mitotic progression. *Genes Dev.* **16,** 1640–1658
2. O'Connell, M. J., Krien, M. J., and Hunter, T. (2003) Never say never. The NIMA-related protein kinases in mitotic control. *Trends Cell Biol.* **13,** 221–228
3. Quarmby, L. M., and Mahjoub, M. R. (2005) Caught Nek-ing: cilia and centrioles. *J. Cell Sci.* **118,** 5161–5169
4. O'regan, L., Blot, J., and Fry, A. M. (2007) Mitotic regulation by NIMA-related kinases. *Cell Div.* **2,** 25
5. Roig, J., Groen, A., Caldwell, J., and Avruch, J. (2005) Active Nercc1 protein kinase concentrates at centrosomes early in mitosis and is necessary for proper spindle assembly. *Mol. Biol. Cell* **16,** 4827–4840
6. Bertran, M. T., Sdelci, S., Regué, L., Avruch, J., Caelles, C., and Roig, J. (2011) Nek9 is a Plk1-activated kinase that controls early centrosome separation through Nek6/7 and Eg5. *EMBO J.* **30,** 2634–2647
7. Rapley, J., Nicolàs, M., Groen, A., Regué, L., Bertran, M. T., Caelles, C., Avruch, J., and Roig, J. (2008) The NIMA-family kinase Nek6 phosphorylates the kinesin Eg5 at a novel site necessary for mitotic spindle formation. *J. Cell Sci.* **121,** 3912–3921
8. Belham, C., Roig, J., Caldwell, J. A., Aoyama, Y., Kemp, B. E., Comb, M., and Avruch, J. (2003) A mitotic cascade of NIMA family kinases. Nercc1/Nek9 activates the Nek6 and Nek7 kinases. *J. Biol. Chem.* **278,** 34897–34909
9. Sdelci, S., Bertran, M. T., and Roig J. (2011) Nek9, Nek6 and Nek7 and the separation of centrosomes. *Cell Cycle* **10,** 3816–3817
10. Yissachar, N., Salem, H., Tennenbaum, T., and Motro, B. (2006) Nek7 kinase is enriched at the centrosome, and is required for proper spindle assembly and mitotic progression. *FEBS Lett.* **580,** 6489–6495
11. Sdelci, S., Schütz, M., Pinyol, R., Bertran, M. T., Regué, L., Caelles, C., Vernos, I., and Roig, J. (2012) Nek9 phosphorylation of NEDD1/GCP-WD contributes to Plk1 control of gamma-tubulin recruitment to the mitotic centrosome. *Curr. Biol.* **22,** 1516–1523
12. Regué, L., Sdelci, S., Bertran, M. T., Caelles, C., Reverter, D., and Roig, J. (2011) DYNLL/LC8 protein controls signal transduction through the Nek9/Nek6 signaling module by regulating Nek6 binding to Nek9. *J. Biol. Chem.* **286,** 18118–18129
13. Rapali, P., Szenes, Á., Radnai, L., Bakos, A., Pál, G., and Nyitray, L. (2011) DYNLL/LC8: a light chain subunit of the dynein motor complex and beyond. *FEBS J.* **278,** 2980–2996
14. King, S. M., and Patel-King, R. S. (1995) The M(r) = 8,000 and 11,000 outer arm dynein light chains from *Chlamydomonas flagella* have cytoplasmic homologues. *J. Biol. Chem.* **270,** 11445–11452
15. King, S. M., Barbarese, E., Dillman, J. F., 3rd, Benashski, S. E., Do, K. T., Patel-King, R. S., and Pfister, K. K. (1998) Cytoplasmic dynein contains a family of differentially expressed light chains. *Biochemistry* **37,** 15033–15041
16. Benashski, S. E., Harrison, A., Patel-King, R. S., and King, S. M. (1997) Dimerization of the highly conserved light chain shared by dynein and myosin V. *J. Biol. Chem.* **272,** 20929–20935
17. Kaiser, F. J., Tavassoli, K., Van den Bemd, G. J., Chang, G. T., Horsthemke, B., Möröy, T., and Lüdecke, H. J. (2003) Nuclear interaction of the dynein light chain LC8a with the TRPS1 transcription factor suppresses the transcriptional repression activity of TRPS1. *Hum. Mol. Genet.* **12,** 1349–1358
18. Puthalakath, H., Huang, D. C., O'Reilly, L. A., King, S. M., and Strasser, A. (1999) The proapoptotic activity of the Bcl-2 family member Bim is regulated by interaction with the dynein motor complex. *Mol. Cell* **3,** 287–296
19. Jaffrey, S. R., and Snyder, S. H. (1996) PIN: an associated protein inhibitor of neuronal nitric oxide synthase. *Science* **274,** 774–777
20. Schnorrer, F., Bohmann, K., and Nüsslein-Volhard, C. (2000) The molecular motor dynein is involved in targeting swallow and bicoid RNA to the anterior pole of *Drosophila* oocytes. *Nat. Cell Biol.* **2,** 185–190
21. Barbar, E. (2008) Dynein light chain LC8 is a dimerization hub essential in diverse protein networks. *Biochemistry* **47,** 503–508
22. Liang, J., Jaffrey, S. R., Guo, W., Snyder, S. H., and Clardy, J. (1999) Structure of the PIN/LC8 dimer with a bound peptide. *Nat. Struct. Biol.* **6,** 735–740
23. Fan, J., Zhang, Q., Tochio, H., Li, M., and Zhang, M. (2001) Structural basis of diverse sequence-dependent target recognition by the 8 kDa dynein light chain. *J. Mol. Biol.* **306,** 97–108
24. Benison, G., Karplus, P. A., and Barbar, E. (2008) The interplay of ligand binding and quaternary structure in the diverse interactions of dynein light chain LC8. *J. Mol. Biol.* **384,** 954–966
25. Lightcap, C. M., Sun, S., Lear, J. D., Rodeck, U., Polenova, T., and Williams, J. C. (2008) Biochemical and structural characterization of the Pak1-LC8 interaction. *J. Biol. Chem.* **283,** 27314–27324
26. Wang, W., Lo, K. W., Kan, H. M., Fan, J. S., and Zhang, M. (2003) Structure of the monomeric 8-kDa dynein light chain and mechanism of the domain-swapped dimer assembly. *J. Biol. Chem.* **278,** 41491–41499
27. Makokha, M., Huang, Y. J., Montelione, G., Edison, A. S., and Barbar, E. (2004) The solution structure of the pH-induced monomer of dynein light-chain LC8 from *Drosophila*. *Protein Sci.* **13,** 727–734
28. Mohan, P. M., Barve, M., Chatterjee, A., and Hosur, R. V. (2006) pH driven conformational dynamics and dimer-to-monomer transition in DLC8. *Protein Sci.* **15,** 335–342
29. Song, Y., Benison, G., Nyarko, A., Hays, T. S., and Barbar, E. (2007) Potential role for phosphorylation in differential regulation of the assembly of

dynein light chains. *J. Biol. Chem.* **282,** 17272–17279
30. Jung, Y., Kim, H., Min, S. H., Rhee, S. G., and Jeong, W. (2008) Dynein light chain LC8 negatively regulates NF-κB through the redox-dependent interaction with IκBα. *J. Biol. Chem.* **283,** 23863–23871
31. Song, C., Wen, W., Rayala, S. K., Chen, M., Ma, J., Zhang, M., and Kumar, R. (2008) Serine 88 phosphorylation of the 8-kDa dynein light chain 1 is a molecular switch for its dimerization status and functions. *J. Biol. Chem.* **283,** 4004–4013
32. Lo, K. W., Naisbitt, S., Fan, J. S., Sheng, M., and Zhang, M. (2001) The 8-kDa dynein light chain binds to its targets via a conserved (K/R)*X*TQT motif. *J. Biol. Chem.* **276,** 14059–14066
33. Rodríguez-Crespo, I., Yélamos, B., Roncal, F., Albar, J. P., Ortiz de Montellano, P. R., and Gavilanes, F. (2001) Identification of novel cellular proteins that bind to the LC8 dynein light chain using a pepscan technique. *FEBS Lett.* **503,** 135–141
34. Radnai, L., Rapali, P., Hódi, Z., Süveges, D., Molnár, T., Kiss, B., Bécsi, B., Erdödi, F., Buday, L., Kardos, J., Kovács, M., and Nyitray, L. (2010) Affinity, avidity, and kinetics of target sequence binding to LC8 dynein light chain isoforms. *J. Biol. Chem.* **285,** 38649–38657
35. Gómez, J., and Freire, E. (1995) Thermodynamic mapping of the inhibitor site of the aspartic protease endothiapepsin. *J. Mol. Biol.* **252,** 337–350
36. Velazquez-Campoy, A., Luque, I., Todd, M. J., Milutinovich, M., Kiso, Y., and Freire, E. (2000) Thermodynamic dissection of the binding energetics of KNI-272, a potent HIV-1 protease inhibitor. *Protein Sci.* **9,** 1801–1809
37. Kabsch, W. (2010) XDS. *Acta Crystallogr. D Biol. Crystallogr.* **66,** 125–132
38. Winn, M. D., Ballard, C. C., Cowtan, K. D., Dodson, E. J., Emsley, P., Evans, P. R., Keegan, R. M., Krissinel, E. B., Leslie, A. G., McCoy, A., McNicholas, S. J., Murshudov, G. N., Pannu, N. S., Potterton, E. A., Powell, H. R., Read, R. J., Vagin, A., and Wilson, K. S. (2011) Overview of the CCP4 suite and current developments. *Acta Crystallogr. D Biol. Crystallogr.* **67,** 235–242
39. Emsley, P., Lohkamp, B., Scott, W. G., and Cowtan, K. (2010) Features and development of Coot. *Acta Crystallogr. D Biol. Crystallogr.* **66,** 486–501
40. Adams, P. D., Afonine, P. V., Bunkóczi, G., Chen, V. B., Davis, I. W., Echols, N., Headd, J. J., Hung, L. W., Kapral, G. J., Grosse-Kunstleve, R. W., McCoy, A. J., Moriarty, N. W., Oeffner, R., Read, R. J., Richardson, D. C., Richardson, J. S., Terwilliger, T. C., and Zwart, P. H. (2010) PHENIX: a comprehensive Python-based system for macromolecular structure solution. *Acta Crystallogr. D Biol. Crystallogr.* **66,** 213–221
41. DeLano, W. L. (2010) *The PyMOL Molecular Graphics System*, version 1.3, Schrödinger, LLC, New York
42. Benison, G., Karplus, P. A., and Barbar, E. (2007) Structure and dynamics of LC8 complexes with K*X*TQT-motif peptides: swallow and dynein intermediate chain compete for a common site. *J. Mol. Biol.* **371,** 457–468
43. Murphy, K. P., and Freire, E. (1992) Thermodynamics of structural stability and cooperative folding behavior in proteins. *Adv. Protein Chem.* **43,** 313–361
44. Manning, G., Whyte, D. B., Martinez, R., Hunter, T., and Sudarsanam, S. (2002) The protein kinase complement of the human genome. *Science* **298,** 1912–1934
45. Lei, K., and Davis, R. J. (2003) JNK phosphorylation of Bim-related members of the Bcl2 family induces Bax-dependent apoptosis. *Proc. Natl. Acad. Sci. U.S.A.* **100,** 2432–2437
46. Wang, L., Hare, M., Hays, T. S., and Barbar, E. (2004) Dynein light chain LC8 promotes assembly of the coiled-coil domain of swallow protein. *Biochemistry* **43,** 4611–4620
47. Nyarko, A., Hare, M., Hays, T. S., and Barbar, E. (2004) The intermediate chain of cytoplasmic dynein is partially disordered and gains structure upon binding to light-chain LC8. *Biochemistry* **43,** 15595–15603
48. Benison, G., Nyarko, A., and Barbar, E. (2006) Heteronuclear NMR identifies a nascent helix in intrinsically disordered dynein intermediate chain: implications for folding and dimerization. *J. Mol. Biol.* **362,** 1082–1093

## 3.2 Publication II:

**Structural characterization of the enzymes composing the arginine deiminase pathway in *Mycoplasma penetrans*.**

Gallego P, Planell R, Benach J, Querol E, Perez-Pons JA, Reverter D.

PLoS One. 2012;7.

OPEN ACCESS Freely available online

PLOS ONE

# Structural Characterization of the Enzymes Composing the Arginine Deiminase Pathway in *Mycoplasma penetrans*

**Pablo Gallego[1], Raquel Planell[1], Jordi Benach[2], Enrique Querol[1], Josep A. Perez-Pons[1], David Reverter[1]***

**1** Institut de Biotecnologia i de Biomedicina and Departament de Bioquímica i de Biologia Molecular, Universitat Autònoma de Barcelona, Barcelona, Spain, **2** Experiments Division, ALBA Synchrotron Light Source, Barcelona, Spain

## Abstract

The metabolism of arginine towards ATP synthesis has been considered a major source of energy for microorganisms such as *Mycoplasma penetrans* in anaerobic conditions. Additionally, this pathway has also been implicated in pathogenic and virulence mechanism of certain microorganisms, i.e. protection from acidic stress during infection. In this work we present the crystal structures of the three enzymes composing the gene cluster of the arginine deiminase pathway from *M. penetrans*: arginine deiminase (ADI), ornithine carbamoyltransferase (OTC) and carbamate kinase (CK). The arginine deiminase (ADI) structure has been refined to 2.3 Å resolution in its apo-form, displaying an ''open'' conformation of the active site of the enzyme in comparison to previous complex structures with substrate intermediates. The active site pocket of ADI is empty, with some of the catalytic and binding residues far from their active positions, suggesting major conformational changes upon substrate binding. Ornithine carbamoyltransferase (OTC) has been refined in two crystal forms at 2.5 Å and 2.6 Å resolution, respectively, both displaying an identical dodecameric structure with a 23-point symmetry. The dodecameric structure of OTC represents the highest level of organization in this protein family and in *M.penetrans* it is constituted by a novel interface between the four catalytic homotrimers. Carbamate kinase (CK) has been refined to 2.5 Å resolution and its structure is characterized by the presence of two ion sulfates in the active site, one in the carbamoyl phosphate binding site and the other in the β-phosphate ADP binding pocket of the enzyme. The CK structure also shows variations in some of the elements that regulate the catalytic activity of the enzyme. The relatively low number of metabolic pathways and the relevance in human pathogenesis of *Mycoplasma penetrans* places the arginine deiminase pathway enzymes as potential targets to design specific inhibitors against this human parasite.

**Citation:** Gallego P, Planell R, Benach J, Querol E, Perez-Pons JA, et al. (2012) Structural Characterization of the Enzymes Composing the Arginine Deiminase Pathway in *Mycoplasma penetrans*. PLoS ONE 7(10): e47886. doi:10.1371/journal.pone.0047886

**Editor:** Annalisa Pastore, National Institute for Medical Research, Medical Research Council London, United Kingdom

**Received** August 2, 2012; **Accepted** September 24, 2012; **Published** October 17, 2012



**Funding:** This work was supported by grants from the ''Ministerio de Ciencia e Innovacion'' of Spain, BFU2008-0364 to DR. and BIO2007-67904-C02-01, BFU2010-22209-C02-01 to EQ, and from the European Community MIRG-CT-2007-200346 to DR. The funders had no role in study design, data collection and analysis, decision to publish, or preparation of the manuscript.

**Competing Interests:** The authors have declared that no competing interests exist.

* E-mail: david.reverter@uab.cat

## Introduction

Mycoplasmas belong to the class *Mollicutes*, a widely distributed group of microorganisms evolved from Gram-positive bacteria by a reduction in their genomes. The loss of genetic information related to metabolic activities and biosynthetic capabilities for essential compounds has emphasized the parasitic mode (of life) of all known *Mycoplasma* species, with each specie usually showing a strict host and tissue specificity [1]. *Mycoplasma penetrans* is a human parasite which persistently colonizes the respiratory and urogenital tracts invading and surviving within infected cells [2]. Lacking a complete tricarboxylic acid cycle and cytochromes, most mollicutes obtain ATP mainly through glycolysis and fermentative metabolism of carbohydrates. However, some *Mycoplasma* species are nonglycolytic or nonfermentative, and for them arginine catabolism has been considered, though not conclusively established, as the major source of energy [3]. In these cases, arginine degradation is done by means of the arginine deiminase (ADI) pathway, an anaerobic route found in Bacteria [4], Archaea [5], and amitochondrial Eukarya [6–8]. In mycoplasmas, the ADI pathway varies at the genomic level, ranging from the complete absence of all the genes in some species, to their presence, even though not necessarily functional, in others [9]. In this regard, *M. penetrans* possesses and expresses the complete set of the ADI pathway genes at the same time while exhibiting a fermentative metabolism.

The ADI pathway is composed by three catalytic enzymes: arginine deiminase (ADI, EC 3.5.3.6), ornithine carbamoyltransferase (OTC, EC 2.1.3.3) and carbamate kinase (CK, EC 2.7.2.2). This pathway performs the conversion of arginine to ornithine, ammonia, $CO_2$ and ATP, yielding one mole of ATP per mole of arginine. ADI catalyzes the first step of the argininine degradation pathway, the deimination of arginine, producing citrulline and ammonium. Subsequently, OTC processes citrulline and uptakes inorganic phosphate to generate ornithine and carbamoyl phosphate. OTC enzymes can also be anabolic and catalyze the reverse reaction. The anabolic OTC can synthesize citrulline to be utilized in the arginine biosynthetic pathway or in the urea cycle. In this sense, some organisms, such as *Pseudomonas aeruginosa*, encode different OTCs genes dedicated to either the ADI pathway

or to the arginine biosynthetic pathways [4,10,11]. In the last step of the ADI pathway, CK catalyzes the hydrolysis of the carbamoyl phosphate to $CO_2$ and ammonia, while the phosphate group is used to phophorylate ADP to generate ATP. Similarly to OTCs, in some organisms such as *Pyrococcus furiosus,* CK can catalyze the opposite reaction synthesizing carbamoyl phosphate from carbamate and ATP [12].

The absence of the arginine deiminase gene (ADI) in the human genome, and the presence and importance of it in pathogenic protozoa like *Giarda intestinalis* [13,14] and pathogenic bacteria like *Pseudomonas aeruginosa* [15–17] (primarily infecting immuno-compromised patients [18]), make the ADI enzyme an attractive therapeutic target for some parasitic and bacterial infections. Additionally, ADI might represent a potential tumor growth inhibitor [19–22]. ADI structures and reaction mechanisms have been described in detail in *Pseudomonas aeruginosa* [23,24] and *Mycoplasma arginini* [25]. In the present work we have resolved the structure of ADI from *Mycoplasma penetrans* at 2.3 Å, and comparison to previous substrate-bound structures of ADI from *M.arginini* reveals substantial structural rearrangements in the active site of the enzyme upon binding of the substrate.

As previously mentioned, OTC (ornithine carbamoyltransferase) can be both anabolic or catabolic in some microorganisms [10,26], possessing different genes for both catabolic and anabolic reactions, such as in *P. aeruginosa*. The anabolic reaction is related to the arginine biosynthesis in plants and to the urea cycle in the mitochondria in mammals [27,28]. OTC is closely related to the aspartate transcarbamoylase (ATCase, EC 2.1.3.2) [29], a well-known example of an allosteric enzyme in the biosynthesis of pyrimidine. All transcarbamylases or carbamoyltransferases share the same basic overall protein fold which contains two domains: a CP-binding domain (carbamoyl phosphate binding domain) and an amino acid binding domain. The basic quaternary structure organization is a homotrimer, with the active site located at the interface between monomers [30,31]. OTC proteins have a wide average range of quaternary structures, the most basic form being a homotrimer [32]. However, in some cases, such as *Lactobacillus hilgardii*, the quaternary assembly is an homohexamer, containing two homotrimers [33]. Additionally, a dodecameric assembly containing four homotrimers has been observed in the catabolic OTC of *P.aeruginosa* [31] and in the hyperthermophilic *Pyrococcus furiosus* [34]. Dodecameric assemblies of OTCs have been suggested to be involved in thermophilic resistance or in allosteric enzyme regulation by cooperativity [31,35,35]. The two crystal structures of OTC from *Mycoplasma penetrans* described in this work possess a quaternary dodecameric assembly, which, despite a similar organization, is unique to *Mycoplasma penetrans* at the interface between the catalytic homotrimers and contain particular interactions.

Carbamate kinase (CK) generates ATP from carbamoyl phosphate and ADP, and this constitutes the last step in the fermentative catabolism of arginine, agmatine and allantoin/oxalurate [4,36–40]. The absence of this protein in animals and its importance in generating energy in some pathogenic microorganisms like *Giardia intestinalis* or *Trichomonas vaginalis* makes CK an attractive therapeutic target [7,41]. Structures of CK bound to ADP and to sulfate ions have already been described in two different organisms, *Enterococcus faecalis* and *Pyrococcus furiosus* [42–44], and in both cases there was a substantial structural rearrangement upon binding of substrates. The structure here of CK from *M.penetrans* differs from the previous structures by the presence of two sulfate ions, one in the carbamoyl phosphate pocket and another in the β-phosphate ADP binding pocket. Particularly interesting in the *M.penetrans* CK structure described here, is the "open" and non-catalytic conformation of the PSD subdomain, despite the presence of a sulfate ion in the carbamoyl phosphate-binding pocket.

## Results

### Protein expression and purification

The expression of arginine deiminase (ADI) from the pET-19b recombinant plasmid as described in Methods produced mostly insoluble protein. Transcription analysis of the *M. penetrans arc* operon, performed by primer extension, indicates the existence of two transcription start sites (unpublished results), giving rise upon translation, to the above described long-ADI and to a short-ADI form initiating at Met43 and ending at Lys452. Remarkably, pairwise and clustal alignments between ADI sequences from different *Mycoplasma* species and from *M. penetrans* start around Met43 residue of the short ADI-form, leaving N-terminal extensions (i.e., residues 1–42) without alignment in relation to the homologous sequences. To check if the recombinant expression of short-ADI would overcome the solubility problems encountered with long-ADI, the corresponding coding sequence was amplified from plasmid pBE-arcA by using adi-7 and adi-6 as forward and reverse primers, respectively (see Table S1). The 5′-end of adi-7 primer also bears an NdeI restriction site, allowing the cloning of the amplified short-ADI coding sequence into the pET-19b expression vector, as described for the long-ADI form. The same protein purification protocol described in Methods was applied to the short-ADI form. The recombinant production of short-ADI substantially improved from the production of the full length or long-ADI form in terms of both expression yields and solubility. Gel filtration of short-ADI, as expressed in *E.coli,* indicated the formation of a dimer, probably representing the biological unit of the protein. The final protein yield was 4 mg of recombinant ADI per liter of culture.

Recombinant production of full-length *M. penetrans* OTC in *E.coli* yielded a high level of expression, and the protein was easily purified by $Ni^{2+}$-affinity interaction through the N-terminal His-tag from the pET-19b vector. Gel filtration chromatography of recombinant OTC indicated the presence of high molecular oligomerization forms, probably corresponding to a dodecameric structure, although other lower molecular weight oligomers could also be isolated. The final protein yield was 15 mg of recombinant OTC per liter of culture. Full-length carbamate kinase (CK) was also produced in *E.coli* in high yields and subsequently purified by $Ni^{2+}$-affinity chromatography. Recombinant *M. penetrans* CK also eluted from the gel filtration column mainly as a dimer, suggesting that such a form might also correspond to the biological unit of the enzyme. The final protein yield was 6 mg of recombinant CK per liter of culture.

Before attempting the crystallization studies, the functionality of the three purified enzymes was tested by performing specific activity assays [45]. Activity data of ADI, OTC, and CK measured from crude cell extracts of *M. penetrans*, compared to the enzymes expressed in *E. coli*, allowed us to conclude that the obtained recombinant proteins behave as their native counterparts (data not shown).

### Crystal structure of arginine deiminase (ADI) from Mycoplasma penetrans

The polypeptide chain of ADI can be clearly and completely traced in the electron density maps from Gly54 to Lys452 (Figure S1). Crystals of *M.penetrans* ADI display a large unit cell composed of twelve molecules in the asymmetric unit. All the molecules in the asymmetric unit display a similar structure, with

an rms deviation of 0.25 Å for the mainchain. Based on results obtained by gel-filtration chromatography, the biological unit can be considered to be a dimer (making up 6 dimers in the asymmetric unit). Structural alignment software (PDBefold) shows homology with the only other two known ADI structures, from *Mycoplasma arginini* (PDB code 1LXY) and from *Pseudomonas aeruginosa* (PDB code 1RXX). These structures display rms deviations with *M.penetrans* ADI of 1.54 Å and 1.85 Å, for 391 and 360 aligned residues with a pair-wise sequence identity, of 59% and 28%, respectively.

The overall protein fold and the secondary structure elements found in previous ADI structures are conserved in *M.penetrans* and consist of the repetition of a three-stranded mixed β sheet and a helix forming five ββαβ modules in a cyclical arrangement (Figure S1). This 5-fold pseudosymmetric moiety is also characteristic of other arginine-catabolizing enzymes such as Arg:Gly amidinotransferase (AT, [46]; PDB code 1JDW), dimethylarginine dimethylaminohydrolase (DDAH, [47]; PDB code 1H70) and agmatine deiminase (AgDI, [48]; PDB code 2JER). This characteristic protein fold seems to have evolved to interact and catalyze reactions containing guanidinium substrates, such as arginine. In the case of the arginine deiminase enzymes (ADI), this 5-fold pseudosymmetric α/β modular domain also contains an additional 85-residue α-helical domain between the first and second module (helices α4 to α8, see Figure S1). The role of this five-helix bundle domain, that is absent in the AT, DDAH and AgDI structures, is still not clear, but it has been speculated that it can participate in the activation of processes such as apoptosis [25].

The active site of the enzyme is located approximately at the center of the structure, forming a buried and compact substrate-binding pocket. Previous structures of *M.arginini* ADI in a covalent complex with two L-arginine substrate intermediates ([25]; PDB code 1LXY and 1S9R) defined the binding pocket and the catalytic residues of the enzyme. In our apo-form structure of ADI from *M.penetrans*, all the substrate binding residues for the enzymatic reaction are conserved, but need to undergo substantial structural rearrangements to carry out the catalytic reaction. The apo-form ADI structure of *M.penetrans* would correspond to the "open" conformation of the enzyme, whereas the intermediate-substrate bound ADI structure of *M.arginini* would represent the "closed" conformation (Figure 1). As observed for many enzymes that follow an induced-fit mechanism, the occurrence of "open" and "closed" conformations are necessary to permit the correct catalytic reaction, which allows for the entrance and the release of the substrate and end product, respectively.

In the intermediate-bound ADI structure from *M.arginini* (PDB code 1LXY), the amino and carboxylate groups of the arginine substrate establish polar and charged interactions with Leu44, Asn155, Arg180, Arg232 and Gly392 (Leu88, Asn198, Arg223, Arg276 and Gly434 in the *M.penetrans* numbering). In our apo-form structure of *M.penetrans* ADI, the carbonyl groups of Leu88 and Gly434 are moved 2 Å away from their binding positions with the amino group of the arginine substrate, whereas Asn198 is located in a similar position. Arg223 and Arg276 (*M.penetrans* numbering), which bind the carboxylate group of the arginine substrate, undertake substantial movements of approximately 4 Å (particularly for Arg276) from their positions in the "open" to the "closed" conformations (Figure 1). The fixation of the aliphatic moiety of the arginine substrate is established by hydrophobic interactions with the Phe158 and Met268 sidechains (Phe201 and Met312 in the *M.penetrans* numbering). Comparison between the "closed" and our apo-form of *M.penetrans* ADI ("open" conformation) indicates that, whereas Phe201 does not move from its location, Met312 needs to move approximately 3 Å to interact with the substrate during the catalytic reaction.

The catalytic reaction of the ADI enzyme is performed by the catalytic triad composed of Cys440, His313 and Glu257, where the sulfur of Cys440 catalyzes a nucleophilic attack on the guanidino carbon of the arginine substrate. The role of Asp204 and Asp315 is also crucial for the stabilization of the tetrahedral intermediates during the catalytic reaction, as observed in the two intermediate complexes of ADI from *Mycoplasma arginini* and *Pseudomonas* [24,25]. In our "open" conformation of *M.penetrans* ADI, Cys440 is located in a similar position as in the "closed" conformation, whereas His313 and Glu257 need to move about 3 Å to interact with the arginine substrate. Asp204 and Asp315 also move in this conformation, albeit to a lesser degree (Figure 1).

Therefore, it is essentially the movement of three loops containing some of the catalytic and binding residues of the active site pocket that is needed to switch from the "open" to the "closed" conformation of the enzyme, namely the loops α9-β5, β6-α10 and β7-α11 (Figure 1B). These three "mobile" loops are essentially shaping one side of the active site pocket, whereas the other side does not seem to undertake any substantial rearrangement upon substrate binding. A similar substrate induced-fit mechanism from the "open" to the "closed" conformation has also been previously described for the *Pseudomonas aeruginosa* ADI [23,24], which has a 28% sequence identity with the ADI from *Mycoplasma*. Interestingly, a notable difference in the *P.aeruginosa* apo-form of ADI is the presence of an arginine residue, which corresponds to Met435 in *M.penetrans*, which is located in the middle of the active site pocket forming a salt bridge with an aspartate residue. This interaction needs to be disrupted and the arginine side chain displaced from the active site to allow the binding of the substrate. This does not occur in the *Mycoplasma* ADI and might be a reason for the large disparity in affinities for the substrate binding displayed by two orders of magnitude difference in the $K_m$ constant [24].

## Crystal structure of ornithine carbamoyltransferase (OTC) from Mycoplasma penetrans

Two different crystal forms of the OTC from *M.penetrans* have been refined. The first one belonged to the $P2_13$ space group and was refined to 2.6 Å, and the second one belonged to a P321 space group and was refined to 2.5 Å. In both crystal forms the polypeptide chain of *M.penetrans* OTC can be clearly and completely traced in the electron density maps (from Met1 to Tyr342). The asymmetric unit of *M.penetrans* OTC is composed of four molecules in both crystals forms, displaying an average rms deviation of 0.35 Å between the four molecules. Structural alignment server (PDBefold) shows high homology with many OTC structures deposited in the PDB data bank, being the top ones from *Pseudomonas aeruginosa* (PDB code 1DXH) and from *Escherichia coli* (PDB code 1AKM). These structures display rms deviations compared with *M.penetrans* OTC of 1.26 Å and 1.21 Å, for 328 and 309 aligned residues with a sequence identity of 47% and 46%, respectively.

Despite the different space groups of the two crystal forms, in both cases an identical dodecameric quaternary structure was observed with an exact 23 point-group symmetry. In the two crystal forms this dodecameric structure was predicted by the PISA server (http://www.ebi.ac.uk/msd-srv/prot_int/pistart.htlm) and might correspond to the biological unit of the protein. The elution time in the gel filtration purification of the recombinant *M.penetrans* OTC also corresponds to the formation of a dodecameric quaternary structure. In most cases the oligomeric structure of OTC corresponds to a homotrimer, which

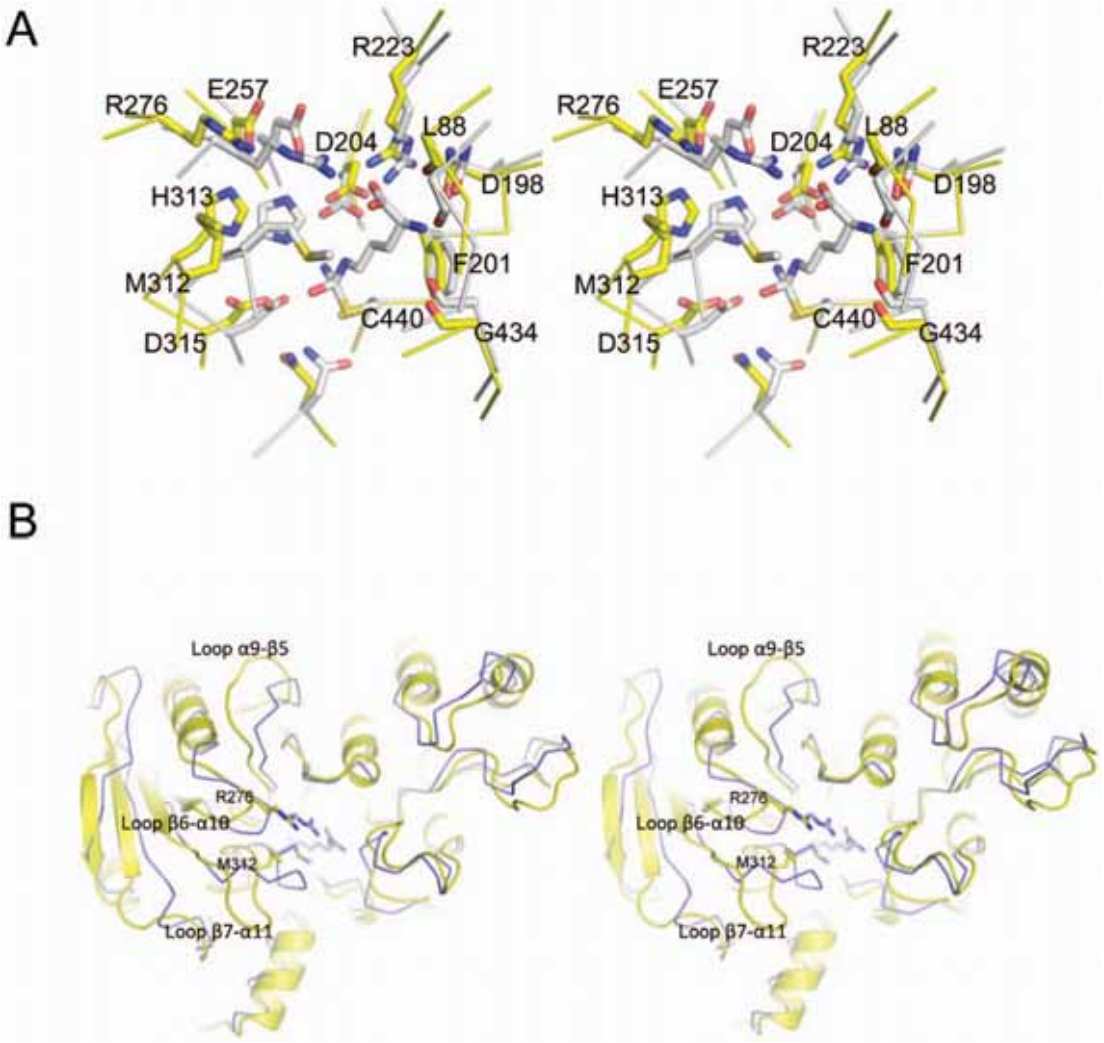


**Figure 1. Conformational changes on the ADI structures upon substrate binding.** (A) Stereo view representation of the superposition of the open active-site of *Mycoplasma penetrans* ADI (yellow) with closed active-site of the *Mycoplasma arginini* ADI in complex with arginine (white). ADI residues involved in the substrate binding and catalysis are labeled and shown in stick representation. (B) Stereo view ribbon representation of the superposition between the *Mycoplasma penetrans* ADI (yellow) with the *Mycoplasma arginini* ADI in complex with arginine (blue). Three major mobile loops of the ADI structure are labeled.
doi:10.1371/journal.pone.0047886.g001

represents the catalytic unit of the enzyme [32]. Only three OTCs have been reported to possess a similar dodecameric quaternary structure as *M.penetrans*, OTCs from *Pseudomonas aeruginosa* ([31]; PDB code 1ORT), *Pyrococus furiosus* ([34]; PDB code 1ALS) and *Thermotoga maritima* (PDB code 1VLV; only deposited). Remarkably, two of them are thermophiles, suggesting a potential role of the quaternary compact structures in high temperature protection in those environments. In all cases the dodecamer structure is formed by the interaction of four homotrimers disposed in a tetrahedral manner [34,49,50]. The four three-fold symmetry axes, located at the vertexes of the tetrahedral, are perpendicular to the center of the opposite homotrimer, and the three two-fold symmetry axes pass through the middle of opposite edges.

The trimeric structure of OTC is conserved in all known structures of OTCs and represents the catalytic unit of the enzyme, displaying one active site per monomer (Figure S2). As with all other known OTCs structures, the monomer consists of two domains of approximately similar size, the carbamoyl phosphate-binding domain (or polar domain, residues 1–150) and the ornithine-binding domain (or equatorial domain, residues 151–320). Each domain is named according to their respective involvement in substrate recognition. The secondary structure of each domain is made up of a five-stranded parallel β-sheet surrounded by α-helices, with helices α5 and α14 of *M.penetrans* OTC linking the two domains (Figure S2). The active site is located in a cleft formed between the two domains, and by comparison with other OTC structures, residues from both domains are involved in the catalytic reaction. By comparison with OTC structures bound to substrate analogs [51,52], the relative positions of residues binding the carbamoyl phosphate moiety are mainly conserved in the *M.penetrans* OTC, including the positive pocket shaped by Ser59, Thr60, Arg61, Thr62, Arg110, His137, Gln140 and Arg328 (*M.penetrans* OTC numbering). Structural comparison between the apo- and the substrate-bound forms of OTCs [51,52] indicate that the carbamoyl phophate-binding domain displays less flexibility than the ornithine-binding

domain, in which larger structural rearrangements are induced during the catalytic reaction. Thus, whereas the catalytic patch formed by residues His275, Cys276 and Leu277 does not vary its position between the apo- and the substrate-bound forms in the ornithine-binding domain [51,52], the loop between Trp237 and Phe247 displays a different conformation in the apo form of the *M.penetrans* OTC. Interestingly, this loop constitutes the main binding site for ornithine and is formed by the conserved DxxxSMG motif (between β8 and α10) in all OTC structures, except in our structure of *M.penetrans* OTC, in which methionine is substituted by leucine. The movement of this SMG-loop seems to be essential for binding of the second substrate and product release during the catalytic reaction [51].

The interfaces between monomers within the catalytic homotrimer are located mainly within the carbamoyl phosphate-binding domain, and are basically formed by the α2 helix and part of the last α14 helix that interacts with the region formed by the β2 strand and the α3 helix from the adjacent monomer (Figure S2). Analysis of the quaternary structure of the homotrimer structures of *M.penetrans* OTC (PISA server) displays a buried average interface of 590 $Å^2$ between monomers. Each monomer contributes 60 residues to the interface, including 12 hydrogen bonds and 9 salt bridges. The total buried surface in the homotrimer structure is 1750 $Å^2$ (indicating an energetically favorable formation of the homotrimer that constitutes the catalytic unit) with some of the interface residues as part of the active site.

The interface between homotrimers that constitute the dodecameric structure is mainly located at the four 3-fold symmetry axes at the vertices of the tetrahedron (Figure 2). This interface is mainly formed by three α1 helices and the loop between α1 and β1 from three monomers from the different catalytic trimers located around each 3-fold symmetry axes. The interface between two monomers buries approximately 330 $A^2$ that would represent a total of 990 $A^2$ for each 3-fold symmetry axes interaction. Each monomer contributes 35 residues to the interface, mainly consisting of the aforementioned α1 helix residues, but with additional residues from the N- and C-terminal regions. Quaternary structure analysis by the PISA server indicates that the interface between two monomers contains 5 hydrogen bonds and 4 salt bridges. In Figure 2 the interface between homotrimers is located around the threefold symmetry axis at one top of the dodecamer. In the *M.penetrans* OTC dodecamer, this interface forms an intermolecular network of hydrogen bonds between Asn42 and Asn43 from the three monomers, which is unique to the sequence of *M.penetrans* OTC (Figure 2C).

Interestingly, the four known dodecameric structures of OTC (including the *M.penetrans* OTC) display completely different chemical profiles of the residues involved in the three-fold interface and only the relative positions of the main chain atoms can be superimposed. In the case of the *P.furiosus* OTC, the interaction around the threefold symmetry axis is mainly hydrophobic (Figure 2E), presenting major interactions between Met29, Trp33 and Lys38 [34]. In the case of the *P.aeruginosa* OTC, the threefold symmetry axis interface is basically charged and polar (Figure 2D), with major contribution of Arg28, Arg32, Thr39 and Gln41 [31]. The fourth dodecamer structure of an OTC is that of *Thermotoga maritima* (PDB code 1VLV; only deposited), and in this case the threefold symmetry axis interface presents a mixture of polar and hydrophobic interactions (Figure 2F). These different interfaces produce minor shifts and rotations between homotrimers in the global quaternary structure arrangement when a catalytic trimer is superimposed within the dodecamer.

In the case of *P.furiosus*, and perhaps in *T.maritima,* the domecameric quaternary structure has been involved in the extreme thermal stability of these microorganisms. It has been suggested that the thermophilic properties of the *P.furiosus* OTC are, in part, the result of the hydrophobic interfaces between homotrimers [49,50]. In the case of *P.aeruginosa*, the dodecameric structure was first directly involved in the allosteric mechanism of the enzyme, which displays a marked cooperativity for carbamoyl phosphate [31], although it was later found than OTC homotrimers could also retain such cooperativity [53,54]. In any case, the presence of higher oligomerization structures might be linked to an increase in the efficiency of the reaction in the ADI pathway, by means of thermal protection or by quaternary structure-induced cooperativity. Interestingly, a tunnel mechanism between OTC and the next catabolic enzyme of the ADI pathway, carbamate kinase (CK), has been suggested, as a means to protect from high temperatures and to efficiently transfer the labile (relatively unstable) product of the OTC reaction, carbamoyl phosphate [55].

## Crystal structure of carbamate kinase (CK) from Mycoplasma penetrans

The polypeptide chain of the *M.penetrans* CK can be traced in the electron density maps from Arg3 to Ser133 and from Lys157 to Ala309 (Figure S3). The gap in the electron density maps corresponds to the flexible PSD domain (''Protruding SubDomain''), and only residues at both ends of the PSD domain and the internal loop from Ala143 to Val150 could be partially modeled in the electron density, all displaying high temperature B-factors and giving as a result a poor agreement between $R_{work}$ and the $R_{free}$ in the final refined structure. Crystals of *M.penetrans* CK display a unit cell composed of one molecule in the asymmetric unit. Based on results obtained by gel-filtration chromatography, by predictions of the PISA server and by previous structures of CK from other organisms, the biological unit can be considered to be a dimer. Structural alignment server PDBefold shows strong homology with the other known CK structures, such as CK from *Pyrococcus furiosus* (PDB code 1E19), from *Giardia lamblia* (PDB code 2KZF) and from *Enterococcus faecalis* (PDB code 2WE5). These structures display rms deviations with *M.penetrans* CK of 1.23 Å, 1.59 Å and 1.54 Å, for 279, 266 and 271 aligned residues with sequence identities of 43%, 37% and 41%, for *P.furiosus*, *G.lamblia* and *E.faecalis*, respectively.

The overall protein fold and the secondary structure elements are conserved in *M.penetrans* CK and basically consist of a central eight-stranded parallel β-sheet, with six strands parallel in one orientation and two strands in an opposite orientation (β12 and β14), surrounded by α-helical elements at both sides of the central β-sheet (Figure S3). As previously described for the first CK structures from *E.faecalis* and *P.furiosus* [42,43], the structure can be divided in two domains, with a large crevice in the middle that creates the binding sites for the two substrates, carbamoyl phosphate (CP) and ADP. The N-terminal domain (residues Met1 to Ala222), rich in α-helices, is composed by two sets of four stranded β-sheets, the first sheet constituted by four parallel strands from the central β-sheet and the second sheet smaller and formed by mixed β-strands. This domain contains three long α-helices, α1, α2 and α3, which make up the entire dimer interface, and the mobile PSD domain (''protruding subdomain'', from Lys126 to Val159), which is involved in the catalytic reaction by an overall ''rigid body'' movement upon substrate binding. The C-terminal domain (residues Asp223 to Ala309) is smaller and formed by the four mixed β-strands from the central β-sheet, surrounded by three α-helices. Whereas the binding residues for carbamoyl phosphate basically emanate from the N-terminal

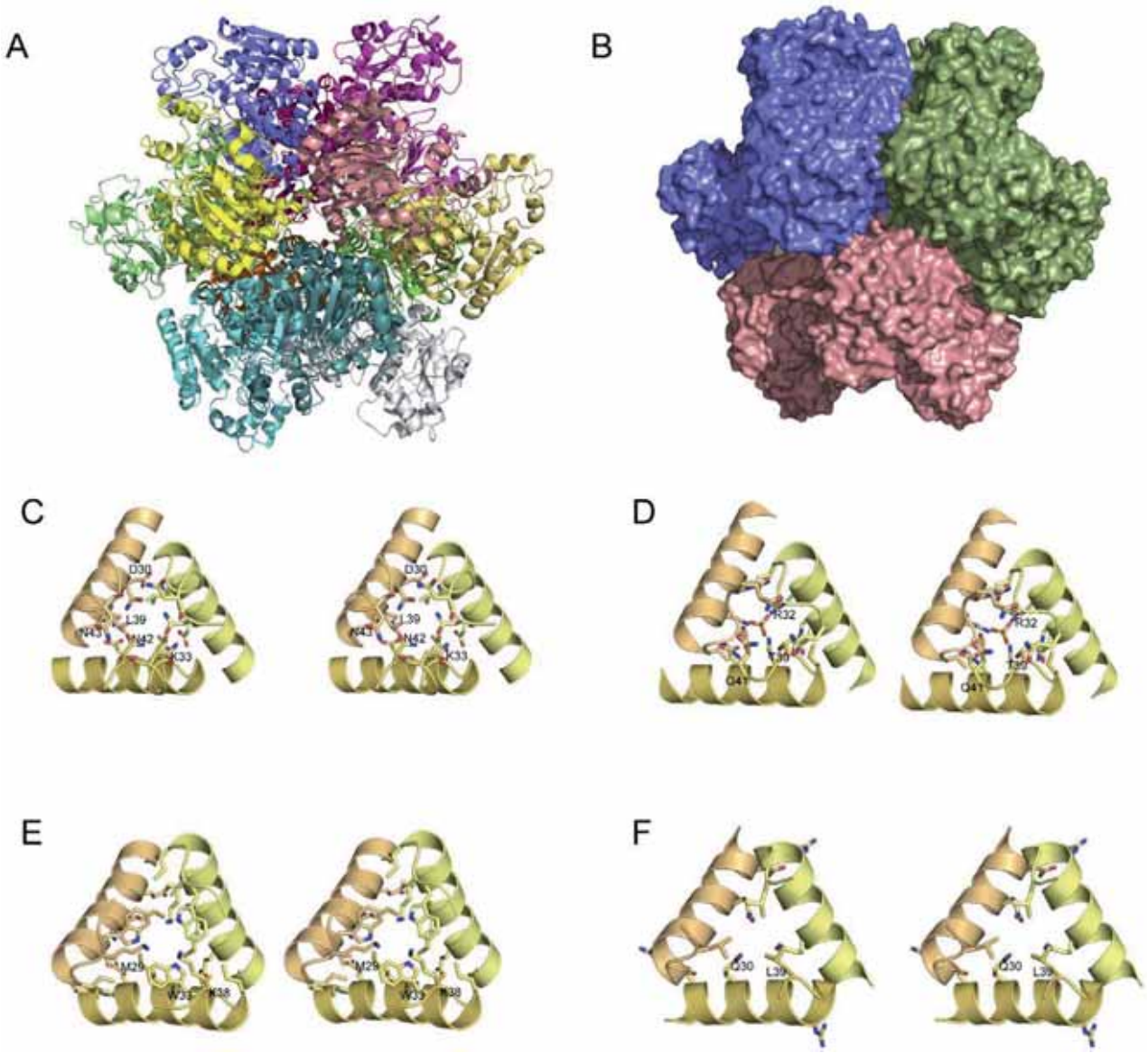


**Figure 2. OTC dodecamer structure and the threefold interface between homotrimers.** (A) Ribbon representation of the *Mycoplasma penetrans* OTC dodecamer. Each monomer is shown with a different colour. (B) Surface view of the *M. penetrans* OTC dodecamer. Each homotrimer is shown with a different color. (C, D, E, F) Stereo ribbon representation of the threefold interface between homotrimers. Residues involved in the dodecamer assembly are labeled and shown in stick representation for different species; (C) *Mycoplasma penetrans*, (D) *Pseudomonas aeruginosa*, (E) *Pyrococcus furiosus*, (F) *Thermotoga maritima*.
doi:10.1371/journal.pone.0047886.g002

domain, the C-terminal domain is responsible for the binding of ADP. Interestingly, in our structure of *M.penetrans* CK, two sulfate ions from the crystallization buffer might be present in the β- and γ-phosphate-binding pockets of the synthesized ATP product molecule, with only present in such position in the CK structures from *E.faecalis* (PDB codes 2WE4 and 2WE5).

In our current structure of *M.penetrans* CK, the location of some of the residues that have been suggested to contact the phosphate group of the carbamoyl phosphate substrate (CP) are conserved. These are the sidechain of Lys209 and the amino backbone nitrogens of Gly10, Asn11, Gly47, and Gly48. However, the putative coordination of the phosphate group of CP shown for the *E.faecalis* CK is not complete in *M.penetrans*, since the sidechain of Lys126 (Lys128 in the structure of the *E.faecalis* CK), which belongs to the mobile PSD domain, is not interacting with the sulfate ion. Interestingly, the inferred position of the PSD domain in the *M.penetrans* CK is in an "open" orientation, more similar to the *E.faecalis* CK-ADP bound structure (PDB code 2WE5) than to the *E.faecalis* CK-$SO_4$-bound structure (PDB code 2WE4) (Figure 3). In our *M.penetrans* CK structure, the PSD domain can only be partially traced in the electron density maps, with all atoms displaying high values of temperature B-factors, indicating a strong tendency of this domain to shift between different conformations. The PSD domain has been postulated to act as a "rigid body" that is triggered upon the binding of the CP molecule to allow the catalytic reaction [43]. However, in our *M.penetrans* CK structure, despite the presence of a sulfate ion occupying a similar CP binding site as in the *E.faecalis* CK-$SO_4$-bound (PDB code 2WE4),

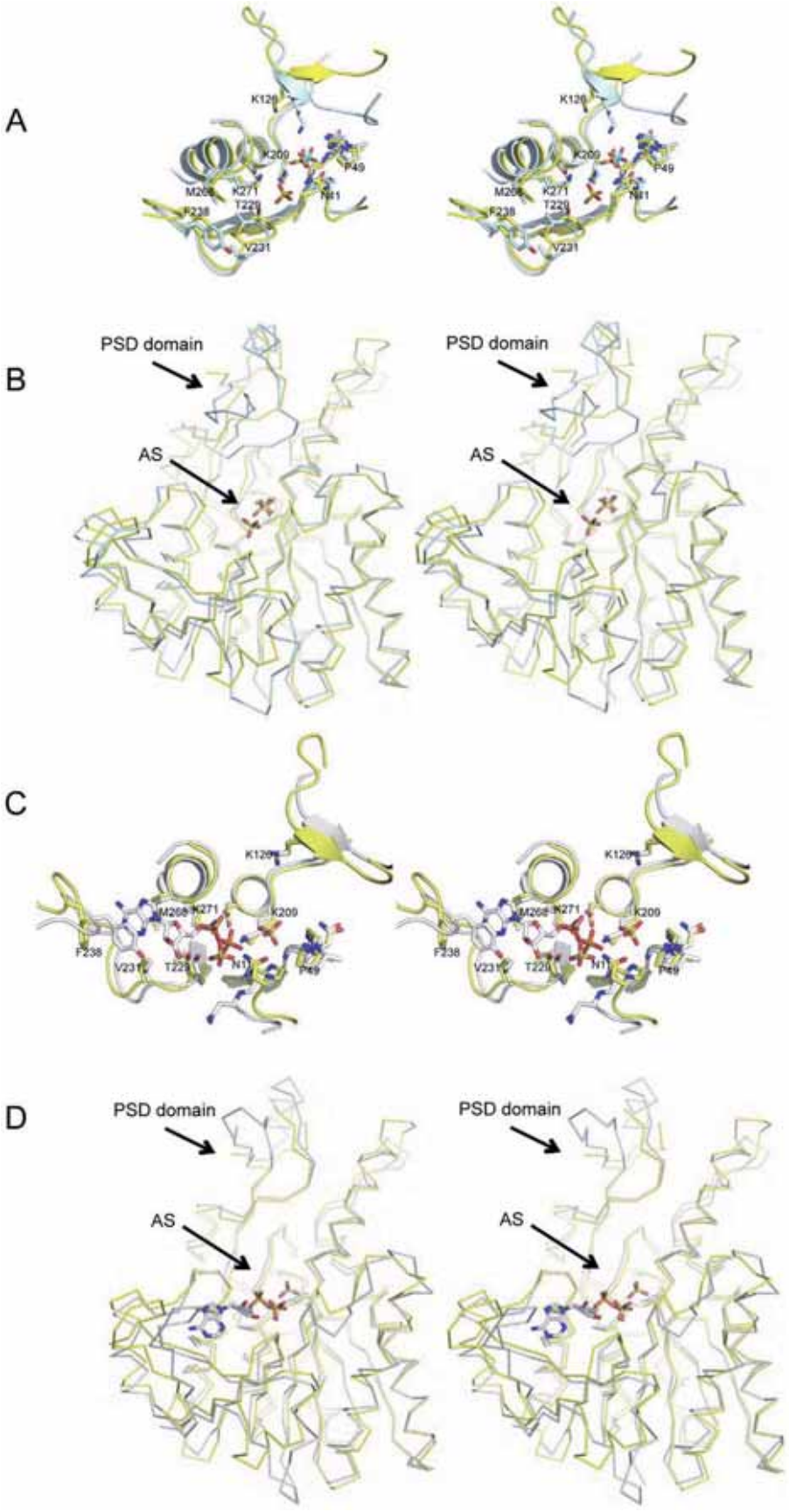
A
K120
K209
P49
M268
K271
T220
N81
F238
V231
B
PSD domain
AS
C
K120
M268
K271
K209
F238
V231
T220
N81
P49
D
PSD domain
AS

**Figure 3. Conformational changes on the CK structures upon substrate binding.** (A) Stereo view representation of the superposition of the active site of CK from *Mycoplasma penetrans* (yellow) and *Enterococcus faecalis* (ligth blue). Sulfate ions are shown in stick representation. CK residues involved in the substrate binding and catalysis are labeled and shown in stick representation. (B) Stereo view ribbon representation of the superposition of the CK from *Mycoplasma penetrans* (yellow) and *Enterococcus faecalis* (ligth blue). Sulfate ions are shown in stick representaion. (C) Stereo view representation of the superposition of the active site of CK from *Mycoplasma penetrans* (yellow) and from *Enterococcus faecalis* in complex with ADP (light blue). Sulfate ions and ADP molecule are shown in stick representation. CK residues involved in the substrate binding and catalysis are labeled and shown in stick representation. (D) Stereo view ribbon representation of the superposition of the CK from *Mycoplasma penetrans* (yellow) and *Enterococcus faecalis* (ligth blue) in complex with ADP.
doi:10.1371/journal.pone.0047886.g003

the PSD domain displays an "open" conformation, not productive for the phosphoryl transfer of the carbamoyl phosphate to the ADP molecule.

The second sulfate ion found in the *M.penetrans* CK structure is located approximately in a similar position as the β-phosphate of the ADP molecule observed in the *E.faecalis* and *P.furiosus* CK-ADP bound structures ([42,43]; PDB codes 2WE5 and 1E19, respectively). Mimicking the ADP β-phosphate, the second sulfate ion interacts with the side chains of Lys271, Thr229 and the amino backbone nitrogen of Ala230. In our *M.penetrans* CK structure this sulfate ion is also at contact distance with the sidechain of Asn11 (3.24 Å), adopting the β1-α1 loop in a conformation similar to the CK-$SO_4$-bound *E.faecalis* structure (PDB code 2WE5). Interestingly, the sidechain of Asn11 can potentially interact with both sulfate ions in our structure, the putative β-phosphate and mobile γ-phosphate of ATP, suggesting a participation of this residue in bridging the transfer of the phosphoryl group during the reaction of the enzyme. The other regions in the structure that might interact with the ADP molecule are in the "open" conformation, as observed in the CK-SO4-bound structure (PDB code 2WE5). These observations support the plasticity observed in most of the active-site regions of enzymes to allow catalysis and release of the end products.

In summary, the *M.penetrans* CK structure bound to two sulfate ions displays some differences in comparison to previous structures (CK-ADP from *E.faecalis* and *P.furiosus*; and CK-$SO_4$ from *E.faecalis*). In the *M.penetrans* CK structure, despite the CP binding site being occupied by a sulfate ion, the PSD domain adopts an "open" orientation, which differs from the "closed" orientation observed in the CK-$SO_4$ complex structure from *E.faecalis*, in which a sulfate ion occupies a similar position or in the *G.lamblia* CK structure ([56]; PDB code 3KZF), in which a glycerol molecule occupies the putative CP binding site. The orientation of the PSD domain in the *M.penetrans* CK resembles the PSD domains in the CK ADP-bound structures from *E.faecalis* and *P.furiosus*, but in both cases without any sulfate ions in the CP binding site (Figure 3D).

The movement of the PSD domain between an "open" and "closed" orientation to interact with the CP molecules has been described to be essential for the catalytic mechanism of the phosphoryl transfer between CP and ADP, allowing the interaction of the sidechain of Lys126 with CP molecule [43]. In our *M.penetrans* CK structure, the "open" orientation of the PSD domain with a sulfate ion occupying the CP binding site has not been observed, and might represent a structural snapshot of the binding of CP before the enzymatic reaction occurs. However/ likewise, it could also be an example of the product complex before the release of the CP from the active site in the anabolic reaction of synthesis of the carbamoyl phosphate from carbamate [42]. Similarly, the binding of the second ion sulfate at the β-phosphate position of the ADP molecule indicates the strong binding tendency of this region to interact with charged ions (sulfates or phosphates). Remarkably, in a previous *E.faecalis* CK sulfate-bound structure, this second binding site pocket was not occupied by any sulfate ion.

## Conclusions

The arginine deiminase pathway (ADI) is the most widespread anaerobic route for arginine degradation in microorganisms and performs the conversion of arginine to ornithine, ammonia, and $CO_2$, generating one mole of ATP per mole of arginine consumed. The ADI pathway constitutes an important source of energy in some microorganisms and like many other enzymatic pathways, it is also organized in a gene cluster to better regulate and optimize the production of the proteins. Here we have described the structure of the three enzymes that constitute the gene cluster in the ADI pathway in *Mycoplasma penetrans* (together with the specific membrane-associated arginine permease coded by *arc*D gene) and compared them to previous structures of the enzymes. Arginine deiminase (ADI), which catalyzes the first step in the ADI pathway, have been crystallized in its apo-form, and differs from the previous substrate-bound structures of *Mycoplasma arginini* by displaying an "open" conformation of the active site. The second enzyme of the pathway is ornitine transcarbamylase (OTC), which can catalyze the reaction in both directions and displays a dodecameric structure in the two crystal forms that have been crystallized. Dodecameric organization of OTC has been described in three microorganisms, *P.aeruginosa, P.furiosus* and *T.maritima,* in other organisms homotrimers can be found as the usual oligomeric form of this enzyme. Interestingly, the interfaces that form the OTC dodecamer in all these organisms are completely different, not showing any sequence homology between them and displaying either charged or hydrophobic interactions in the 3-fold symmetry axes of the dodecamer. Our current structure of *M.penetrans* OTC shows a novel interface forming the dodecamer. The last enzyme of the pathway is the carbamate kinase (CK), which is responsible for the formation of new molecules of ATP from carbamoyl phosphate. The crystal structure of CK contains two sulfate ions in the active site pocket, mimicking the binding of the β- and γ-phosphate of the ATP product molecule before the phosphorylation reaction has occurred. Interestingly, in our CK structure the position of the mobile PSD domain is in an "open" and non-catalytic conformation, despite the CP binding site being occupied by a sulfate ion, and might represent a structural snapshot of the binding of the substrates before the catalytic reaction occurs. The structural characterization of the enzymes of the ADI pathway in *Mycoplasma penetrans* has shed light to particular features of these proteins that eventually might provide new tools to interfere in the growing and proliferation of this pathogenic organism in humans.

## Methods

### Gene cloning and mutagenesis

A 3749-bp fragment (namely ArcABC) containing the genes for arginine deiminase (*arcA*), ornithine carbamoyltransferase (*arcB*), and carbamate kinase (*arcC*) was isolated from *Mycoplasma penetrans* GTU-54 strain (kindly provided by J. Baseman, University of Texas, San Antonio, USA) genomic DNA by PCR amplification using the set of primers Arc1penetr (forward) and Arc2penetr

(reverse); see Table S1 for their respective sequences. The ArcABC fragment was blunt-end cloned into the *Eco*RV site of plasmid vector pBE, a derivative of pBSKII (Stratagene, CA) in which the multicloning site has been removed and substituted by a single *Eco*RV site [57]; the recombinant plasmid pBE-ArcABC was transformed into *E. coli* XL1-Blue strain. TGA is a stop codon in the universal genetic code but mycoplasmas translate such a codon as a tryptophan. Therefore, before attempting the heterologous expression in *E. coli* of mycoplasma gene products, any TGA in a coding region should be changed to TGG in order to incorporate the native Trp residue into the corresponding polypeptide. The *arcA* gene of *M. penetrans* contains two TGA codons that code for Trp317 and Trp339 in the arginine deiminase (ADI) amino acid sequence; equally, the *arcB* gene contains two TGA codons that code for Trp129 and Trp237 in the ornithine carbamoyltransferase (OTC). On the contrary, *arcC* gene coding for carbamate kinase (CK) does not contain any TGA codon. TGA codons were changed to TGG by site-directed mutagenesis, performing for each gene (*arcA* and *arcB*) six consecutive PCR steps, as outlined in Figure S4. The different couples of primers for each PCR reaction (numbered 1–6) and each gene (ADI and OTC) are indicated in Table S1, along with the length (in base pairs) of the amplified fragment. Mutagenic primers correspond to numbers 2, 3, 4, and 5; moreover, primers 2 and 4 are fully complementary to primers 3 and 5, respectively, and include the same point mutations (indicated with a bold character in Table S1). Phusion DNA polymerase (New England Biolabs) and 2 mM $MgCl_2$ were used in all PCR reactions. Briefly, using the pBE-ArcABC recombinant plasmid as a template, a first PCR (PCR1 in Figure S4) amplifies from the start codon of the corresponding coding sequence to the first TGA codon to be mutated; a second PCR (PCR2) amplifies from the first TGA codon to the second one; and, finally a third PCR3 amplifies from the second TGA to the stop codon of the coding sequence. Next, using primers 1 and 4 and as DNA template the products of PCR1 and PCR2 reactions, PCR4 allowed to amplify from the start codon to the second TGA (already changed to TGG); in the same way, with the use of primers 3 and 6 and PCR2 plus PCR3 products as templates, PCR5 amplifies from the first TGA (TGG) to the stop codon. Note that PCR1, PCR2, and PCR3 products overlap at the ends including the mutated TGA codons (see Figure S4). Finally, the complete gene incorporating both changed TGG codons was obtained with PCR6 by using primers 1 and 6 and PCR4+PCR5 reaction products as templates; in this case, the complementary overlapping sequence between both PCR products corresponds to the DNA region expanding from the first to the second TGG. Not being necessary to change any TGA codon, the *arcC* gene was directly amplified from pBE-ArcABC using the corresponding primers 1 and 6 (ck-1 and ck-6 in Table S1, respectively). The products of the three PCR6 reactions (corresponding to *arcC*, and the mutated *arcA* and *arcB* genes) were cloned into the *Eco*RV site of the pBE vector and the recombinant plasmids pBE-ArcA, pBE-ArcB, and pBE-ArcC were transformed into *E. coli* XL1-Blue strain. For each gene, three independent clones were sequenced. Sequencing reactions with fluorescent dideoxynucleotides were performed using the Big Dye 3.0 Terminator kit (Applied Biosystems) following the manufacturer's instructions and analyzed in an ABI 3100 Genetic Analyzer (Applied Biosystems). The substitution of TGA by TGG codons was confirmed in the *arcA* and *arcB* genes, and no other change with regard to the native sequences (including the *arcC* gene) was observed.

## Protein expression and purification

For the recombinant expression of individual proteins, TGA mutated *arcA* (long-ADI, see below), *arcB*, and *arcC* genes were cloned into pET-19b plasmid vector (Novagen) as follows. Mutated genes were excised from the corresponding pBE derivative (see above) by digestion with *Nde*I and *Bam*HI restriction enzymes, whose recognition sequences were borne by the 5′-end of PCR primers 1 and 6, respectively (underlined in Table S1). The *Nde*I-*Bam*HI fragments were ligated to pET-19b expression vector, previously linearized with the same restriction enzymes, allowing the fusion of a $His_{10}$-tag coding sequence to the 5′-end of each gene. Finally, the obtained recombinant plasmids were transformed into *E. coli* host expression strain BL21 (DE3).

Cells were grown at 37°C in Luria–Bertani (LB) growth medium supplemented with ampicillin (50 mg/L) to an optical density at 600 nm of 0.9 for ADI expression or 0.7 for OTC and CK expression. Protein expression was then induced by addition of 1 mM isopropyl β-D-1-thiogalactopyranoside (IPTG) to the culture medium, followed by shaking at 37°C for 3 hours. Induced cells were harvested by centrifugation, and resuspended in 5 mM imidazole, 0.5 M NaCl, 20 mM Tris-HCl (pH 7.9) (namely Binding Buffer), containing 1 mM phenylmethanesulfonyl fluoride (PMSF). Cells were disrupted by sonication, and the insoluble material removed by centrifugation at $40000 \times g$ for 20 minutes; supernatants were recovered and passed through a 0.45 μm filter. The histidine-tagged recombinant proteins were purified by loading the supernatants onto Hi-Trap Chelating Sepharose (GE Healthcare) chromatography columns equilibrated in Binding Buffer. Columns were washed with 60 mM imidazole, 0.5 M NaCl, 20 mM Tris-HCl (pH 7.9), and His-tagged retained proteins were eluted with 1 M imidazole, 0.5 M NaCl, 20 mM Tris-HCl (pH 7.9). Fractions containing the eluted proteins were pooled, dialyzed against 50 mM NaCl, 20 mM Tris–HCl (pH 8.0) buffer, and then loaded onto a HiLoad Superdex 200 26/60 gel-filtration column (GE Healthcare) previously equilibrated with the same buffer, as a final polishing purification step. Eluted fractions were analyzed by SDS-PAGE, and the purest samples were pooled, frozen in liquid-$N_2$, and stored at −80°C. Protein concentration was estimated by the Coomassie-binding method of Bradford, using bovine serum albumin as a standard.

## Crystallization and data collection

Crystals of arginine deininase (ADI) were obtained at 18°C by sitting drop vapor diffusion methods. The reservoir solution contained 0.9M Trisodium citrate, 0.1M Sodium cacodylate pH 6.5. Single crystals appeared after 2 days from equal volumes of protein solution (5 mg/ml in 5 mM Tris pH 8.0, 50 mM NaCl) and reservoir solution. Crystals of ornithine carbamoyltransferase (OTC) were grown at 18°C by sitting drop vapor diffusion methods in two different reservoir conditions: in 0.2M ammonium acetate, 39% MPD, 0.1M tri-sodium citrate pH 5.5 (trigonal space group) and in 15% PEG20000 and 0.1M MES pH 6.5 (cubic space group). Crystals of carbamate kinase (CK) were obtained at 18°C by sitting drop vapor diffusion methods in a reservoir condition with 1.8M ammonium sulfate, 2% PEG400, 0.1M HEPES pH 7.0. All crystals were cryo-protected in reservoir buffer containing 12% glycerol and flash-frozen in liquid nitrogen prior to diffraction analysis. Diffraction data were recorded from cryo-cooled crystals (100K) at Grenoble beamline ID23-2. Data were integrated and merged using XDS [58] and scaled, reduced and further analyzed using CCP4 [59] (Table 1).

**Table 1.** Data collection and refinement statistics.

| Data Collection | ADI | OTC (crystal 1) | OTC (crystal 2) | CK |
|---|---|---|---|---|
| Space group | $P2_1$ | P321 | $P2_13$ | $P3_221$ |
| Cell dimensions | | | | |
| a, b, c (Å) | 120.5, 128.8, 220.3 | 183.6, 183.6, 117.3 | 167.9, 167.9, 167.9 | 51.8, 51.8, 174.2 |
| α, β, γ (°) | 90, 91.4, 90 | 90, 90, 120 | 90, 90, 120 | 90, 90, 120 |
| Resolution (Å)[a] | 30–2.3 (2.40– 2.30) | 49–2.5 (2.64–2.50) | 50–2.6 (2.74–2.60) | 45–2.38 (2.51–2.38) |
| $R_{merge}$[b] | 0.060 (0.367) | 0.090 (0.436) | 0.094 (0.367) | 0.068 (0.388) |
| $I/\sigma_I$ | 9.8 (2.0) | 12.1 (2.6) | 8.7 (2.4) | 11.8 (2.5) |
| Completeness (%) | 97.6 (96.1) | 98.2 (89.7) | 98.6 (95.4) | 97.7 (92.2) |
| Redundancy | 1.9 (1.9) | 4.8 (3.4) | 2.4 (2.3) | 4.8 (4.5) |
| Refinement | | | | |
| Resolution (Å) | 30–2.3 | 49–2.5 | 48–2.6 | 45–2.5 |
| No. Reflections | 288889 | 74328 | 47453 | 9819 |
| $R_{work}/R_{free}$[c] | 21.60/24.23 | 17.01/21.51 | 17.9/23.9 | 23.19/28.68 |
| No. Atoms | 39631 | 11190 | 11035 | 2558 |
| No. aa protein | 4788 | 1376 | 1368 | 309 |
| Water | 1615 | 418 | 339 | 33 |
| R.m.s deviations | | | | |
| Bond lengths (Å) | 0.007 | 0.008 | 0.009 | 0.008 |
| Bond angles (°) | 1.33 | 1.154 | 1.206 | 1.155 |
| PDB code | 4E4J | 4AMU | 4ANF | 4AXS |

[a]Statistic for highest resolution shell is shown in parentheses.
[b]$R_{merge} = \sum |I_i - < I >|/\sum I_i$, where $I_i$ is the ith measurement of the intensity of an individual reflection or its symmetry-equivalent reflections and <I> is the average intensity of that reflection and its symmetry-equivalent reflections.
[c]$R_{work} = \sum ||F_o| - |F_c||/\sum |F_o|$ for all reflections and $R_{free} = \sum ||F_o| - |F_c||/\sum |F_o|$, calculated based on the 5% of data excluded from refinement.
doi:10.1371/journal.pone.0047886.t001

## Structure determination and refinement

The structure of ADI was determined from the x-ray data by molecular replacement using the PDB from *Mycoplasma arginini* (PDB code 1S9S) as a model. The two structures of OTC were determined from the x-ray data by molecular replacement using the PDB from *Pseudomonas aeruginosa* (PDB code 1DXH) as a model. The structure of CK was determined from the x-ray data by molecular replacement using the PDB from *Enterococcus faecalis* (PDB code 2WE5) as a model. The initial electron density maps produced from molecular replacement programs were manually improved to build up complete models for ADI, OTC and CK using the program COOT [60]. Model refinement was performed with CNS [61] and Phenix [62]. ADI contained 12 molecules in the asymmetric unit and the Ramachandran analysis shows 95.36% of residues (4543) are in preferred regions, 4.47% of residues (213) are in allowed regions and 0.17% of residues (8) are in outlier regions. OTC crystal 1 contained four molecules in the asymmetric unit and the Ramachandran analysis shows 94.71% of residues (1288) are in preferred regions, 4.41% of residues (60) are in allowed regions and 0.88% of residues (12) are in outlier regions. OTC crystal 2 also contained four molecules in the asymmetric unit and the Ramachandran analysis shows 94.34% of residues (1283) are in preferred regions, 4.34% of residues (59) are in allowed regions and 1.32% of residues (18) are in outlier regions. CK contained one molecule in the asymmetric unit and the Ramachandran analysis shows 90.88% of residues (259) are in preferred regions, 7.37% of residues (21) are in allowed regions and 1.75% of residues (5) are in outlier regions. Refinement and data statistics are provided in Table 1. Structural representations were prepared with PyMOL [63].

## Accession codes

Protein Data Bank: Coordinates and structure factors from the three structures were deposited in the PDB data with accession ID codes 4E4J (MpADI), 4AMU (MpOTC), 4ANF (MpOTC) and 4AXS (MpCK).

## Supporting Information

**Figure S1 ADI structure and sequence alignment.** (A) Ribbon representation of the ADI structure from *Mycoplasma penetrans*. The α-helix and β- strands are represented in red and golden, respectively, and are labeled sequentially from N-terminus. (B) Surface representation of ADI from *M.penetrans*. AS indicates the active site pocket. (C) Surface representation of ADI from *M.arginini* (PDB code) in complex with arginine in the active site (colored in magenta). AS indicates the active site pocket. (D) Topology-based sequence alignment of ADI from *Mycomplasma penetrans*, *Mycoplasma arginini* and *Pseudomonas aeruginosa*. The secondary structural elements are labelled and shown above the sequence as rectangles or arrows for α-helix and β-strands, respectively. Active site residues are colored in red. Identical or highly conserved residues are highlighted in yellow.
(PDF)

**Figure S2 OTC structure and sequence alignment.** (A) Ribbon representation of the structure of the OTC monomer from *Mycoplasma penetrans*. The α-helix and β-strands are represented in

red and golden, respectively, and are labeled sequentially from the N-terminus. Residues involved in the active-site are shown in stick representation. (B) Ribbon representation of the OTC homotrimer structure. (C) Topology-based sequence alignment of OTC from *Mycoplasma penetrans*, *Pseudomonas aeruginosa*, *Themortoga maritima*, *Pyrococcus furiosus*, *Lactobacillus hilgardii*, *Gleobacter violacius* and *Escherichia coli*. The secondary structural elements are labeled and shown above the sequence as rectangles or arrows for α-helices or for β- strands, respectively. Active site residues are colored in red. Identical or highly conserved residues are highlighted in yellow.
(PDF)

**Figure S3 Structure of the CK from M. penetrans and sequence alignment.** (A) Ribbon representation of CK from *Mycoplasma penetrans*. The α-helix and β-strands are represented in red and golden, respectively, and are labeled sequentially from the N-terminus. Residues involved in the active-site are shown in stick representation. (B) Ribbon representation of the dimer of CK. In one of the monomers, the N-terminal domain is in colored in light blue, the C-terminal domain in forest green and the PSD domain in lime green. The two sulfate ions are shown in stick representation. (D) Topology-based sequence alignment of CK from *Mycoplasma penetrans*, *Enterococcus faecalis*, *Pyrococcus furiosus* and *Giardia lamblia*. The secondary structural elements are labeled and shown above the sequence as rectangles or arrows for α- helices or forβ-strands, respectively. Active site residues are colored in red. Identical or highly conserved residues are highlighted in yellow.
(PDF)

**Figure S4 Mutagenesis strategy.** Scheme illustrating the strategy followed to change the two TGA, coding for tryptophan in *M. penetrans*, by TGG codons before the heterologous expression of *arc*A (ADI) and *arc*B (OTC) genes in *E. coli*. Numbered arrows indicate the primers (see Table S1 for primer sequences and features). The successive six PCR amplifications carried out are also indicated. Cloning of *arc*C gene, which does not contain any TGA codon, was performed in a single reaction (PCR6) using primers 1 and 6.
(PDF)

**Table S1 Primers.** Underlining indicates the restriction sites introduced at the 5′ end of selected primers. A bold lowercase character indicates the changed base in mutagenic primers.
(PDF)

## Acknowledgments

We acknowledge Fernando Gil-Ortiz and Kamela O. Alegre for suggestions and stimulating discussion on the work. D.R. acknowledges the Ramon y Cajal program from the "Ministerio de Ciencia e Innovacion" of Spain. P.G. acknowledges a FPI fellowship from the "Ministerio de Ciencia e Innovacion" of Spain and R.P. from the Centre de Referència de R+D de Biotecnologia de la Generalitat de Catalunya.

## Author Contributions

Conceived and designed the experiments: JAPP EQ DR. Performed the experiments: PG RP. Analyzed the data: PG RP JB DR. Wrote the paper: JAPP EQ DR.

## References

1. Razin S (1978) The mycoplasmas. Microbiol Rev 42:414–470.
2. Razin S, Yogev D, Naot Y (1998) Molecular biology and pathogenicity of mycoplasmas. Microbiol Mol Biol Rev 62:1094–156.
3. Pollack JD, Williams MV, McElhaney RN (1997) The comparative metabolism of the Mollicutes *(Mycoplasmas)*: the utility for taxonomic classification and the relationship of putative gene annotation and phylogeny to enzymatic function in the smallest free-living cells. Critical Rev Microbiol 23:269–354.
4. Cunin R, Glansdorff N, Piérard A, Stalon V (1986) Biosynthesis and metabolism of arginine in bacteria. Microbiol Rev 50:314–52.
5. Ruepp A, Soppa J (1993) Fermentative arginine degradation in *Halobacterium salinarium* (formerly *Halobacterium halobium*): genes, gene products, and transcripts of the arcRACB gene cluster. Plant Physiol 101:429–34.
6. Ludwig RA (1992) Arabidopsis chloroplasts dissimilate L-arginine and L-citrulline for use as N source. Mol Biochem Parasitol 51:29–36.
7. Schofield PJ, Edwards MR, Matthews J, Wilson JR (1992) The pathway of arginine catabolism in *Giardia intestinalis*. Mol Biochem Parasitol 51:29–36.
8. Yarlett N, Lindmark DG, Goldberg B, Moharrami MA, Bacchi CJ (1994) Subcellular localization of the enzymes of the arginine dihydrolase pathway in *Trichomonas vaginalis* and *Tritrichomonas foetus*. J Eukaryot Microbiol 41:554–9.
9. Pollack JD (1997). *Mycoplasm*a genes: a case for reflective annotation. Trends Microbiol. 5, 413–419.
10. Stalon V, Ramos F, Piérard A, Wiame JM (1967) The occurrence of a catabolic and an anabolic ornithine carbamoyltransferase in *Pseudomonas*. Biochim Biophys Acta 139:91–7.
11. Vander Wauven C, Piérard A, Kley-Raymann M, Haas D (1984) *Pseudomonas aeruginosa* mutants affected in anaerobic growth on arginine: evidence for a four-gene cluster encoding the arginine deiminase pathway. J Bacteriol 160:928–34.
12. Uriarte M, Marina A, Ramón-Maiques S, Fita I, Rubio V (1999) The carbamoyl-phosphate synthetase of *Pyrococcus furiosus* is enzymologically and structurally a carbamate kinase. J Biol Chem 274:16295–303.
13. Knodler LA, Sekyere EO, Stewart TS, Schofield PJ, Edwards MR (1998) Cloning and expression of a prokaryotic enzyme, arginine deiminase, from a primitive eukaryote *Giardia intestinalis*. J Biol Chem 273:4470–7.
14. Biagini GA, Yarlett N, Ball GE, Billetz AC, Lindmark DG, et al. (2003) Bacterial-like energy metabolism in the amitochondriate protozoon *Hexamita inflata*. Mol Biochem Parasitol 128:11–9.
15. Baur H, Luethi E, Stalon V, Mercenier A, Haas D (1989) Sequence analysis and expression of the arginine-deiminase and carbamate-kinase genes of *Pseudomonas aeruginosa*. Eur J Biochem 179:53–60.
16. Gamper M, Zimmermann A, Haas D (1991) Anaerobic regulation of transcription initiation in the arcDABC operon of *Pseudomonas aeruginosa*. J Bacteriol 173:4742–50.
17. Lüthi E, Mercenier A, Haas D (1986) The arcABC operon required for fermentative growth of *Pseudomonas aeruginosa* on arginine: Tn5-751-assisted cloning and localization of structural genes. J Gen Microbiol 132:2667–75.
18. Smith RS, Iglewski BH (2003) P. aeruginosa quorum-sensing systems and virulence. Curr Opin Microbiol 6:56–60.
19. Dillon BJ, Holtsberg FW, Ensor CM, Bomalaski JS, Clark MA (2002) Biochemical characterization of the arginine degrading enzymes arginase and arginine deiminase and their effect on nitric oxide production. Med Sci Monit 8: BR248–53.
20. Miyazaki K, Takaku H, Umeda M, Fujita T, Huang WD, et al. (1990) Potent growth inhibition of human tumor cells in culture by arginine deiminase purified from a culture medium of a *Mycoplasma*-infected cell line. Cancer Res 50:4522–7.
21. Philip R, Campbell E, Wheatley DN (2003) Arginine deprivation, growth inhibition and tumour cell death: 2. Enzymatic degradation of arginine in normal and malignant cell cultures. Br J Cancer 88:613–23.
22. Terayama H, Koji T, Kontani M, Okumoto T (1982) Arginase as an inhibitory principle in liver plasma membranes arresting the growth of various mammalian cells in vitro. Biochim Biophys Acta 720:188–92.
23. Galkin A, Kulakova L, Sarikaya E, Lim K, Howard A, et al. (2004) Structural insight into arginine degradation by arginine deiminase, an antibacterial and parasite drug target. J Biol Chem 279:14001–8.
24. Galkin A, Lu X, Dunaway-Mariano D, Herzberg O (2005) Crystal structures representing the Michaelis complex and the thiouronium reaction intermediate of *Pseudomonas aeruginosa* arginine deiminase. J Biol Chem 280:34080–7.
25. Das K, Butler GH, Kwiatkowski V, Clark AD Jr, Yadav P, et al. (2004) Crystal structures of arginine deiminase with covalent reaction intermediates; implications for catalytic mechanism. Structure 12:657–67.
26. Falmagne P, Portetelle D, Stalon V (1985) Immunological and structural relatedness of catabolic ornithine carbamoyltransferases and the anabolic enzymes of enterobacteria. J. Bacteriol 161:714–9.
27. Brady BS, Hyman BC, Lovatt CJ (2010) Regulation of CPSase, ACTase, and OCTase genes in *Medicago truncatula*: Implications for carbamoylphosphate synthesis and allocation to pyrimidine and arginine de novo biosynthesis. Gene 462:18–25.
28. Díaz-Muñoz M, Hernández-Muñoz R (2010) Molecular and biochemical features of the mitochondrial enzyme ornithine transcarbamylase: a possible new role as a signaling factor. Curr Med Chem 17:2253–60.
29. Houghton JE, Bencini DA, O'Donovan GA, Wild JR (1984) Protein differentiation: a comparison of aspartate transcarbamoylase and ornithine transcarbamoylase from *Escherichia coli* K-12. Proc Natl Acad Sci U S A 81:4864–8.

30. Honzatko RB, Crawford JL, Monaco HL, Ladner JE, Ewards BF, et al. (1982) Crystal and molecular structures of native and CTP-liganded aspartate carbamoyltransferase from *Escherichia coli*. J Mol Biol 160:219–63.
31. Villeret V, Tricot C, Stalon V, Dideberg O (1995) Crystal structure of *Pseudomonas aeruginosa* catabolic ornithine transcarbamoylase at 3.0-A resolution: a different oligomeric organization in the transcarbamoylase family. Proc Natl Acad Sci U S A 92:10762–6.
32. Legrain C, Stalon V, Noullez JP, Mercenier A, Simon JP, et al. (1977) Structure and function of ornithine carbamoyltransferases. Eur J Biochem 80:401–9.
33. de las Rivas B, Fox GC, Angulo I, Ripoll MM, Rodríguez H, et al. (2009) Crystal structure of the hexameric catabolic ornithine transcarbamylase from *Lactobacillus hilgardii*: Structural insights into the oligomeric assembly and metal binding. J Mol Biol 393:425–34.
34. Villeret V, Clantin B, Tricot C, Legrain C, Roovers M, et al. (1998) The crystal structure of *Pyrococcus furiosus* ornithine carbamoyltransferase reveals a key role for oligomerization in enzyme stability at extremely high temperatures. Proc Natl Acad Sci U S A 95:2801–6.
35. Baur H, Tricot C, Stalon V, Haas D (1990) Converting catabolic ornithine carbamoyltransferase to an anabolic enzyme. J Biol Chem 265:14728–31.
36. Abdelal AT (1979) Arginine catabolism by microorganisms. Annu Rev Microbiol 33:139–68.
37. Simon JP, Stalon V (1982) Enzymes of agmatine degradation and the control of their synthesis in *Streptococcus faecalis*. J Bacteriol 152:676–81.
38. Griswold AR, Jameson-Lee M, Burne RA (2006) Regulation and physiologic significance of the agmatine deiminase system of *Streptococcus mutans* UA159. J Bacteriol 188:834–41.
39. Vander Wauven C, Simon JP, Slos P, Stalon V (1986) Control of enzyme synthesis in the oxalurate catabolic pathway of *Streptococcus faecalis* ATCC 11700: evidence for the existence of a third carbamate kinase. Arch Microbiol 145:386–90.
40. Cusa E, Obradors N, Baldomà L, Badía J, Aguilar J (1999) Genetic analysis of a chromosomal region containing genes required for assimilation of allantoin nitrogen and linked glyoxylate metabolism in *Escherichia coli*. J Bacteriol 181:7479–84.
41. Linstead D, Cranshaw MA (1983) The pathway of arginine catabolism in the parasitic flagellate *Trichomonas vaginalis*. Mol Biochem Parasitol 8:241–52.
42. Ramón-Maiques S, Marina A, Uriarte M, Fita I, Rubio V (2000) The 1.5 A resolution crystal structure of the carbamate kinase-like carbamoyl phosphate synthetase from the hyperthermophilic Archaeon *Pyrococcus furiosus*, bound to ADP, confirms that this thermostable enzyme is a carbamate kinase, and provides insight into substrate binding and stability in carbamate kinases. J Mol Biol 299:463–76.
43. Ramón-Maiques S, Marina A, Guinot A, Gil-Ortiz F, Uriarte M, et al. (2010) Substrate binding and catalysis in carbamate kinase ascertained by crystallographic and site-directed mutagenesis studies: movements and significance of a unique globular subdomain of this key enzyme for fermentative ATP production in bacteria. J Mol Biol 397:1261–75.
44. Marina A, Uriarte M, Barcelona B, Fresquet V, Cervera J, et al. (1998) Carbamate kinase from *Enterococcus faecalis* and *Enterococcus faecium* – cloning of the genes, studies on the enzyme expressed in Escherichia coli, and sequence similarity with N-acetyl-L-glutamate kinase. Eur J Biochem 253:280–91.
45. Planell R (2008) PhD Thesis, Universitat Autònoma Barcelona.
46. Humm A, Fritsche E, Steinbacher S, Huber R (1997) Crystal structure and mechanism of human L-arginine: glycine amidinotransferase: a mitochondrial enzyme involved in creatine biosynthesis. EMBO J 16:3373–85.
47. Murray-Rust J, Leiper J, McAlister M, Phelan J, Tilley S, et al. (2001) Structural insights into the hydrolysis of cellular nitric oxide synthase inhibitors by dimethylarginine dimethylaminohydrolase. *Nat Struct Biol* 8:679–83.
48. Llácer JL, Polo LM, Tavárez S, Alarcón B, Hilario R, et al. (2007) The gene cluster for agmatine catabolism of *Enterococcus faecalis*: study of recombinant putrescine transcarbamylase and agmatine deiminase and a snapshot of agmatine deiminase catalyzing its reaction. J Bacteriol 189:1254–65.
49. Massant J, Wouters J, Glansdorff N (2003) Refined structure of *Pyrococcus furiosus* ornithine carbamoyltransferase at 1.87 A. Acta Crystallogr D Biol Crystallogr 59:2140–9.
50. Clantin B, Tricot C, Lonhienne T, Stalon V, Villeret V (2001) Probing the role of oligomerization in the high thermal stability of *Pyrococcus furiosus* ornithine carbamoyltransferase by site-specific mutants. Eur J Biochem 268:3937–42.
51. Langley DB, Templeton MD, Fields BA, Mitchell RE, Collyer CA (2000) Mechanism of inactivation of ornithine transcarbamoylase by Ndelta -(N'-Sulfodiaminophosphinyl)-L-ornithine, a true transition state analogue? Crystal structure and implications for catalytic mechanism. J Biol Chem 275:20012–9.
52. Sankaranarayanan R, Cherney MM, Cherney LT, Garen CR, Moradian F, et al. (2008) The crystal structures of ornithine carbamoyltransferase from *Mycobacterium tuberculosis* and its ternary complex with carbamoyl phosphate and L-norvaline reveal the enzyme's catalytic mechanism. J Mol Biol 375:1052–63.
53. Nguyen VT, Baker DP, Tricot C, Baur H, Villeret V, et al. (1996) Catabolic ornithine carbamoyltransferase of *Pseudomonas aeruginosa*. Importance of the N-terminal region for dodecameric structure and homotropic carbamoylphosphate cooperativity. Eur J Biochem 236:283–93.
54. Mouz N, Tricot C, Ebel C, Petillot Y, Stalon V, et al. (1996) Use of a designed fusion protein dissociates allosteric properties from the dodecameric state of Pseudomonas aeruginosa catabolic ornithine carbamoyltransferase. Proc Natl Acad Sci U S A 93:9414–9.
55. Massant J, Glansdorff N (2004) Metabolic channelling of carbamoyl phosphate in the hyperthermophilic archaeon *Pyrococcus furiosus*: dynamic enzyme-enzyme interactions involved in the formation of the channelling complex. Biochem Soc Trans 32:306–9.
56. Galkin A, Kulakova L, Wu R, Nash TE, Dunaway-Mariano D, et al. (2010) X-ray structure and characterization of carbamate kinase fromthe human parasite Giardia lamblia. Acta Crystallogr Sect F Struct Biol Cryst Commun 66:386–90.
57. Pich O, Burgos O, Planell R, Querol E, Piñol J (2006) Comparative analysis of antibiotic resistance gene markers in *Mycoplasma genitalium*: application to studies of the minimal gene complement. Microbiology 152:519–527.
58. Kabsch W (2010) XDS. Acta Crystallogr D Biol Crystallogr 66, 125–132.
59. Winn MD, Ballard CC, Cowtan KD, Dodson EJ, Emsley P, et al. (2011) Overview of the CCP4 suite and current developments. Acta Crystallogr D Biol Crystallogr 67:235–242.
60. Emsley P, Lohkamp B, Scott WG, Cowtan K (2010) Features and development of Coot. Acta Crystallogr D Biol Crystallogr 66: 486–501.
61. Brunger AT (2007) Version 1.2 of the Crystallography and NMR system. Nat Protoc 2: 2728–2733.
62. Adams PD, Afonine PV, Bunkoczi G, Chen VB, Davis IW, et al. (2010) PHENIX: a comprehensive Python-based system for macromolecular structure solution. Acta Crystallogr D Biol Crystallogr 66:213–221.
63. Schrödinger LLC (2010) The PyMOL Molecular Graphics System, Version 1.3.

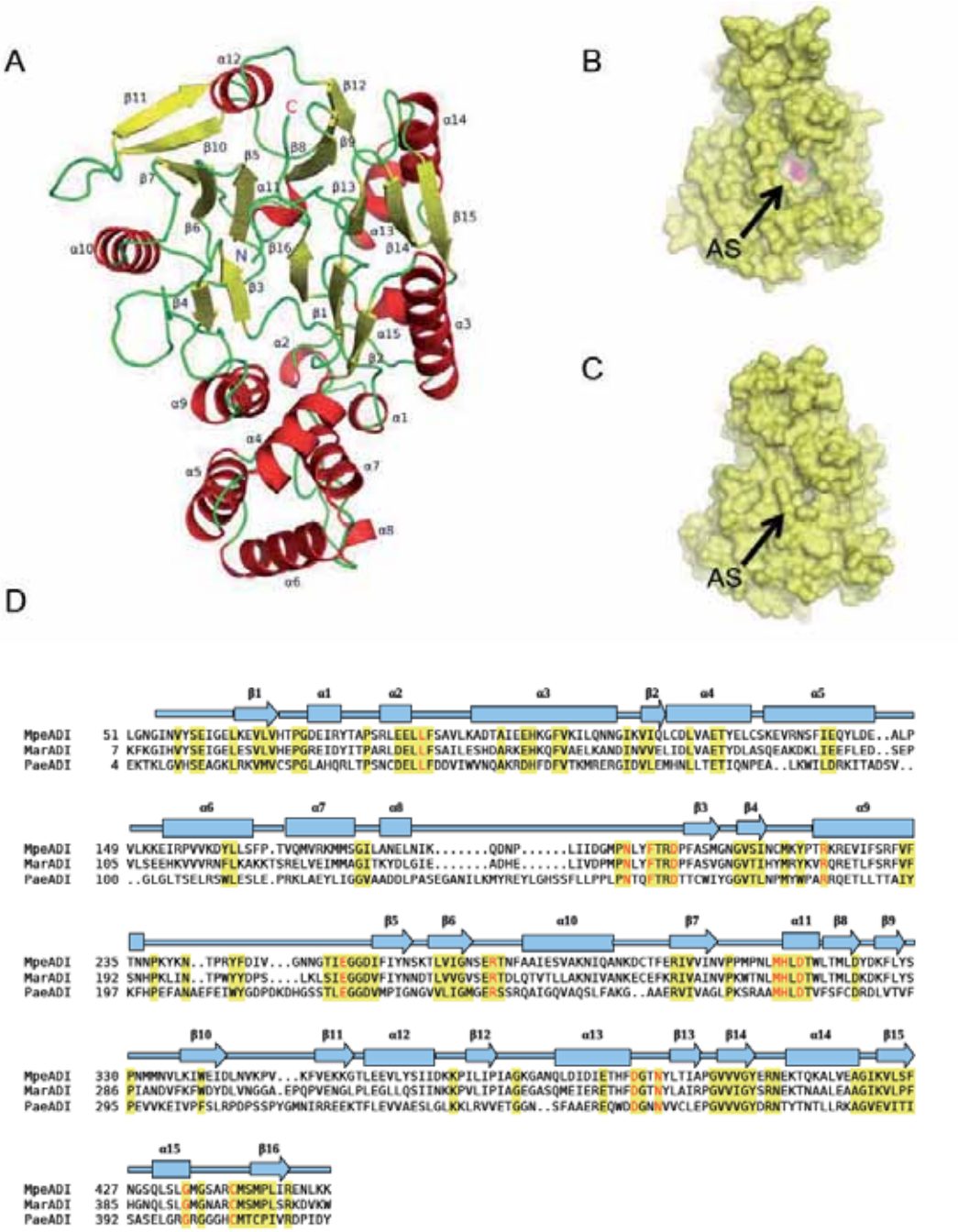


**Supplemental figure (S1). ADI** structure **and sequence alignment.**

Ribbon representation of the ADI structure from*Mycoplasma penetrans*. The α-helix and β-strands are represented in red and golden, respectively, and are labeled sequentially from N-terminus. (B) Surface representation of ADI from *M.penetrans*. AS indicates the active site pocket. (C) Surface representation of ADI from*M.arginini* (PDB code) in complex with arginine in the active site (colored in magenta). AS indicates the active site pocket. (D) Topology-based sequence alignment of ADI from*Mycomplasma penetrans*, *Mycoplasma arginini* and *Pseudomonas aeruginosa*. The secondary structural elements are labelled and shown above the sequence as rectangles or arrows for α-helix and β-strands, respectively. Active site residues are colored in red. Identical or highly conserved residues are highlighted in yellow.

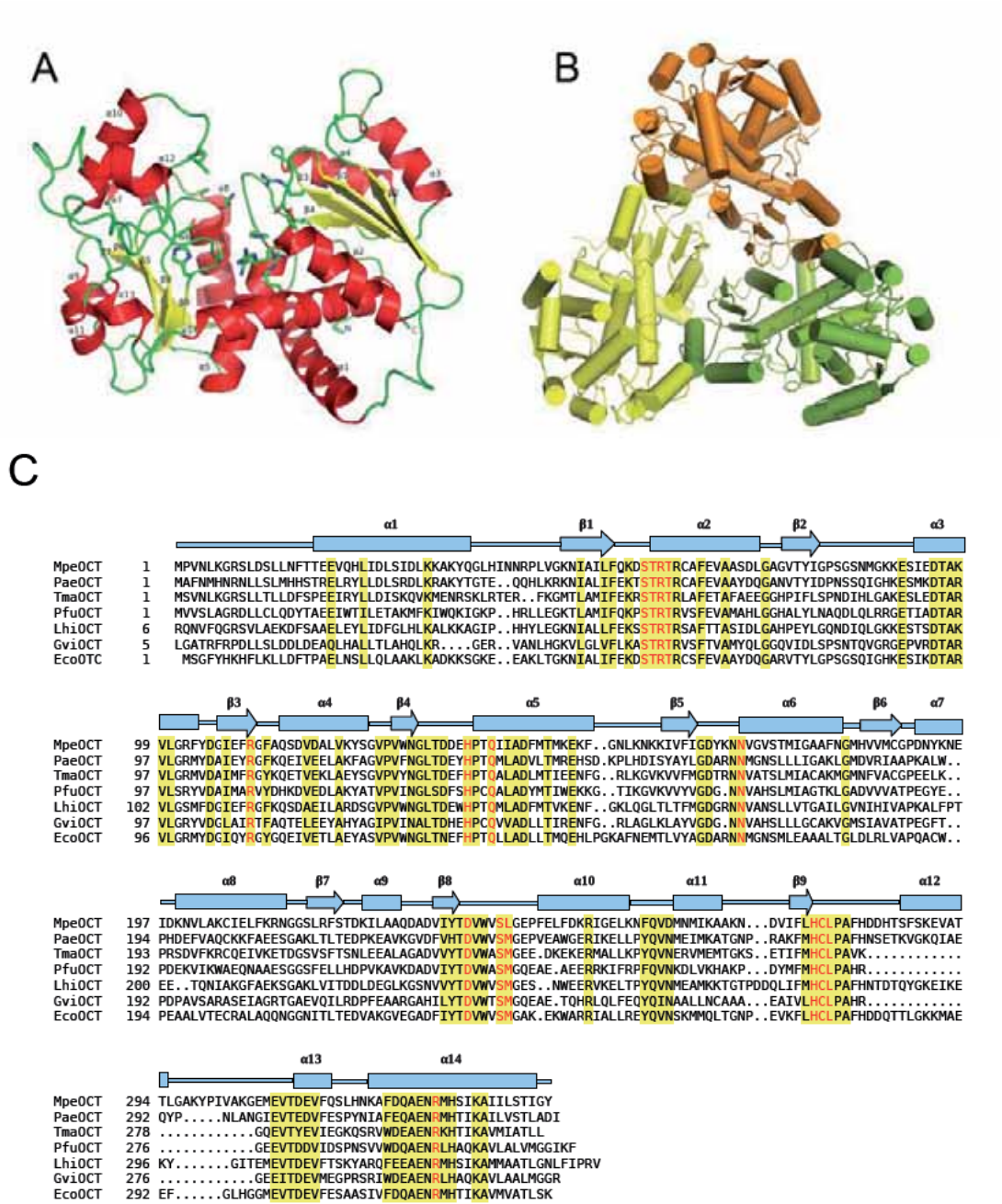


**Supplemental figure (S2). OTC structure and sequence alignment.**

(A) Ribbon representation of the structure of the OTC monomer from *Mycoplasma penetrans*. The α-helix and β-strands are represented in red and golden, respectively, and are labeled sequentially from the N-terminus. Residues involved in the active-site are shown in stick representation. (B) Ribbon representation of the OTC homotrimer structure. (C) Topology-based sequence alignment of OTC from *Mycoplasma penetrans*, *Pseudomonas aeruginosa*, *Themortoga maritima*, *Pyrococcus furiosus*, *Lactobacillus hilgardii*, *Gleobacter violacius* and *Escherichia coli*. The secondary structural elements are labeled and shown above the sequence as rectangles or arrows for α-helices or for β- strands, respectively. Active site residues are colored in red. Identical or highly conserved residues are highlighted in yellow.

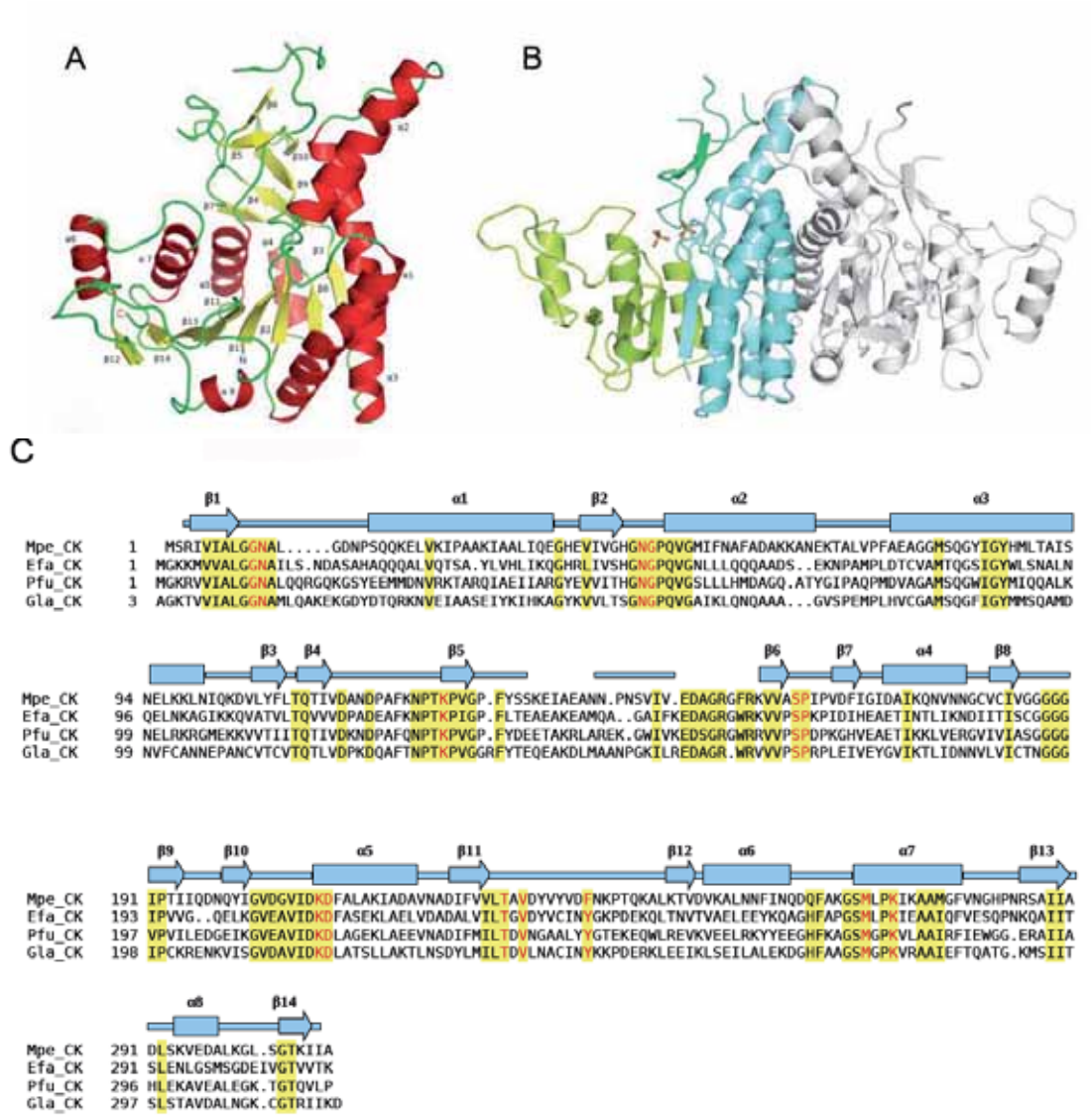


**Supplemental figure (S3). Structure of the CK from M. penetrans and sequence alignment.**

(A) Ribbon representation of CK from *Mycoplasma penetrans*. The α-helix and β-strands are represented in red and golden, respectively, and are labeled sequentially from the N-terminus. Residues involved in the active-site are shown in stick representation. (B) Ribbon representation of the dimer of CK. In one of the monomers, the N-terminal domain is in colored in light blue, the C-terminal domain in forest green and the PSD domain in lime green. The two sulfate ions are shown in stick representation. (D) Topology-based sequence alignment of CK from *Mycoplasma penetrans*,*Enterococcus faecalis*, *Pyrococcus furiosus* and *Giardia lamblia*. The secondary structural elements are labeled and shown above the sequence as rectangles or arrows for α- helices or forβ-strands, respectively. Active site residues are colored in red. Identical or highly conserved residues are highlighted in yellow.

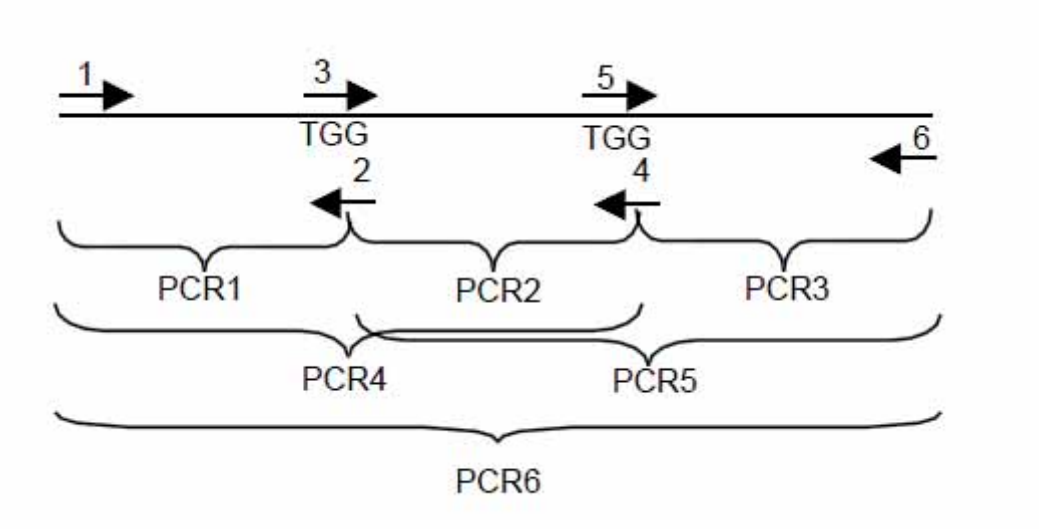


**Supplemental figure (S4). Mutagenesis strategy.**

Scheme illustrating the strategy followed to change the two TGA, coding for tryptophan in *M. penetrans*, by TGG codons before the heterologous expression of*arc*A (ADI) and *arc*B (OTC) genes in *E. coli*. Numbered arrows indicate the primers (see Table S1 for primer sequences and features). The successive six PCR amplifications carried out are also indicated. Cloning of *arc*C gene, which does not contain any TGA codon, was performed in a single reaction (PCR6) using primers 1 and 6.

| Primer | Sequence (5'- 3') |
|---|---|
| Arc1‡ | GTCGACCCACATGAGCTTAAAGGGATAG |
| Arc2‡ | GTCGACTACTTGTTGGAGCTTGAGAAATTC |
| adi-1 | CATATGTTGGTTATTACAATTGCACTAAATAT |
| adi-2* | CTAACATTGTTAA**c**CAAGTATCTAAATGCATTAG |
| adi-3* | CTAATGCATTTAGATACTTG**g**TTAACAATGTTAG |
| adi-4* | GGTTTAACATTTAGATCAATTTC**c**CAAATCTTTAATACATTC |
| adi-5* | GAATGTATTAAAGATTTG**g**GAAATTGATCTAAATGTTAAACC |
| adi-6 | GGATCCTTATTTTTTTAAATTTTCTCTAATTAAAGG |
| adi-7 | CATATGATGAGTAGTATTGATAAAAATTCAC |
| otc-1 | CATATGATGCCAGTAAATTTAAAAGGAAGAAG |
| otc-2* | CTGTTAACCCATT**c**CAAACTGGAACTCCAG |
| otc-3* | CTGGAGTTCCAGTTTG**g**AATGGGTTAACAG |
| otc-4* | CTCCAAGAGATAC**c**CAAACGTCTGTATAG |
| otc-5* | CTATACAGACGTTTG**g**GTATCTCTTGGAG |
| otc-6 | GGATCCCTAGTAACCAATTGTAGACAGAATG |
| ck-1 | CATATGATGTCTAGAATTGTTATTGCTTTAG |
| ck-6 | GGATCCTTAAGCAATTATTTTTGTACCACTTAATC |

‡ Used to perform PCR amplification of the DNA fragment containing *arc*A, *arc*B, and *arc*C genes from *M. penetrans* genomic DNA.
* Mutagenic primers used to change the two TGA by TGG codons in each *arc*A and *arc*B coding sequence.

**Suplemental Table (S1) Primers.**

Underlining indicates the restriction sites introduced at the 5′ end of selected primers. A bold lowercase character indicates the changed base in mutagenic primers.

# 4. Discussion.

The results in this thesis include the structural analysis of the NIMA-pathway and of the ADI pathway. In both instances the role of protein-protein interactions, the functional implications of their association manner, and the importance of protein crystallization as a major structural technique have been explored.

Our studies in the NIMA-pathway include two crystal structures of LC8 with a peptide corresponding to the intrinsically disordered Nek9 LC8-binding motif with and without a phosphate on Ser944. These structures, together with other biophysical analysis techniques, have shed light into a novel regulatory mechanism that interferes with LC8 protein-protein interaction upon phosphorylation. Additionally, we also present three different crystal structures of the enzymes composing the ADI pathway in *M.penetrans*: arginine deiminase, ornithine carbamoyl transferase amd carbamate kinase. Different structural features are analyzed for each enzyme of the pathway. For instance, the dodecameric structure of OTC allows us to study in depth how the dodecameric assemble occurs and modifies between mesophyll and thermophile organisms.

## 4.1 Regulation of the DYNLL/LC8 binding to Nek9 by phosphorylation.

Phosphorylation is one of the most common post-translational modifications that occur within the cell. Phosphorylation/dephosphorylation cycles can regulate many protein-protein interactions, and therefore, many signaling pathways inside the cell [44,64]. Nek9 is a kinase involved in the control of early events of mitosis, which controls the formation of the mitotic spindle through the activation of the related kinases Nek6/7 [57,83]. Although DYNLL/LC8 was initially described as an accessory subunit of the large dynein motor complexes [103,114,115], it has been recently postulated to act as a dimerization hub in protein complexes promoting dimerization, structural stabilization of IDPs and could hence allosteric regulation in its binding partners in diverse complexes and networks [128]. The protein kinase Nek9 is one of these LC8 partners, it has been shown to interact with LC8 through a canonical consensus region located in a partially disordered region of the C-terminal tail. As a result of LC8 binding on Nek9, it has been proposed that LC8 negatively

controls the binding of Nek9 to Nek6/7 and consequently their activation cascade [63,64].Thus suggest that LC8 binding may have additional functions, besides oligomerization, in the context of specific complexes in the Nek9-Nek6/7 cassette. In this thesis, we have shown that Nek9 autophosphorylation on Ser944 weakens the interaction with LC8 and thus supports the idea that phosphorylation of LC8 binding partners can have a role in the regulation of the LC8 interaction *in vivo* [63].

It is proposed that LC8 acts as “chaperone-like” protein. During interaction with different partners, it can behave as a hub protein promoting dimerization, it can stabilize IDPs and it can also increase the α-helical content by stabilization of coiled-coil structures in proteins with coiled-coil regions next to the LC8 binding consensus motif. This is the case of dynein intermediate chain (DIC 1 and 2) and Swallow [145,192]. For the dynein intermediate chain, LC8 was first described to act as a cargo adapter, nonetheless the current view is that the dynein intermediate chain is partially disordered and gains structure upon binding to LC8, meanwhile the cargo binding ability is only indirectly affected by the binding to LC8 [146,192].

In the present thesis, our CD experiments show a high content of α-helical structure in the C-terminal region of Nek9 (from 893 to 974) (see figure 1, publication I), probably indicating the presence of the predicted coiled-coil structure [57]. This is supported by the higher ordered multimeric structures that appear during the gel filtration purification of the recombinant Nek9-CC protein [63]. In our LC8/Nek9-CC binding experiments, the comparison of the CD spectra of a mixture of the two proteins, LC8 and Nek9-CC constructs, and the sum of their individual spectra suggest variations in the composition of secondary structure elements. In particular, the increase in ellipticity at 222 nm may indicate changes in the β/α contain. These results are in agreement with crystal structures of LC8·peptide complexes, with the formation of an extra β-strand upon binding to LC8 [110].

Two point mutants for the LC8 consensus-binding motif perturb binding to LC8; the highly conserved Gln948 (Nek9-CC Q948A), and the phospho-mimetic mutation on Ser944 (Nek9-CC S944E). Individual CD spectra of both Nek9-CC point mutants display similar profiles as the wild-type form, probably

indicating the formation of a coiled-coil structure. However, the CD spectra of the mixture of LC8 with both Nek9-CC point mutants show differences in the CD profile compared with wild-type, in particular in the region around 222 nm. This reduction in the ellipticity probably indicates a decrease in the affinity of LC8 for both Nek9 mutants. Interestingly, the two point mutants display differences in the CD spectra in the region around 210 nm. In addition to the reduction of binding to LC8, these changes at 210 nm could also indicate changes in the stability of the predicted Nek9 coiled-coil, thus affecting the Nek9 oligomerization state, as suggested in previous experiments [63].

An interesting methodology optimized in this thesis in the measuring of the binding interaction of the complex LC8-Nek9 by measuring CD changes around the β-signal [110]. The increase of the ellipticity at 220 nm indicates a gain of β-structure produced by the binding of the Nek9 peptide. Identical CD titration experiments were carried out with the Nek9 peptide and with the Nek9 P-peptide. The 18-fold reduction in the binding constant with the Nek9 P-peptide measured from the CD titration experiments is a direct indication of the perturbation of the interaction produced by the presence of the phosphate group on Ser944.

Protein stability of the LC8 alone, LC8·peptide and LC8·P-peptide complexes was also analyzed by changes of the intrinsic fluorescence during thermal denaturation. The LC8 and its peptide-complexes unfold at the same temperature, but the major enthalpy of the complex between LC8 and the unmodified Nek9 peptide indicates a major energy released for the disruption of the complex. Moreover, the LC8 Nek9 P-peptide complex shares a similar enthalpy value with LC8 alone indicating that Nek9 P-peptide interacts weaker with the LC8 protein.

Finally, the thermodynamic values extracted from the isothermal titration calorimetry experiments (ITC) also show a 6-fold decrease of the dissociation constant (Kd) for the Nek9 P-peptide. This can be attributed basically to less favorable enthalpic interactions, probably indicating a reduction in the number of bonds formed in the complex and combined by a partial compensation from more favorable entropic interactions.

All these three different biophysical methods indicate a direct perturbation

of the complex between LC8 and Nek9 upon phosphorylation on Ser944.

In the present thesis crystals of LC8 with both Nek9 peptides (+ and – phosphate) were grown in a similar reservoir condition, but displayed different crystallographic space groups. Both crystal forms display a similar LC8 homodimeric structure established in the recent years by different structures, either in the apo form or in complex with peptides [61,103,104,106,110]. The interaction of both Nek9 peptides to LC8 is carried out by a similar β-like antiparallel strand from Gly941 to Thr949, forming a total number of eight backbone β-sheet hydrogen bonds between the Nek9 peptide and β3 strand of LC8. However, comparisons between the six LC8 monomers in the asymmetric unit indicate that the phosphate negative charge on Ser944 perturbs the interaction with LC8, displaying a high degree of flexibility that affects mainly the binding of the first half of the peptide, from positions −7 to −4 (Gly941 to Ser944, being Gln948 the position 0). The position of Ser944 in the LC8 binding motif of Nek9, located at -4, varies from Asp, Ser, Asn and Thr in the consensus sequence analysis for LC8 binding partners [61]. Interestingly, some of them are residues susceptible of being phosphorylated or residues with an inherent negative charge. The formation of fairly similar LC8·Nek9 complex structures for both peptides is due the high protein concentration in crystallization even with the lower affinity for the Nek9 P-peptide and the important binding differences described *in vivo* [63]. However, such high concentration of proteins is difficult to occur in the cellular context, and the reported Kd values strongly suggest that the differences between the unmodified and the Nek9 P-peptide are sufficient to perturb binding in vivo.

Detailed comparison of both LC8 complexes indicates a high conservation for most of the interactions. Nevertheless, structural differences include the backbone hydrogen bond of the carbonyl group of Gly941, which is not formed in some of the P-peptide molecules, and the hydrogen bond between Ser944 and LC8 Thr67, which is disrupted in all cases by the presence of the phosphate group at Ser944.

Moreover, structural superposition of the six different peptides found in the asymmetric unit show that the Nek9 P-peptides display a high degree of flexibility when compared with the unmodified Nek9 peptides, which displays an

almost identical superposition. This increase of flexibility displayed by the Nek9 P-peptide is more prominent at the N-terminal part of the P-peptide (from Val940 to His943). These results suggest that phosphorylation on Ser944, which is located at -4, affects the interaction of the Nek9 peptide to LC8 by producing a destabilization of the complex, mostly affecting positions from -7 to -4.

When comparing both structures, a shift in one of the LC8 monomers with respect to the other monomer comes out in the LC8 homodimer. This shift is produced in the LC8 homodimer structure upon binding to the Nek9 P-peptide. This shift might be attributed to the presence of a phosphate group at Ser944, in which its negative charge might somehow interfere in the dimer interface. It is possible that the lysine residues from the opposite subunit next to the phosphate group are affected by the negative charge of the phosphate group. We suggest that this movement in the homodimer quaternary structure upon Ser944 phosphorylation could be significant to perturb the binding and stability of the Nek9 peptide to LC8.

Accordingly, in addition to the biophysical experiments, the comparison of the two crystal structures can be summarized in a slight shift in the LC8 homodimer interface, in two disrupted hydrogen bonds in the Nek9 P-peptide complex and in a high flexibility of the bound Nek9 P-peptides, thus resulting in a binding reduction on LC8 upon Ser944 phosphorylation.

Interestingly, in agreement with Laura Regué's work [63] the binding reduction on LC8 upon Nek9 Ser944 phosphorylation totally disrupts the interaction *in vivo*. Considering that the significant but not restrictive *in vitro* $K_d$ decrease upon phosphorylation induces such changes *in vivo,* probably it entails an unknown direct or indirect environmental factor in *in vivo*. Taking into account the LC8 function as a hub protein in a wide variety of partners with high presence in the cell, like the dynein motor complex, and also the relative low concentration in the cell of major protein kinases, like Nek9, we suggest that slight changes of LC8 binding $K_d$ can result in a complete dissociation due to protein binding competition.

Regulation of protein-protein interaction by phosphorylation is one of the most common ways to regulate cellular signaling pathways. In the case of the

mitotic Nek9/Nek6/Nek7 cassette, LC8 seems to interfere in this pathway by a direct binding competition with the downstream kinases Nek6/7, regulation that can be reversed by direct phosphorylation on the interface between the two proteins. In the present work we provide *in vitro* experimental data directly indicating that phosphorylation can regulate the binding of LC8 to a particular protein partner, in this case, Nek9. The fact that LC8 has many of its multiple binding partners contain Ser/Thr residues in the consensus binding motifs and that it is ubiquitously present; suggest that phosphorylation on this motif might be a general mechanism of controlling LC8 interaction in different cellular contexts.

## 4.2 ADI pathway in *M.penetrans*.

In the present thesis we present the crystal structures of the three enzymes composing the ADI pathway: arginine deiminase (ADI, EC 3.5.3.6), ornithine carbamoyltransferase (OTC, EC 2.1.3.3) and carbamate kinase (CK, EC 2.7.2.2).

The arginine deiminase (ADI), which catalyzes the first step in the ADI pathway, has been crystallized in its apo-form. It displays an “open” conformation of the active site and differs from the previous substrate-bound structures of *Mycoplasma arginini* that represents the “closed” conformation. Based on results obtained by gel-filtration chromatography and crystallization, the biological unit can be considered to be a dimer. The occurrence of “open” and “closed” conformations are necessary to permit the correct catalytic reaction, which allows for the entrance and the release of the substrate and end product, respectively, following an induced-fit mechanism.

In our “open” structure of *M.penetrans* ADI, the carbonyl groups of Leu88 and Gly434 are moved 2 Å away from their binding positions with the amino group of the arginine substrate, whereas Asn198 is located in a similar position and Phe201 does not move from its location. Met312 needs to move approximately 3 Å to interact with the substrate during the catalytic reaction, and Arg223 and Arg276, which bind the carboxylate group of the arginine substrate, must undertake substantial movements of approximately 4 Å from their positions in the “open” to the “closed” conformations.

In summary, three loops, namely α9-β5, β6-α10 and β7-α11 (see figure 1,

publication II), containing some of the catalytic and binding residues of the active site pocket, are responsible for switching between the “open” and the “closed” conformation of the enzyme.

Two different crystal forms of the ornithine carbamoyltransferase (OTC) from *M.penetrans* have been solved. In both crystal forms the asymmetric unit is composed of four molecules, which is arranged in a dodecameric quaternary structure. This dodecameric structure was also confirmed by the PISA server (http://www.ebi.ac.uk/pdbe/pisa/) and based on gel filtration experiments, probably corresponds to the biological unit of the protein.

Only three OTCs have been reported to possess a similar dodecameric quaternary structure as *M.penetrans,* from *Pseudomonas aeruginosa* ([156]; PDB code 1ORT), from *Pyrococus furiosus* ([157]; PDB code 1ALS) and from *Thermotoga maritima* (PDB code 1VLV; only deposited). Remarkably, two of them are thermophiles, suggesting a potential role of the quaternary compact structures in high temperature protection in those environments. In all cases the dodecamer structure is formed by the interaction of four homotrimers disposed in a tetrahedral manner [56,157,193].

The interface between homotrimers is mainly formed by three α-helices (α1-helix) and the loop between α1-helix and β1-sheet from three monomers from the different catalytic trimers located around each 3-fold symmetry axis. The four known dodecameric structures do not share any sequence similarity. For example, in the *M.penetrans,* the OTC dodecamer interface forms an intermolecular network of hydrogen bonds between Asn42 and Asn43 from the three monomers, which is unique to the sequence of *M.penetrans* OTC. In the case of the *P.furiosus* OTC the interaction around the threefold symmetry axis is mainly hydrophobic presenting major interactions between Met29, Trp33 and Lys38 [157]; in the case of the *P.aeruginosa* OTC the threefold symmetry axis interface is basically charged and polar, with major contribution of Arg28, Arg32, Thr39 and Gln41 [156]; and in the case of *T.maritima* (PDB code 1VLV; only deposited) the threefold symmetry axis interface presents a mixture of polar and hydrophobic interactions. Thus, comparison of the four known dodecameric OTC structures results in a similar helical interface but with completely different chemical profiles of the residues involved in the three-fold interface and only

the relative positions of the main chain atoms can be superimposed.

Comparison of *M.penetrans* and *T.maritima* OTCs by using the PISA server displays a similar solvation free energy gain by forming the homotrimers interface (one to one) and also a similar number of hydrogen bonds and salt bridges in a analogous buried area (Table 4.1). In the case of the hyper-thermophillic *P.furiosus* OTC, its homotrimer interfaces differs substantially from the other dodecamers, its high protein affinity and reduced buried area increases the compactness and despite their diminished number hydrogen bonds, the connectivity increases by the formation of new hydrophobic interactions. Finally, for *P.aeruginosa* OTC, a mesophyll like *M.penetrans*, the number of salt bridges and hydrogen bonds are similar to *M.penetrans* but differs in decrease number of hydrophobic interactions. All dodecameric OTC studied in this thesis do not show any sequence homology but instead they have similar relative positions of the interacting residues.

In the case of *P.furiosus*, and probably also in *T.maritima,* the domecameric quaternary structure for OTC can be a consequence of the extreme thermal stability of these microorganisms. It has been suggested that the thermophilic stability properties of the *P.furiosus* OTC are the result of the hydrophobic interfaces between homotrimers [56,193]. Other features that differ significantly between thermophillic and mesophyll organisms proteins are the higher compactness and connectivity generally increasing the number of highly connected residues in thermophillic proteins [194]. In the case of *P.aeruginosa*, the dodecameric structure was firstly assumed to be directly involved in the allosteric mechanism of the enzyme, which displays a marked cooperativity for carbamoyl phosphate [156]. However later studies found than OTC homotrimers could also retain such cooperativity [195,196]. In any case, OTC high oligomerization structures might be connected to an increase in the efficiency of the reaction in the ADI pathway, by means of thermal protection, by quaternary structure-induced cooperativity or by increasing the local concentration of the carbamoyl phosphate achieving an efficient product/substrate transfer between enzymes. In this way, a tunnel mechanism between OTC and the next catabolic enzyme, carbamate kinase (CK), has been suggested as a means to protect carbamoyl phosphate from high

temperatures and enhancing the product transfer and reducing its life time in cytoplasm [189]. Taking into account that *M.penetrans* OTC homotrimers interface has similar properties than the thermophillic organism *T.maritima,* we suggest that the dodecamer assemble might be an important feature in a cell to increase the local concentration of the carbamoyl phosphate and to optimize the product transfer to CK enzyme, which has been shown to directly interact with OTC [188–190].

| **OTC homotrimers interface** | **Buried Area ($A^2$)** | **ΔiG (kcal/mol)** | **$N_{HB}$** | **$N_{SB}$** |
|---|---|---|---|---|
| *P.furiosus* | 604.1 | -8.3 | 3 | 5 |
| *T.maritima* | 703.1 | -3.4 | 8 | 2 |
| *M.penetrans* | 687.4 | -3.5 | 7 | 4 |
| *P.aeruginosa* | 737.1 | -0.6 | 8 | 1 |

**Table 4.1: OTCs engaged homotrimer interfaces physicochemical properties.**

Buried area indicates, in $Å^2$, the interface area calculated as difference in total accessible surface areas of isolated and interfacing structures divided by two. ΔiG indicates the solvation free energy gain upon formation of the interface, in kcal/mol. The value is calculated as difference in total solvation energies of isolated and interfacing structures. Negative ΔiG corresponds to hydrophobic interfaces, or positive protein affinity. This value does not include the effect of satisfied hydrogen bonds and salt bridges across the interface. $N_{HB}$ indicates the number of potential hydrogen bonds across the interface. Each hydrogen bond contributes about 0.5 kcal/mol into the free energy of protein binding. $N_{SB}$ indicates the number of potential salt bridges across the interface. Each salt bridge contributes about 0.3 kcal/mol into the free energy of protein binding.

Finally, the crystal structure of the *M.penetrans* carbamate kinase (CK), the last enzyme of the ADI pathway, has been determined. The structure displays a homodimer assembly organization, as predictions of the PISA server, supported by gel-filtration chromatography and reported in previous CK structures from other organisms. Our CK structure is bound to two sulfate ions and displays substantial differences compared to other reported CK structures, such as the complex CK-ADP from *P.furiosus* and *E.faecalis* ([184,186]; PDB codes 1E19 and 2WE5, respectively); and CK-$SO_4$ from *E.faecalis* ([186]; PDB code 2WE4).

A distinctive feature of the *M,penetrans* CK structure is the orientation of the PSD sub-domain. In the CK-$SO_4$ complex structure from *E.faecalis*, in which a sulfate ion occupies a similar position, or in the *G.lamblia* CK structure ([197]; PDB code 3KZF), where a glycerol molecule occupies the putative CP binding site, their PSD domain adopts the “closed” orientation. However, in our *M.penetrans* CK structure, despite the CP binding site being occupied by a sulfate ion, the PSD domain displays an “open” orientation. In fact, the orientation of the PSD domain in the *M.penetrans* CK resembles the PSD domains in the CK ADP-bound structures from *E.faecalis* and *P.furiosus*, in both cases without any sulfate ions occupying the CP binding site. Taking into account that the movement of the PSD domain between an “open” and “closed” orientation to interact with the carbamoyl phosphate (CP) molecules has been described to be an essential mechanism for the phosphoryl transfer between substrates [186], the *M.penetrans* CK structure, with an “open” orientation of the PSD domain and a sulfate ion occupying the CP binding site, might represent a structural snapshot of the binding of CP before the enzymatic reaction occurs. Otherwise, it could also be an example of the product complex before the release of the CP from the active site in the anabolic reaction of synthesis of the carbamoyl phosphate from carbamate [184].

# **5.** Conclusions

## 5.1 Publication I: Structural analysis of the regulation of the DYNLL/LC8 binding to Nek9 by phosphorylation.

5.1.1 Nek9 peptide binding to LC8 induces a β-strand formation on the LC8 binding motif, which is intrinsically disordered in solution.

5.1.2 Phosphorylation on Nek9 Ser944 induces a direct perturbation on the LC8 and Nek9 complex that results in a significant decrease of the dissociation constant (Kd).

5.1.3 The negative charge of the phosphate on Ser944 perturbs the interaction with LC8 by increasing the degree of flexibility of the N-terminal region of the Nek9 peptide (from Gly941 to Ser944).

5.1.4 Additionally, two interface hydrogen bonds are disrupted upon phosphorylation on Ser944, resulting in reduction of the binding to LC8.

5.1.5 LC8 binding to Nek9 produces changes in the predicted Nek9 coiled-coil structure, which can affect the Nek9 oligomerization state.

## 5.2 Publication II: Structural characterization of the enzymes composing the arginine deiminase pathway in *Mycoplasma penetrans.*

5.2.1 The crystal structure of the three enzymes of the ADI pathway in *Mycoplasma penetrans* has disclosed to particular features that eventually might provide new tools to interfere in the proliferation of this pathogenic organism in humans.

5.2.2 The “open” conformation of the crystal structure of arginine deiminase reveals the “induced fit” mechanism of the enzyme. Basically three loops containing some of the catalytic and binding residues of the active site pocket switch from the “open” to the “closed” conformation.

5.2.3 These three “mobile” loops are essentially shaping one side of the active site pocket, whereas the other side does not seem to undertake any substantial rearrangement upon substrate binding.

5.2.4 Ornitine transcarbamylase (OTC) displays a dodecameric structure, which has only been described in three other microorganisms, *P.aeruginosa, P.furiosus* and *T.maritima*. (homotrimers are the usual oligomeric form).

5.2.5 Our *M.penetrans* OTC shows a novel type of interface forming the dodecamer. In all organisms with dodecamer interfaces are different, not showing any sequence homology and displaying either charged or hydrophobic interactions.

5.2.6 We suggest that the OTC dodecamer assembly might be an important feature to increase the local concentration of the carbamoyl phosphate and improving the transfer to the CK enzyme.

5.2.7 The crystal structure of CK contains two sulfate ions in the active site pocket, mimicking the binding of the β- and γ-phosphate of the ATP product molecule before the phosphate transfer.

5.2.8 Interestingly, in *M.penetrans* CK structure the position of the mobile PSD domain is in an “open” and non-catalytic conformation, despite the carbamoyl phosphate binding site being occupied by a sulfate ion, and might represent a structural snapshot of the binding of the substrates before catalysis.

## **6.** References.

1. Nelson DL, Cox MM (2004) Lehninger Principles of Biochemistry, Fourth Edition with CDROM. W. H. Freeman. Available: http://www.amazon.com/Lehninger-Principles-Biochemistry-Fourth-Edition/dp/071676265X. Accessed 3 February 2014.

2. Crick F (1970) Central dogma of molecular biology. Nature 227: 561–563. Available: http://www.ncbi.nlm.nih.gov/pubmed/4913914. Accessed 3 February 2014.

3. Murray RK, Bender DA, Botham KM, Kennelly PJ, Rodwell VW, et al. (2012) Harpers Illustrated Biochemistry (Lange Medical Book). McGraw-Hill Medical. Available: http://www.amazon.com/Harpers-Illustrated-Biochemistry-Lange-Medical/dp/007176576X. Accessed 5 February 2014.

4. Anfinsen CB (1973) Principles that govern the folding of protein chains. Science 181: 223–230. Available: http://www.ncbi.nlm.nih.gov/pubmed/4124164. Accessed 22 January 2014.

5. Kabsch W, Sander C (1983) Dictionary of protein secondary structure: pattern recognition of hydrogen-bonded and geometrical features. Biopolymers 22: 2577–2637. Available: http://www.ncbi.nlm.nih.gov/pubmed/6667333. Accessed 27 January 2014.

6. Introduction To Protein Structure 2 E Branden C And Tooze J - Free DOC downloads (n.d.). Available: http://ebookily.net/doc/introduction-to-protein-structure-2-e-branden-c-and-tooze-j. Accessed 5 February 2014.

7. Frank J (2006) Three-Dimensional Electron Microscopy of Macromolecular Assemblies: Visualization of Biological Molecules in Their Native State. Oxford University Press, USA. Available: http://www.amazon.com/Three-Dimensional-Electron-Microscopy-Macromolecular-Assemblies/dp/0195182189. Accessed 5 February 2014.

8. Bruce Alberts, Alexander Johnson, Julian Lewis, Martin Raff, Keith Roberts and PW (2002) Molecular Biology of the Cell. Available: http://www.ncbi.nlm.nih.gov/books/NBK21054/. Accessed 5 February 2014.

9. Uversky VN (2012) Intrinsically disordered proteins and novel strategies for drug discovery. Expert Opin Drug Discov 7: 475–488. Available: http://informahealthcare.com/doi/abs/10.1517/17460441.2012.686489. Accessed 5 February 2014.

10. Travaglini-Allocatelli C, Ivarsson Y, Jemth P, Gianni S (2009) Folding and stability of globular proteins and implications for function. Curr Opin Struct Biol 19: 3–7. Available: http://www.ncbi.nlm.nih.gov/pubmed/19157852. Accessed 5 February 2014.

11. Karp G (n.d.) Cell and Molecular Biology: Concepts and Experiments (Karp, Cell and Molecular Biology). Wiley. Available: http://www.amazon.com/Cell-Molecular-Biology-Concepts-Experiments/dp/0470483377. Accessed 5 February 2014.

12. Miroshnikov KA, Marusich EI, Cerritelli ME, Cheng N, Hyde CC, et al. (1998) Engineering trimeric fibrous proteins based on bacteriophage T4 adhesins. Protein Eng 11: 329–332. Available: http://www.ncbi.nlm.nih.gov/pubmed/9680195. Accessed 5 February 2014.

13. Tompa P (2012) Intrinsically disordered proteins: a 10-year recap. Trends Biochem Sci 37: 509–516. Available: http://www.ncbi.nlm.nih.gov/pubmed/22989858. Accessed 20 January 2014.

14. Mathews CK, Holde KE van, Ahern KG (1999) Biochemistry. Addison Wesley Longman. Available: http://www.amazon.co.uk/Biochemistry-Christopher-K-Mathews/dp/0201702355. Accessed 5 February 2014.

15. Lodish H, Berk A, Kaiser CA, Krieger M, Scott MP, et al. (2007) Molecular Cell Biology (Lodish, Molecular Cell Biology). W. H. Freeman. Available: http://www.amazon.com/Molecular-Cell-Biology-Lodish/dp/0716776014. Accessed 5 February 2014.

16. Elgar G, Vavouri T (2008) Tuning in to the signals: noncoding sequence conservation in vertebrate genomes. Trends Genet 24: 344–352. Available: http://www.ncbi.nlm.nih.gov/pubmed/18514361. Accessed 24 January 2014.

17. Atwood T, Campbell P, Parish H, Smith T, Stirling J, et al. (n.d.) Oxford Dictionary of Biochemistry and Molecular Biology. Oxford University Press, USA. Available: http://www.amazon.com/Oxford-Dictionary-Biochemistry-Molecular-Biology/dp/0198529171. Accessed 5 February 2014.

18. Garrett RH, Grisham CM (1999) Biochemistry. Harcourt College Pub. Available: http://www.amazon.com/Biochemistry-Reginald-H-Garrett/dp/0030211875. Accessed 5 February 2014.

19. Michaelis L, Menten ML, Johnson KA, Goody RS (2011) The original Michaelis constant: translation of the 1913 Michaelis-Menten paper. Biochemistry 50: 8264–8269. Available: http://www.pubmedcentral.nih.gov/articlerender.fcgi?artid=3381512&tool=pmcentrez&rendertype=abstract. Accessed 30 January 2014.

20. Silverthorn DU (2012) Human Physiology: An Integrated Approach, Books a la Carte Edition (6th Edition). Pearson. Available: http://www.amazon.com/Human-Physiology-Integrated-Approach-Edition/dp/0321814835. Accessed 5 February 2014.

21. Campbell NA, Reece JB (2007) Biology. Pearson. Available: http://www.amazon.co.uk/Biology-Neil-A-Campbell/dp/0321536169. Accessed 5 February 2014.

22. Dhanasekaran N, Premkumar Reddy E (1998) Signaling by dual specificity kinases. Oncogene 17: 1447–1455. Available: http://www.ncbi.nlm.nih.gov/pubmed/9779990. Accessed 5 February 2014.

23. Knighton DR, Zheng JH, Ten Eyck LF, Xuong NH, Taylor SS, et al. (1991) Structure of a peptide inhibitor bound to the catalytic subunit of cyclic adenosine monophosphate-dependent protein kinase. Science 253: 414–420. Available: http://www.ncbi.nlm.nih.gov/pubmed/1862343. Accessed 5 February 2014.

24. Petsko DRGA (n.d.) Protein Structure and Function. Oxford University Press. Available: http://www.amazon.com/Protein-Structure-Function-Dagmar-Gregory/dp/0199556849. Accessed 5 February 2014.

25. Pawson T, Nash P (2000) Protein-protein interactions define specificity in signal transduction. Genes Dev 14: 1027–1047. Available: http://www.ncbi.nlm.nih.gov/pubmed/10809663. Accessed 5 February 2014.

26. Hardy J, Allsop D (1991) Amyloid deposition as the central event in the aetiology of Alzheimer's disease. Trends Pharmacol Sci 12: 383–388. Available: http://www.ncbi.nlm.nih.gov/pubmed/1763432. Accessed 5 February 2014.

27. Jones S, Thornton JM (1996) Principles of protein-protein interactions. Proc Natl Acad Sci U S A 93: 13–20. Available: http://www.pubmedcentral.nih.gov/articlerender.fcgi?artid=40170&tool=pmcentrez&rendertype=abstract. Accessed 3 February 2014.

28. Welchman RL, Gordon C, Mayer RJ (2005) Ubiquitin and ubiquitin-like proteins as multifunctional signals. Nat Rev Mol Cell Biol 6: 599–609. Available: http://www.ncbi.nlm.nih.gov/pubmed/16064136. Accessed 22 January 2014.

29. Westermarck J, Ivaska J, Corthals GL (2013) Identification of protein interactions involved in cellular signaling. Mol Cell Proteomics 12: 1752–1763. Available: http://www.ncbi.nlm.nih.gov/pubmed/23481661. Accessed 5 February 2014.

30. Yan C, Wu F, Jernigan RL, Dobbs D, Honavar V (2008) Characterization of protein-protein interfaces. Protein J 27: 59–70. Available: http://www.pubmedcentral.nih.gov/articlerender.fcgi?artid=2566606&tool=pmcentrez&rendertype=abstract. Accessed 5 February 2014.

31. Jones S, Thornton JM (1997) Analysis of protein-protein interaction sites using surface patches. J Mol Biol 272: 121–132. Available: http://www.ncbi.nlm.nih.gov/pubmed/9299342. Accessed 5 February 2014.

32. Chothia C, Janin J (1975) Principles of protein-protein recognition. Nature 256: 705–708. Available: http://www.ncbi.nlm.nih.gov/pubmed/1153006. Accessed 6 February 2014.

33. Janin J, Chothia C (1990) The structure of protein-protein recognition sites. J Biol Chem 265: 16027–16030. Available: http://www.ncbi.nlm.nih.gov/pubmed/2204619. Accessed 21 January 2014.

34. Phizicky EM, Fields S (1995) Protein-protein interactions: methods for detection and analysis. Microbiol Rev 59: 94–123. Available:

http://www.pubmedcentral.nih.gov/articlerender.fcgi?artid=239356&tool=pmcentrez&rendertype=abstract. Accessed 6 February 2014.

35. Wand AJ, Englander SW (1996) Protein complexes studied by NMR spectroscopy. Curr Opin Biotechnol 7: 403–408. Available: http://www.pubmedcentral.nih.gov/articlerender.fcgi?artid=3442359&tool=pmcentrez&rendertype=abstract. Accessed 6 February 2014.

36. Vinogradova O, Qin J (2012) NMR as a unique tool in assessment and complex determination of weak protein-protein interactions. Top Curr Chem 326: 35–45. Available: http://www.pubmedcentral.nih.gov/articlerender.fcgi?artid=3676910&tool=pmcentrez&rendertype=abstract. Accessed 6 February 2014.

37. Rajagopala S V, Sikorski P, Caufield JH, Tovchigrechko A, Uetz P (2012) Studying protein complexes by the yeast two-hybrid system. Methods 58: 392–399. Available: http://www.pubmedcentral.nih.gov/articlerender.fcgi?artid=3517932&tool=pmcentrez&rendertype=abstract. Accessed 6 February 2014.

38. Barillot E, Calzone L, Hupe P, Vert J-P, Zinovyev A (2012) Computational Systems Biology of Cancer. CRC Press. Available: http://books.google.com/books?id=7AgN224pgq4C&pgis=1. Accessed 10 May 2014.

39. Brettner LM, Masel J (2012) Protein stickiness, rather than number of functional protein-protein interactions, predicts expression noise and plasticity in yeast. BMC Syst Biol 6: 128. Available: http://www.pubmedcentral.nih.gov/articlerender.fcgi?artid=3527306&tool=pmcentrez&rendertype=abstract. Accessed 6 February 2014.

40. Wodak SJ, Vlasblom J, Turinsky AL, Pu S (2013) Protein-protein interaction networks: the puzzling riches. Curr Opin Struct Biol 23: 941–953. Available: http://www.ncbi.nlm.nih.gov/pubmed/24007795. Accessed 22 January 2014.

41. Greenfield NJ (2004) Circular dichroism analysis for protein-protein interactions. Methods Mol Biol 261: 55–78. Available: http://www.ncbi.nlm.nih.gov/pubmed/15064449. Accessed 6 February 2014.

42. Velazquez-Campoy A, Leavitt SA, Freire E (2004) Characterization of protein-protein interactions by isothermal titration calorimetry. Methods Mol Biol 261: 35–54. Available: http://www.ncbi.nlm.nih.gov/pubmed/15064448. Accessed 6 February 2014.

43. Petschnigg J, Snider J, Stagljar I (2011) Interactive proteomics research technologies: recent applications and advances. Curr Opin Biotechnol 22: 50–58. Available: http://www.ncbi.nlm.nih.gov/pubmed/20884196. Accessed 6 February 2014.

44. Russell RJ, Hough DW, Danson MJ, Taylor GL (1994) The crystal structure of citrate synthase from the thermophilic archaeon, Thermoplasma acidophilum. Structure 2:

1157–1167. Available: http://www.ncbi.nlm.nih.gov/pubmed/7704526. Accessed 6 February 2014.

45. Chan MK, Mukund S, Kletzin A, Adams MW, Rees DC (1995) Structure of a hyperthermophilic tungstopterin enzyme, aldehyde ferredoxin oxidoreductase. Science 267: 1463–1469. Available: http://www.ncbi.nlm.nih.gov/pubmed/7878465. Accessed 6 February 2014.

46. Delboni LF, Mande SC, Rentier-Delrue F, Mainfroid V, Turley S, et al. (1995) Crystal structure of recombinant triosephosphate isomerase from Bacillus stearothermophilus. An analysis of potential thermostability factors in six isomerases with known three-dimensional structures points to the importance of hydrophobic interactions. Protein Sci 4: 2594–2604. Available: http://www.pubmedcentral.nih.gov/articlerender.fcgi?artid=2143043&tool=pmcentrez&rendertype=abstract. Accessed 6 February 2014.

47. Korolev S, Nayal M, Barnes WM, Di Cera E, Waksman G (1995) Crystal structure of the large fragment of Thermus aquaticus DNA polymerase I at 2.5-A resolution: structural basis for thermostability. Proc Natl Acad Sci U S A 92: 9264–9268. Available: http://www.pubmedcentral.nih.gov/articlerender.fcgi?artid=40965&tool=pmcentrez&rendertype=abstract. Accessed 6 February 2014.

48. Burley SK, Petsko GA (1985) Aromatic-aromatic interaction: a mechanism of protein structure stabilization. Science 229: 23–28. Available: http://www.ncbi.nlm.nih.gov/pubmed/3892686. Accessed 6 February 2014.

49. Georis J, de Lemos Esteves F, Lamotte-Brasseur J, Bougnet V, Devreese B, et al. (2000) An additional aromatic interaction improves the thermostability and thermophilicity of a mesophilic family 11 xylanase: structural basis and molecular study. Protein Sci 9: 466–475. Available: http://www.pubmedcentral.nih.gov/articlerender.fcgi?artid=2144569&tool=pmcentrez&rendertype=abstract. Accessed 6 February 2014.

50. Yip KS, Britton KL, Stillman TJ, Lebbink J, de Vos WM, et al. (1998) Insights into the molecular basis of thermal stability from the analysis of ion-pair networks in the glutamate dehydrogenase family. Eur J Biochem 255: 336–346. Available: http://www.ncbi.nlm.nih.gov/pubmed/9716374. Accessed 6 February 2014.

51. Matsumura M, Signor G, Matthews BW (1989) Substantial increase of protein stability by multiple disulphide bonds. Nature 342: 291–293. Available: http://www.ncbi.nlm.nih.gov/pubmed/2812028. Accessed 6 February 2014.

52. Kohlhoff M, Dahm A, Hensel R (1996) Tetrameric triosephosphate isomerase from hyperthermophilic Archaea. FEBS Lett 383: 245–250. Available: http://www.ncbi.nlm.nih.gov/pubmed/8925906. Accessed 6 February 2014.

53. Aoki M, Uchiumi T, Tsuji E, Hachimori A (1998) Effect of replacement of His-118, His-125 and Trp-143 by alanine on the catalytic activity and subunit assembly of inorganic pyrophosphatase from thermophilic bacterium PS-3. Biochem J 331 ( Pt 1: 143–148.

Available: http://www.pubmedcentral.nih.gov/articlerender.fcgi?artid=1219331&tool=pmcentrez&rendertype=abstract. Accessed 6 February 2014.

54. Maes D, Zeelen JP, Thanki N, Beaucamp N, Alvarez M, et al. (1999) The crystal structure of triosephosphate isomerase (TIM) from Thermotoga maritima: a comparative thermostability structural analysis of ten different TIM structures. Proteins 37: 441–453. Available: http://www.ncbi.nlm.nih.gov/pubmed/10591103. Accessed 6 February 2014.

55. Vetriani C, Maeder DL, Tolliday N, Yip KS, Stillman TJ, et al. (1998) Protein thermostability above 100 degreesC: a key role for ionic interactions. Proc Natl Acad Sci U S A 95: 12300–12305. Available: http://www.pubmedcentral.nih.gov/articlerender.fcgi?artid=22826&tool=pmcentrez&rendertype=abstract. Accessed 6 February 2014.

56. Clantin B, Tricot C, Lonhienne T, Stalon V, Villeret V (2001) Probing the role of oligomerization in the high thermal stability of Pyrococcus furiosus ornithine carbamoyltransferase by site-specific mutants. Eur J Biochem 268: 3937–3942. Available: http://www.ncbi.nlm.nih.gov/pubmed/11453986. Accessed 6 February 2014.

57. Roig J, Mikhailov A, Belham C, Avruch J (2002) Nercc1, a mammalian NIMA-family kinase, binds the Ran GTPase and regulates mitotic progression. Genes Dev 16: 1640–1658. Available: http://www.pubmedcentral.nih.gov/articlerender.fcgi?artid=186374&tool=pmcentrez&rendertype=abstract. Accessed 6 February 2014.

58. O'Connell MJ, Krien MJE, Hunter T (2003) Never say never. The NIMA-related protein kinases in mitotic control. Trends Cell Biol 13: 221–228. Available: http://www.ncbi.nlm.nih.gov/pubmed/12742165. Accessed 6 February 2014.

59. Quarmby LM, Mahjoub MR (2005) Caught Nek-ing: cilia and centrioles. J Cell Sci 118: 5161–5169. Available: http://www.ncbi.nlm.nih.gov/pubmed/16280549. Accessed 6 February 2014.

60. O'Regan L, Blot J, Fry AM (2007) Mitotic regulation by NIMA-related kinases. Cell Div 2: 25. Available: http://www.pubmedcentral.nih.gov/articlerender.fcgi?artid=2018689&tool=pmcentrez&rendertype=abstract. Accessed 23 January 2014.

61. Rapali P, Szenes Á, Radnai L, Bakos A, Pál G, et al. (2011) DYNLL/LC8: a light chain subunit of the dynein motor complex and beyond. FEBS J 278: 2980–2996. Available: http://www.ncbi.nlm.nih.gov/pubmed/21777386. Accessed 25 January 2014.

62. Rapley J, Nicolàs M, Groen A, Regué L, Bertran MT, et al. (2008) The NIMA-family kinase Nek6 phosphorylates the kinesin Eg5 at a novel site necessary for mitotic spindle formation. J Cell Sci 121: 3912–3921. Available: http://www.ncbi.nlm.nih.gov/pubmed/19001501. Accessed 20 January 2014.

63. Regué L, Sdelci S, Bertran MT, Caelles C, Reverter D, et al. (2011) DYNLL/LC8 protein controls signal transduction through the Nek9/Nek6 signaling module by regulating Nek6 binding to Nek9. J Biol Chem 286: 18118–18129. Available: http://www.pubmedcentral.nih.gov/articlerender.fcgi?artid=3093884&tool=pmcentrez&rendertype=abstract. Accessed 27 January 2014.

64. Gallego P, Velazquez-Campoy A, Regué L, Roig J, Reverter D (2013) Structural analysis of the regulation of the DYNLL/LC8 binding to Nek9 by phosphorylation. J Biol Chem 288: 12283–12294. Available: http://www.ncbi.nlm.nih.gov/pubmed/23482567. Accessed 6 February 2014.

65. Morris NR (1975) Mitotic mutants of Aspergillus nidulans. Genet Res 26: 237–254. Available: http://www.ncbi.nlm.nih.gov/pubmed/773766. Accessed 20 January 2014.

66. Fry AM, Nigg EA (1995) Cell cycle. The NIMA kinase joins forces with Cdc2. Curr Biol 5: 1122–1125. Available: http://www.ncbi.nlm.nih.gov/pubmed/8548283. Accessed 6 February 2014.

67. Osmani SA, Ye XS (1996) Cell cycle regulation in Aspergillus by two protein kinases. Biochem J 317 ( Pt 3: 633–641. Available: http://www.pubmedcentral.nih.gov/articlerender.fcgi?artid=1217533&tool=pmcentrez&rendertype=abstract. Accessed 6 February 2014.

68. Parker JDK, Bradley BA, Mooers AO, Quarmby LM (2007) Phylogenetic analysis of the Neks reveals early diversification of ciliary-cell cycle kinases. PLoS One 2: e1076. Available: http://www.pubmedcentral.nih.gov/articlerender.fcgi?artid=2031824&tool=pmcentrez&rendertype=abstract. Accessed 6 February 2014.

69. Melixetian M, Klein DK, Sørensen CS, Helin K (2009) NEK11 regulates CDC25A degradation and the IR-induced G2/M checkpoint. Nat Cell Biol 11: 1247–1253. Available: http://www.ncbi.nlm.nih.gov/pubmed/19734889. Accessed 23 January 2014.

70. Shalom O, Shalva N, Altschuler Y, Motro B (2008) The mammalian Nek1 kinase is involved in primary cilium formation. FEBS Lett 582: 1465–1470. Available: http://www.ncbi.nlm.nih.gov/pubmed/18387364. Accessed 6 February 2014.

71. Shiba D, Manning DK, Koga H, Beier DR, Yokoyama T (2010) Inv acts as a molecular anchor for Nphp3 and Nek8 in the proximal segment of primary cilia. Cytoskeleton (Hoboken) 67: 112–119. Available: http://www.ncbi.nlm.nih.gov/pubmed/20169535. Accessed 6 February 2014.

72. Chang J, Baloh RH, Milbrandt J (2009) The NIMA-family kinase Nek3 regulates microtubule acetylation in neurons. J Cell Sci 122: 2274–2282. Available: http://www.pubmedcentral.nih.gov/articlerender.fcgi?artid=2723145&tool=pmcentrez&rendertype=abstract. Accessed 20 January 2014.

73. Doles J, Hemann MT (2010) Nek4 status differentially alters sensitivity to distinct microtubule poisons. Cancer Res 70: 1033–1041. Available:

http://www.pubmedcentral.nih.gov/articlerender.fcgi?artid=2946156&tool=pmcentrez&rendertype=abstract. Accessed 6 February 2014.

74. Pelegrini AL, Moura DJ, Brenner BL, Ledur PF, Maques GP, et al. (2010) Nek1 silencing slows down DNA repair and blocks DNA damage-induced cell cycle arrest. Mutagenesis 25: 447–454. Available: http://www.ncbi.nlm.nih.gov/pubmed/20501547. Accessed 6 February 2014.

75. Lee M-Y, Kim H-J, Kim M-A, Jee HJ, Kim AJ, et al. (2008) Nek6 is involved in G2/M phase cell cycle arrest through DNA damage-induced phosphorylation. Cell Cycle 7: 2705–2709. Available: http://www.pubmedcentral.nih.gov/articlerender.fcgi?artid=3769414&tool=pmcentrez&rendertype=abstract. Accessed 6 February 2014.

76. Moniz LS, Stambolic V (2011) Nek10 mediates G2/M cell cycle arrest and MEK autoactivation in response to UV irradiation. Mol Cell Biol 31: 30–42. Available: http://www.pubmedcentral.nih.gov/articlerender.fcgi?artid=3019845&tool=pmcentrez&rendertype=abstract. Accessed 6 February 2014.

77. Maiato H (2010) Mitosis: wisdom, knowledge, and information. Cell Mol Life Sci 67: 2141–2143. Available: http://www.ncbi.nlm.nih.gov/pubmed/20213271. Accessed 6 February 2014.

78. Trinkle-Mulcahy L, Lamond AI (2006) Mitotic phosphatases: no longer silent partners. Curr Opin Cell Biol 18: 623–631. Available: http://www.ncbi.nlm.nih.gov/pubmed/17030123. Accessed 3 February 2014.

79. Sagona AP, Stenmark H (2010) Cytokinesis and cancer. FEBS Lett 584: 2652–2661. Available: http://www.ncbi.nlm.nih.gov/pubmed/20371245. Accessed 30 January 2014.

80. Nigg EA (2001) Mitotic kinases as regulators of cell division and its checkpoints. Nat Rev Mol Cell Biol 2: 21–32. Available: http://www.ncbi.nlm.nih.gov/pubmed/11413462. Accessed 4 February 2014.

81. Salaun P, Rannou Y, Prigent C (2008) Cdk1, Plks, Auroras, and Neks: the mitotic bodyguards. Adv Exp Med Biol 617: 41–56. Available: http://www.pubmedcentral.nih.gov/articlerender.fcgi?artid=2533106&tool=pmcentrez&rendertype=abstract. Accessed 6 February 2014.

82. Simpson-Lavy KJ, Oren YS, Feine O, Sajman J, Listovsky T, et al. (2010) Fifteen years of APC/cyclosome: a short and impressive biography. Biochem Soc Trans 38: 78–82. Available: http://www.ncbi.nlm.nih.gov/pubmed/20074039. Accessed 6 February 2014.

83. Belham C, Roig J, Caldwell JA, Aoyama Y, Kemp BE, et al. (2003) A mitotic cascade of NIMA family kinases. Nercc1/Nek9 activates the Nek6 and Nek7 kinases. J Biol Chem 278: 34897–34909. Available: http://www.ncbi.nlm.nih.gov/pubmed/12840024. Accessed 3 February 2014.

84. Holland PM, Milne A, Garka K, Johnson RS, Willis C, et al. (2002) Purification, cloning, and characterization of Nek8, a novel NIMA-related kinase, and its candidate substrate Bicd2. J Biol Chem 277: 16229–16240. Available: http://www.ncbi.nlm.nih.gov/pubmed/11864968. Accessed 27 January 2014.

85. Roig J, Groen A, Caldwell J, Avruch J (2005) Active Nercc1 protein kinase concentrates at centrosomes early in mitosis and is necessary for proper spindle assembly. Mol Biol Cell 16: 4827–4840. Available: http://www.pubmedcentral.nih.gov/articlerender.fcgi?artid=1237086&tool=pmcentrez&rendertype=abstract. Accessed 6 February 2014.

86. Hadjebi O, Casas-Terradellas E, Garcia-Gonzalo FR, Rosa JL (2008) The RCC1 superfamily: from genes, to function, to disease. Biochim Biophys Acta 1783: 1467–1479. Available: http://www.ncbi.nlm.nih.gov/pubmed/18442486. Accessed 6 February 2014.

87. Tan BC-M, Lee S-C (2004) Nek9, a novel FACT-associated protein, modulates interphase progression. J Biol Chem 279: 9321–9330. Available: http://www.ncbi.nlm.nih.gov/pubmed/14660563. Accessed 6 February 2014.

88. Pelka P, Scimè A, Mandalfino C, Joch M, Abdulla P, et al. (2007) Adenovirus E1A proteins direct subcellular redistribution of Nek9, a NimA-related kinase. J Cell Physiol 212: 13–25. Available: http://www.ncbi.nlm.nih.gov/pubmed/17443675. Accessed 6 February 2014.

89. Bertran MT, Sdelci S, Regué L, Avruch J, Caelles C, et al. (2011) Nek9 is a Plk1-activated kinase that controls early centrosome separation through Nek6/7 and Eg5. EMBO J 30: 2634–2647. Available: http://www.pubmedcentral.nih.gov/articlerender.fcgi?artid=3155310&tool=pmcentrez&rendertype=abstract. Accessed 23 January 2014.

90. Wiese C, Zheng Y (2006) Microtubule nucleation: gamma-tubulin and beyond. J Cell Sci 119: 4143–4153. Available: http://www.ncbi.nlm.nih.gov/pubmed/17038541. Accessed 20 January 2014.

91. Tanenbaum ME, Macůrek L, Galjart N, Medema RH (2008) Dynein, Lis1 and CLIP-170 counteract Eg5-dependent centrosome separation during bipolar spindle assembly. EMBO J 27: 3235–3245. Available: http://www.pubmedcentral.nih.gov/articlerender.fcgi?artid=2609737&tool=pmcentrez&rendertype=abstract. Accessed 6 February 2014.

92. Ferenz NP, Paul R, Fagerstrom C, Mogilner A, Wadsworth P (2009) Dynein antagonizes eg5 by crosslinking and sliding antiparallel microtubules. Curr Biol 19: 1833–1838. Available: http://www.pubmedcentral.nih.gov/articlerender.fcgi?artid=2783793&tool=pmcentrez&rendertype=abstract. Accessed 6 February 2014.

93. Hoogenraad CC, Akhmanova A, Howell SA, Dortland BR, De Zeeuw CI, et al. (2001) Mammalian Golgi-associated Bicaudal-D2 functions in the dynein-dynactin pathway by interacting with these complexes. EMBO J 20: 4041–4054. Available:

http://www.pubmedcentral.nih.gov/articlerender.fcgi?artid=149157&tool=pmcentrez&rendertype=abstract. Accessed 6 February 2014.

94. Behrends C, Sowa ME, Gygi SP, Harper JW (2010) Network organization of the human autophagy system. Nature 466: 68–76. Available: http://www.pubmedcentral.nih.gov/articlerender.fcgi?artid=2901998&tool=pmcentrez&rendertype=abstract. Accessed 21 January 2014.

95. Pfister KK, Fay RB, Witman GB (1982) Purification and polypeptide composition of dynein ATPases from Chlamydomonas flagella. Cell Motil 2: 525–547. Available: http://www.ncbi.nlm.nih.gov/pubmed/6220806. Accessed 6 February 2014.

96. Wickstead B, Gull K (2007) Dyneins across eukaryotes: a comparative genomic analysis. Traffic 8: 1708–1721. Available: http://www.pubmedcentral.nih.gov/articlerender.fcgi?artid=2239267&tool=pmcentrez&rendertype=abstract. Accessed 21 January 2014.

97. Sakakibara H, Oiwa K (2011) Molecular organization and force-generating mechanism of dynein. FEBS J 278: 2964–2979. Available: http://www.ncbi.nlm.nih.gov/pubmed/21777385. Accessed 6 February 2014.

98. Pfister KK, Shah PR, Hummerich H, Russ A, Cotton J, et al. (2006) Genetic analysis of the cytoplasmic dynein subunit families. PLoS Genet 2: e1. Available: http://www.pubmedcentral.nih.gov/articlerender.fcgi?artid=1331979&tool=pmcentrez&rendertype=abstract. Accessed 27 January 2014.

99. Dick T, Ray K, Salz HK, Chia W (1996) Cytoplasmic dynein (ddlc1) mutations cause morphogenetic defects and apoptotic cell death in Drosophila melanogaster. Mol Cell Biol 16: 1966–1977. Available: http://www.pubmedcentral.nih.gov/articlerender.fcgi?artid=231184&tool=pmcentrez&rendertype=abstract. Accessed 6 February 2014.

100. Kamath RS, Fraser AG, Dong Y, Poulin G, Durbin R, et al. (2003) Systematic functional analysis of the Caenorhabditis elegans genome using RNAi. Nature 421: 231–237. Available: http://www.ncbi.nlm.nih.gov/pubmed/12529635. Accessed 22 January 2014.

101. Hall J, Karplus PA, Barbar E (2009) Multivalency in the assembly of intrinsically disordered Dynein intermediate chain. J Biol Chem 284: 33115–33121. Available: http://www.pubmedcentral.nih.gov/articlerender.fcgi?artid=2785153&tool=pmcentrez&rendertype=abstract. Accessed 25 January 2014.

102. Williams JC, Xie H, Hendrickson WA (2005) Crystal structure of dynein light chain TcTex-1. J Biol Chem 280: 21981–21986. Available: http://www.ncbi.nlm.nih.gov/pubmed/15701632. Accessed 6 February 2014.

103. Fan J, Zhang Q, Tochio H, Li M, Zhang M (2001) Structural basis of diverse sequence-dependent target recognition by the 8 kDa dynein light chain. J Mol Biol 306: 97–108. Available: http://www.ncbi.nlm.nih.gov/pubmed/11178896. Accessed 6 February 2014.

104. Benison G, Karplus PA, Barbar E (2008) The interplay of ligand binding and quaternary structure in the diverse interactions of dynein light chain LC8. J Mol Biol 384: 954–966. Available: http://www.ncbi.nlm.nih.gov/pubmed/18948118. Accessed 6 February 2014.

105. Day CL, Puthalakath H, Skea G, Strasser A, Barsukov I, et al. (2004) Localization of dynein light chains 1 and 2 and their pro-apoptotic ligands. Biochem J 377: 597–605. Available: http://www.pubmedcentral.nih.gov/articlerender.fcgi?artid=1223895&tool=pmcentrez&rendertype=abstract. Accessed 6 February 2014.

106. Lightcap CM, Sun S, Lear JD, Rodeck U, Polenova T, et al. (2008) Biochemical and structural characterization of the Pak1-LC8 interaction. J Biol Chem 283: 27314–27324. Available: http://www.pubmedcentral.nih.gov/articlerender.fcgi?artid=2556000&tool=pmcentrez&rendertype=abstract. Accessed 6 February 2014.

107. Vedadi M, Lew J, Artz J, Amani M, Zhao Y, et al. (2007) Genome-scale protein expression and structural biology of Plasmodium falciparum and related Apicomplexan organisms. Mol Biochem Parasitol 151: 100–110. Available: http://www.ncbi.nlm.nih.gov/pubmed/17125854. Accessed 24 January 2014.

108. Benison G, Karplus PA, Barbar E (2007) Structure and dynamics of LC8 complexes with KXTQT-motif peptides: swallow and dynein intermediate chain compete for a common site. J Mol Biol 371: 457–468. Available: http://www.ncbi.nlm.nih.gov/pubmed/17570393. Accessed 6 February 2014.

109. Benison G, Chiodo M, Karplus PA, Barbar E (2009) Structural, thermodynamic, and kinetic effects of a phosphomimetic mutation in dynein light chain LC8. Biochemistry 48: 11381–11389. Available: http://www.pubmedcentral.nih.gov/articlerender.fcgi?artid=2821902&tool=pmcentrez&rendertype=abstract. Accessed 6 February 2014.

110. Liang J, Jaffrey SR, Guo W, Snyder SH, Clardy J (1999) Structure of the PIN/LC8 dimer with a bound peptide. Nat Struct Biol 6: 735–740. Available: http://www.ncbi.nlm.nih.gov/pubmed/10426949. Accessed 6 February 2014.

111. Rapali P, Radnai L, Süveges D, Harmat V, Tölgyesi F, et al. (2011) Directed evolution reveals the binding motif preference of the LC8/DYNLL hub protein and predicts large numbers of novel binders in the human proteome. PLoS One 6: e18818. Available: http://www.pubmedcentral.nih.gov/articlerender.fcgi?artid=3078936&tool=pmcentrez&rendertype=abstract. Accessed 27 January 2014.

112. Song C, Wen W, Rayala SK, Chen M, Ma J, et al. (2008) Serine 88 phosphorylation of the 8-kDa dynein light chain 1 is a molecular switch for its dimerization status and functions. J Biol Chem 283: 4004–4013. Available: http://www.ncbi.nlm.nih.gov/pubmed/18084006. Accessed 6 February 2014.

113. Song Y, Benison G, Nyarko A, Hays TS, Barbar E (2007) Potential role for phosphorylation in differential regulation of the assembly of dynein light chains. J Biol

Chem 282: 17272–17279. Available: http://www.ncbi.nlm.nih.gov/pubmed/17428790. Accessed 6 February 2014.

114. Rodríguez-Crespo I, Yélamos B, Roncal F, Albar JP, Ortiz de Montellano PR, et al. (2001) Identification of novel cellular proteins that bind to the LC8 dynein light chain using a pepscan technique. FEBS Lett 503: 135–141. Available: http://www.ncbi.nlm.nih.gov/pubmed/11513870. Accessed 6 February 2014.

115. Lo KW, Naisbitt S, Fan JS, Sheng M, Zhang M (2001) The 8-kDa dynein light chain binds to its targets via a conserved (K/R)XTQT motif. J Biol Chem 276: 14059–14066. Available: http://www.ncbi.nlm.nih.gov/pubmed/11148209. Accessed 6 February 2014.

116. Hódi Z, Németh AL, Radnai L, Hetényi C, Schlett K, et al. (2006) Alternatively spliced exon B of myosin Va is essential for binding the tail-associated light chain shared by dynein. Biochemistry 45: 12582–12595. Available: http://www.ncbi.nlm.nih.gov/pubmed/17029413. Accessed 6 February 2014.

117. Wagner W, Fodor E, Ginsburg A, Hammer JA (2006) The binding of DYNLL2 to myosin Va requires alternatively spliced exon B and stabilizes a portion of the myosin's coiled-coil domain. Biochemistry 45: 11564–11577. Available: http://www.ncbi.nlm.nih.gov/pubmed/16981716. Accessed 6 February 2014.

118. García-Mayoral MF, Martínez-Moreno M, Albar JP, Rodríguez-Crespo I, Bruix M (2010) Structural basis for the interaction between dynein light chain 1 and the glutamate channel homolog GRINL1A. FEBS J 277: 2340–2350. Available: http://www.ncbi.nlm.nih.gov/pubmed/20412299. Accessed 6 February 2014.

119. Crooks GE, Hon G, Chandonia J-M, Brenner SE (2004) WebLogo: a sequence logo generator. Genome Res 14: 1188–1190. Available: http://www.pubmedcentral.nih.gov/articlerender.fcgi?artid=419797&tool=pmcentrez&rendertype=abstract. Accessed 24 January 2014.

120. Mammen M, Choi S-K, Whitesides GM (1998) Polyvalent Interactions in Biological Systems: Implications for Design and Use of Multivalent Ligands and Inhibitors. Angew Chemie Int Ed 37: 2754–2794. Available: http://doi.wiley.com/10.1002/(SICI)1521-3773(19981102)37:20<2754::AID-ANIE2754>3.0.CO;2-3. Accessed 6 February 2014.

121. Espindola FS, Suter DM, Partata LB, Cao T, Wolenski JS, et al. (2000) The light chain composition of chicken brain myosin-Va: calmodulin, myosin-II essential light chains, and 8-kDa dynein light chain/PIN. Cell Motil Cytoskeleton 47: 269–281. Available: http://www.ncbi.nlm.nih.gov/pubmed/11093248. Accessed 6 February 2014.

122. Lee KH, Lee S, Kim B, Chang S, Kim SW, et al. (2006) Dazl can bind to dynein motor complex and may play a role in transport of specific mRNAs. EMBO J 25: 4263–4270. Available: http://www.pubmedcentral.nih.gov/articlerender.fcgi?artid=1570426&tool=pmcentrez&rendertype=abstract. Accessed 6 February 2014.

123. Navarro C, Puthalakath H, Adams JM, Strasser A, Lehmann R (2004) Egalitarian binds dynein light chain to establish oocyte polarity and maintain oocyte fate. Nat Cell Biol 6: 427–435. Available: http://www.ncbi.nlm.nih.gov/pubmed/15077115. Accessed 6 February 2014.

124. Puthalakath H, Huang DC, O'Reilly LA, King SM, Strasser A (1999) The proapoptotic activity of the Bcl-2 family member Bim is regulated by interaction with the dynein motor complex. Mol Cell 3: 287–296. Available: http://www.ncbi.nlm.nih.gov/pubmed/10198631. Accessed 24 January 2014.

125. Williams JC, Roulhac PL, Roy AG, Vallee RB, Fitzgerald MC, et al. (2007) Structural and thermodynamic characterization of a cytoplasmic dynein light chain-intermediate chain complex. Proc Natl Acad Sci U S A 104: 10028–10033. Available: http://www.pubmedcentral.nih.gov/articlerender.fcgi?artid=1885999&tool=pmcentrez&rendertype=abstract. Accessed 6 February 2014.

126. Hall J, Hall A, Pursifull N, Barbar E (2008) Differences in dynamic structure of LC8 monomer, dimer, and dimer-peptide complexes. Biochemistry 47: 11940–11952. Available: http://www.ncbi.nlm.nih.gov/pubmed/18942858. Accessed 27 January 2014.

127. Wu H, Maciejewski MW, Takebe S, King SM (2005) Solution structure of the Tctex1 dimer reveals a mechanism for dynein-cargo interactions. Structure 13: 213–223. Available: http://www.ncbi.nlm.nih.gov/pubmed/15698565. Accessed 6 February 2014.

128. Barbar E (2008) Dynein light chain LC8 is a dimerization hub essential in diverse protein networks. Biochemistry 47: 503–508. Available: http://www.ncbi.nlm.nih.gov/pubmed/18092820. Accessed 27 January 2014.

129. Chen Y-M, Gerwin C, Sheng Z-H (2009) Dynein light chain LC8 regulates syntaphilin-mediated mitochondrial docking in axons. J Neurosci 29: 9429–9438. Available: http://www.ncbi.nlm.nih.gov/pubmed/19641106. Accessed 27 January 2014.

130. Fejtova A, Davydova D, Bischof F, Lazarevic V, Altrock WD, et al. (2009) Dynein light chain regulates axonal trafficking and synaptic levels of Bassoon. J Cell Biol 185: 341–355. Available: http://www.pubmedcentral.nih.gov/articlerender.fcgi?artid=2700376&tool=pmcentrez&rendertype=abstract. Accessed 22 January 2014.

131. Stelter P, Kunze R, Flemming D, Höpfner D, Diepholz M, et al. (2007) Molecular basis for the functional interaction of dynein light chain with the nuclear-pore complex. Nat Cell Biol 9: 788–796. Available: http://www.ncbi.nlm.nih.gov/pubmed/17546040. Accessed 25 January 2014.

132. Den Hollander P, Kumar R (2006) Dynein light chain 1 contributes to cell cycle progression by increasing cyclin-dependent kinase 2 activity in estrogen-stimulated cells. Cancer Res 66: 5941–5949. Available: http://www.ncbi.nlm.nih.gov/pubmed/16740735. Accessed 6 February 2014.

133. Nakano H, Funasaka T, Hashizume C, Wong RW (2010) Nucleoporin translocated promoter region (Tpr) associates with dynein complex, preventing chromosome lagging formation during mitosis. J Biol Chem 285: 10841–10849. Available: http://www.pubmedcentral.nih.gov/articlerender.fcgi?artid=2856290&tool=pmcentrez&rendertype=abstract. Accessed 6 February 2014.

134. Batlevi Y, Martin DN, Pandey UB, Simon CR, Powers CM, et al. (2010) Dynein light chain 1 is required for autophagy, protein clearance, and cell death in Drosophila. Proc Natl Acad Sci U S A 107: 742–747. Available: http://www.pubmedcentral.nih.gov/articlerender.fcgi?artid=2818958&tool=pmcentrez&rendertype=abstract. Accessed 20 January 2014.

135. Fimia GM, Stoykova A, Romagnoli A, Giunta L, Di Bartolomeo S, et al. (2007) Ambra1 regulates autophagy and development of the nervous system. Nature 447: 1121–1125. Available: http://www.ncbi.nlm.nih.gov/pubmed/17589504. Accessed 27 January 2014.

136. Crépieux P, Kwon H, Leclerc N, Spencer W, Richard S, et al. (1997) I kappaB alpha physically interacts with a cytoskeleton-associated protein through its signal response domain. Mol Cell Biol 17: 7375–7385. Available: http://www.pubmedcentral.nih.gov/articlerender.fcgi?artid=232593&tool=pmcentrez&rendertype=abstract. Accessed 6 February 2014.

137. Jung Y, Kim H, Min SH, Rhee SG, Jeong W (2008) Dynein light chain LC8 negatively regulates NF-kappaB through the redox-dependent interaction with IkappaBalpha. J Biol Chem 283: 23863–23871. Available: http://www.pubmedcentral.nih.gov/articlerender.fcgi?artid=3259766&tool=pmcentrez&rendertype=abstract. Accessed 27 January 2014.

138. Fuhrmann JC, Kins S, Rostaing P, El Far O, Kirsch J, et al. (2002) Gephyrin interacts with Dynein light chains 1 and 2, components of motor protein complexes. J Neurosci 22: 5393–5402. Available: http://www.ncbi.nlm.nih.gov/pubmed/12097491. Accessed 6 February 2014.

139. Kim EY, Schrader N, Smolinsky B, Bedet C, Vannier C, et al. (2006) Deciphering the structural framework of glycine receptor anchoring by gephyrin. EMBO J 25: 1385–1395. Available: http://www.pubmedcentral.nih.gov/articlerender.fcgi?artid=1422172&tool=pmcentrez&rendertype=abstract. Accessed 5 February 2014.

140. Maas C, Tagnaouti N, Loebrich S, Behrend B, Lappe-Siefke C, et al. (2006) Neuronal cotransport of glycine receptor and the scaffold protein gephyrin. J Cell Biol 172: 441–451. Available: http://www.pubmedcentral.nih.gov/articlerender.fcgi?artid=2063653&tool=pmcentrez&rendertype=abstract. Accessed 6 February 2014.

141. Zhang W, Chan HM, Gao Y, Poon R, Wu Z (2007) BS69 is involved in cellular senescence through the p53-p21Cip1 pathway. EMBO Rep 8: 952–958. Available: http://www.pubmedcentral.nih.gov/articlerender.fcgi?artid=2002549&tool=pmcentrez&rendertype=abstract. Accessed 6 February 2014.

142. Kaiser FJ, Tavassoli K, Van den Bemd G-J, Chang GTG, Horsthemke B, et al. (2003) Nuclear interaction of the dynein light chain LC8a with the TRPS1 transcription factor suppresses the transcriptional repression activity of TRPS1. Hum Mol Genet 12: 1349–1358. Available: http://www.ncbi.nlm.nih.gov/pubmed/12761050. Accessed 6 February 2014.

143. Rayala SK, den Hollander P, Balasenthil S, Yang Z, Broaddus RR, et al. (2005) Functional regulation of oestrogen receptor pathway by the dynein light chain 1. EMBO Rep 6: 538–544. Available: http://www.pubmedcentral.nih.gov/articlerender.fcgi?artid=1369089&tool=pmcentrez&rendertype=abstract. Accessed 5 February 2014.

144. Rayala SK, den Hollander P, Manavathi B, Talukder AH, Song C, et al. (2006) Essential role of KIBRA in co-activator function of dynein light chain 1 in mammalian cells. J Biol Chem 281: 19092–19099. Available: http://www.ncbi.nlm.nih.gov/pubmed/16684779. Accessed 6 February 2014.

145. Nyarko A, Hare M, Hays TS, Barbar E (2004) The intermediate chain of cytoplasmic dynein is partially disordered and gains structure upon binding to light-chain LC8. Biochemistry 43: 15595–15603. Available: http://www.ncbi.nlm.nih.gov/pubmed/15581372. Accessed 6 February 2014.

146. Benison G, Nyarko A, Barbar E (2006) Heteronuclear NMR identifies a nascent helix in intrinsically disordered dynein intermediate chain: implications for folding and dimerization. J Mol Biol 362: 1082–1093. Available: http://www.ncbi.nlm.nih.gov/pubmed/16949604. Accessed 6 February 2014.

147. Pollack JD, Williams M V, McElhaney RN (1997) The comparative metabolism of the mollicutes (Mycoplasmas): the utility for taxonomic classification and the relationship of putative gene annotation and phylogeny to enzymatic function in the smallest free-living cells. Crit Rev Microbiol 23: 269–354. Available: http://www.ncbi.nlm.nih.gov/pubmed/9439886. Accessed 23 January 2014.

148. Knodler LA, Sekyere EO, Stewart TS, Schofield PJ, Edwards MR (1998) Cloning and expression of a prokaryotic enzyme, arginine deiminase, from a primitive eukaryote Giardia intestinalis. J Biol Chem 273: 4470–4477. Available: http://www.ncbi.nlm.nih.gov/pubmed/9468500. Accessed 6 February 2014.

149. Biagini GA, Yarlett N, Ball GE, Billetz AC, Lindmark DG, et al. (2003) Bacterial-like energy metabolism in the amitochondriate protozoon Hexamita inflata. Mol Biochem Parasitol 128: 11–19. Available: http://www.ncbi.nlm.nih.gov/pubmed/12706792. Accessed 6 February 2014.

150. Baur H, Luethi E, Stalon V, Mercenier A, Haas D (1989) Sequence analysis and expression of the arginine-deiminase and carbamate-kinase genes of Pseudomonas aeruginosa. Eur J Biochem 179: 53–60. Available: http://www.ncbi.nlm.nih.gov/pubmed/2537202. Accessed 6 February 2014.

151. Gamper M, Zimmermann A, Haas D (1991) Anaerobic regulation of transcription initiation in the arcDABC operon of Pseudomonas aeruginosa. J Bacteriol 173: 4742–

4750. Available: http://www.pubmedcentral.nih.gov/articlerender.fcgi?artid=208152&tool=pmcentrez&rendertype=abstract. Accessed 6 February 2014.

152. Lüthi E, Mercenier A, Haas D (1986) The arcABC operon required for fermentative growth of Pseudomonas aeruginosa on arginine: Tn5-751-assisted cloning and localization of structural genes. J Gen Microbiol 132: 2667–2675. Available: http://www.ncbi.nlm.nih.gov/pubmed/3040889. Accessed 6 February 2014.

153. Smith RS, Iglewski BH (2003) P. aeruginosa quorum-sensing systems and virulence. Curr Opin Microbiol 6: 56–60. Available: http://www.ncbi.nlm.nih.gov/pubmed/12615220. Accessed 6 February 2014.

154. Gallego P, Planell R, Benach J, Querol E, Perez-Pons JA, et al. (2012) Structural characterization of the enzymes composing the arginine deiminase pathway in Mycoplasma penetrans. PLoS One 7: e47886. Available: http://www.pubmedcentral.nih.gov/articlerender.fcgi?artid=3474736&tool=pmcentrez&rendertype=abstract. Accessed 6 February 2014.

155. Legrain C, Stalon V, Noullez JP, Mercenier A, Simon JP, et al. (1977) Structure and function of ornithine carbamoyltransferases. Eur J Biochem 80: 401–409. Available: http://www.ncbi.nlm.nih.gov/pubmed/923586. Accessed 6 February 2014.

156. Villeret V, Tricot C, Stalon V, Dideberg O (1995) Crystal structure of Pseudomonas aeruginosa catabolic ornithine transcarbamoylase at 3.0-A resolution: a different oligomeric organization in the transcarbamoylase family. Proc Natl Acad Sci U S A 92: 10762–10766. Available: http://www.pubmedcentral.nih.gov/articlerender.fcgi?artid=40692&tool=pmcentrez&rendertype=abstract. Accessed 6 February 2014.

157. Villeret V, Clantin B, Tricot C, Legrain C, Roovers M, et al. (1998) The crystal structure of Pyrococcus furiosus ornithine carbamoyltransferase reveals a key role for oligomerization in enzyme stability at extremely high temperatures. Proc Natl Acad Sci U S A 95: 2801–2806. Available: http://www.pubmedcentral.nih.gov/articlerender.fcgi?artid=19649&tool=pmcentrez&rendertype=abstract. Accessed 6 February 2014.

158. Baur H, Tricot C, Stalon V, Haas D (1990) Converting catabolic ornithine carbamoyltransferase to an anabolic enzyme. J Biol Chem 265: 14728–14731. Available: http://www.ncbi.nlm.nih.gov/pubmed/2118516. Accessed 6 February 2014.

159. Das K, Butler GH, Kwiatkowski V, Clark AD, Yadav P, et al. (2004) Crystal structures of arginine deiminase with covalent reaction intermediates; implications for catalytic mechanism. Structure 12: 657–667. Available: http://www.ncbi.nlm.nih.gov/pubmed/15062088. Accessed 6 February 2014.

160. Razin S, Yogev D, Naot Y (1998) Molecular biology and pathogenicity of mycoplasmas. Microbiol Mol Biol Rev 62: 1094–1156. Available: http://www.pubmedcentral.nih.gov/articlerender.fcgi?artid=98941&tool=pmcentrez&rendertype=abstract. Accessed 4 February 2014.

161. Inamine JM, Ho KC, Loechel S, Hu PC (1990) Evidence that UGA is read as a tryptophan codon rather than as a stop codon by Mycoplasma pneumoniae, Mycoplasma genitalium, and Mycoplasma gallisepticum. J Bacteriol 172: 504–506. Available: http://www.pubmedcentral.nih.gov/articlerender.fcgi?artid=208464&tool=pmcentrez&rendertype=abstract. Accessed 6 February 2014.

162. Fraser CM, Gocayne JD, White O, Adams MD, Clayton RA, et al. (1995) The minimal gene complement of Mycoplasma genitalium. Science 270: 397–403. Available: http://www.ncbi.nlm.nih.gov/pubmed/7569993. Accessed 6 February 2014.

163. Sasaki Y, Ishikawa J, Yamashita A, Oshima K, Kenri T, et al. (2002) The complete genomic sequence of Mycoplasma penetrans, an intracellular bacterial pathogen in humans. Nucleic Acids Res 30: 5293–5300. Available: http://www.pubmedcentral.nih.gov/articlerender.fcgi?artid=137978&tool=pmcentrez&rendertype=abstract. Accessed 6 February 2014.

164. Woese CR, Maniloff J, Zablen LB (1980) Phylogenetic analysis of the mycoplasmas. Proc Natl Acad Sci U S A 77: 494–498. Available: http://www.pubmedcentral.nih.gov/articlerender.fcgi?artid=348298&tool=pmcentrez&rendertype=abstract. Accessed 6 February 2014.

165. Miles RJ (1992) Catabolism in mollicutes. J Gen Microbiol 138: 1773–1783. Available: http://www.ncbi.nlm.nih.gov/pubmed/1402786. Accessed 23 January 2014.

166. Degnan BA, Fontaine MC, Doebereiner AH, Lee JJ, Mastroeni P, et al. (2000) Characterization of an isogenic mutant of Streptococcus pyogenes Manfredo lacking the ability to make streptococcal acid glycoprotein. Infect Immun 68: 2441–2448. Available: http://www.pubmedcentral.nih.gov/articlerender.fcgi?artid=97444&tool=pmcentrez&rendertype=abstract. Accessed 6 February 2014.

167. Casiano-Colón A, Marquis RE (1988) Role of the arginine deiminase system in protecting oral bacteria and an enzymatic basis for acid tolerance. Appl Environ Microbiol 54: 1318–1324. Available: http://www.pubmedcentral.nih.gov/articlerender.fcgi?artid=202656&tool=pmcentrez&rendertype=abstract. Accessed 6 February 2014.

168. Fenske JD, Kenny GE (1976) Role of arginine deiminase in growth of Mycoplasma hominis. J Bacteriol 126: 501–510. Available: http://www.pubmedcentral.nih.gov/articlerender.fcgi?artid=233306&tool=pmcentrez&rendertype=abstract. Accessed 6 February 2014.

169. Schimke RT, Berlin CM, Sweeney EW, Carroll WR (1966) The generation of energy by the arginine dihydrolase pathway in Mycoplasma hominis 07. J Biol Chem 241: 2228–2236. Available: http://www.ncbi.nlm.nih.gov/pubmed/5911610. Accessed 6 February 2014.

170. Galkin A, Kulakova L, Sarikaya E, Lim K, Howard A, et al. (2004) Structural insight into arginine degradation by arginine deiminase, an antibacterial and parasite drug

target. J Biol Chem 279: 14001–14008. Available: http://www.ncbi.nlm.nih.gov/pubmed/14701825. Accessed 6 February 2014.

171. Vallance P, Bush HD, Mok BJ, Hurtado-Guerrero R, Gill H, et al. (2005) Inhibition of dimethylarginine dimethylaminohydrolase (DDAH) and arginine deiminase (ADI) by pentafluorophenyl (PFP) sulfonates. Chem Commun (Camb): 5563–5565. Available: http://www.ncbi.nlm.nih.gov/pubmed/16358064. Accessed 6 February 2014.

172. Galkin A, Lu X, Dunaway-Mariano D, Herzberg O (2005) Crystal structures representing the Michaelis complex and the thiouronium reaction intermediate of Pseudomonas aeruginosa arginine deiminase. J Biol Chem 280: 34080–34087. Available: http://www.ncbi.nlm.nih.gov/pubmed/16091358. Accessed 6 February 2014.

173. Humm A, Fritsche E, Steinbacher S, Huber R (1997) Crystal structure and mechanism of human L-arginine:glycine amidinotransferase: a mitochondrial enzyme involved in creatine biosynthesis. EMBO J 16: 3373–3385. Available: http://www.pubmedcentral.nih.gov/articlerender.fcgi?artid=1169963&tool=pmcentrez&rendertype=abstract. Accessed 6 February 2014.

174. Murray-Rust J, Leiper J, McAlister M, Phelan J, Tilley S, et al. (2001) Structural insights into the hydrolysis of cellular nitric oxide synthase inhibitors by dimethylarginine dimethylaminohydrolase. Nat Struct Biol 8: 679–683. Available: http://www.ncbi.nlm.nih.gov/pubmed/11473257. Accessed 6 February 2014.

175. Llácer JL, Polo LM, Tavárez S, Alarcón B, Hilario R, et al. (2007) The gene cluster for agmatine catabolism of Enterococcus faecalis: study of recombinant putrescine transcarbamylase and agmatine deiminase and a snapshot of agmatine deiminase catalyzing its reaction. J Bacteriol 189: 1254–1265. Available: http://www.pubmedcentral.nih.gov/articlerender.fcgi?artid=1797358&tool=pmcentrez&rendertype=abstract. Accessed 6 February 2014.

176. Cunin R, Glansdorff N, Piérard A, Stalon V (1986) Biosynthesis and metabolism of arginine in bacteria. Microbiol Rev 50: 314–352. Available: http://www.pubmedcentral.nih.gov/articlerender.fcgi?artid=373073&tool=pmcentrez&rendertype=abstract. Accessed 3 February 2014.

177. Stalon V, Ramos F, Piérard A, Wiame JM (1967) The occurrence of a catabolic and an anabolic ornithine carbamoyltransferase in Pseudomonas. Biochim Biophys Acta 139: 91–97. Available: http://www.ncbi.nlm.nih.gov/pubmed/4962140. Accessed 6 February 2014.

178. Vander Wauven C, Piérard A, Kley-Raymann M, Haas D (1984) Pseudomonas aeruginosa mutants affected in anaerobic growth on arginine: evidence for a four-gene cluster encoding the arginine deiminase pathway. J Bacteriol 160: 928–934. Available: http://www.pubmedcentral.nih.gov/articlerender.fcgi?artid=215798&tool=pmcentrez&rendertype=abstract. Accessed 6 February 2014.

179. Brady BS, Hyman BC, Lovatt CJ (2010) Regulation of CPSase, ACTase, and OCTase genes in Medicago truncatula: Implications for carbamoylphosphate synthesis and allocation to pyrimidine and arginine de novo biosynthesis. Gene 462: 18–25. Available: http://www.ncbi.nlm.nih.gov/pubmed/20451592. Accessed 6 February 2014.

180. Díaz-Muñoz M, Hernández-Muñoz R (2010) Molecular and biochemical features of the mitochondrial enzyme ornithine transcarbamylase: a possible new role as a signaling factor. Curr Med Chem 17: 2253–2260. Available: http://www.ncbi.nlm.nih.gov/pubmed/20459380. Accessed 6 February 2014.

181. Honzatko RB, Crawford JL, Monaco HL, Ladner JE, Ewards BF, et al. (1982) Crystal and molecular structures of native and CTP-liganded aspartate carbamoyltransferase from Escherichia coli. J Mol Biol 160: 219–263. Available: http://www.ncbi.nlm.nih.gov/pubmed/6757446. Accessed 6 February 2014.

182. Schofield PJ, Edwards MR, Matthews J, Wilson JR (1992) The pathway of arginine catabolism in Giardia intestinalis. Mol Biochem Parasitol 51: 29–36. Available: http://www.ncbi.nlm.nih.gov/pubmed/1314332. Accessed 6 February 2014.

183. Linstead D, Cranshaw MA (1983) The pathway of arginine catabolism in the parasitic flagellate Trichomonas vaginalis. Mol Biochem Parasitol 8: 241–252. Available: http://www.ncbi.nlm.nih.gov/pubmed/6312311. Accessed 6 February 2014.

184. Ramón-Maiques S, Marina A, Uriarte M, Fita I, Rubio V (2000) The 1.5 A resolution crystal structure of the carbamate kinase-like carbamoyl phosphate synthetase from the hyperthermophilic Archaeon pyrococcus furiosus, bound to ADP, confirms that this thermostable enzyme is a carbamate kinase, and provides insight in. J Mol Biol 299: 463–476. Available: http://www.ncbi.nlm.nih.gov/pubmed/10860751. Accessed 6 February 2014.

185. Marina A, Uriarte M, Barcelona B, Fresquet V, Cervera J, et al. (1998) Carbamate kinase from Enterococcus faecalis and Enterococcus faecium--cloning of the genes, studies on the enzyme expressed in Escherichia coli, and sequence similarity with N-acetyl-L-glutamate kinase. Eur J Biochem 253: 280–291. Available: http://www.ncbi.nlm.nih.gov/pubmed/9578487. Accessed 6 February 2014.

186. Ramón-Maiques S, Marina A, Guinot A, Gil-Ortiz F, Uriarte M, et al. (2010) Substrate binding and catalysis in carbamate kinase ascertained by crystallographic and site-directed mutagenesis studies: movements and significance of a unique globular subdomain of this key enzyme for fermentative ATP production in bacteria. J Mol Biol 397: 1261–1275. Available: http://www.ncbi.nlm.nih.gov/pubmed/20188742. Accessed 18 May 2014.

187. Legrain C, Demarez M, Glansdorff N, Pierard A (1995) Ammonia-dependent synthesis and metabolic channelling of carbamoyl phosphate in the hyperthermophilic archaeon Pyrococcus furiosus. Microbiology 141: 1093–1099. Available: http://mic.sgmjournals.org/content/141/5/1093.abstract. Accessed 6 February 2014.

188. Massant J, Verstreken P, Durbecq V, Kholti A, Legrain C, et al. (2002) Metabolic channeling of carbamoyl phosphate, a thermolabile intermediate: evidence for physical interaction between carbamate kinase-like carbamoyl-phosphate synthetase and ornithine carbamoyltransferase from the hyperthermophile Pyrococcus furiosus. J Biol Chem 277: 18517–18522. Available: http://www.ncbi.nlm.nih.gov/pubmed/11893735. Accessed 6 February 2014.

189. J M, N G (2004) Metabolic channelling of carbamoyl phosphate in the hyperthermophilic archaeon Pyrococcus furiosus: dynamic enzyme–enzyme interactions involved in the formation of the channelling complex. Available: http://www.biochemsoctrans.org/bst/032/0306/bst0320306.htm. Accessed 17 May 2014.

190. Massant J, Glansdorff N (2005) New experimental approaches for investigating interactions between Pyrococcus furiosus carbamate kinase and carbamoyltransferases, enzymes involved in the channeling of thermolabile carbamoyl phosphate. Archaea 1: 365–373. Available: http://www.pubmedcentral.nih.gov/articlerender.fcgi?artid=2685582&tool=pmcentrez&rendertype=abstract. Accessed 6 February 2014.

191. Rhodes G (1999) Crystallography Made Crystal Clear, Second Edition: A Guide for Users of Macromolecular Models (Complementary Science). Academic Press. Available: http://www.amazon.com/Crystallography-Crystal-Clear-Second-Edition/dp/0125870728. Accessed 6 February 2014.

192. Wang L, Hare M, Hays TS, Barbar E (2004) Dynein light chain LC8 promotes assembly of the coiled-coil domain of swallow protein. Biochemistry 43: 4611–4620. Available: http://www.ncbi.nlm.nih.gov/pubmed/15078108. Accessed 18 May 2014.

193. Massant J, Wouters J, Glansdorff N (2003) Refined structure of Pyrococcus furiosus ornithine carbamoyltransferase at 1.87 A. Acta Crystallogr D Biol Crystallogr 59: 2140–2149. Available: http://www.ncbi.nlm.nih.gov/pubmed/14646072. Accessed 18 May 2014.

194. Robinson-Rechavi M, Alibés A, Godzik A (2006) Contribution of electrostatic interactions, compactness and quaternary structure to protein thermostability: lessons from structural genomics of Thermotoga maritima. J Mol Biol 356: 547–557. Available: http://www.ncbi.nlm.nih.gov/pubmed/16375925. Accessed 18 May 2014.

195. Mouz N, Tricot C, Ebel C, Petillot Y, Stalon V, et al. (1996) Use of a designed fusion protein dissociates allosteric properties from the dodecameric state of Pseudomonas aeruginosa catabolic ornithine carbamoyltransferase. Proc Natl Acad Sci U S A 93: 9414–9419. Available: http://www.pubmedcentral.nih.gov/articlerender.fcgi?artid=38442&tool=pmcentrez&rendertype=abstract. Accessed 18 May 2014.

196. Nguyen VT, Baker DP, Tricot C, Baur H, Villeret V, et al. (1996) Catabolic ornithine carbamoyltransferase of Pseudomonas aeruginosa. Importance of the N-terminal region for dodecameric structure and homotropic carbamoylphosphate cooperativity.

Eur J Biochem 236: 283–293. Available: http://www.ncbi.nlm.nih.gov/pubmed/8617277. Accessed 18 May 2014.

197. Galkin A, Kulakova L, Wu R, Nash TE, Dunaway-Mariano D, et al. (2010) X-ray structure and characterization of carbamate kinase from the human parasite Giardia lamblia. Acta Crystallogr Sect F Struct Biol Cryst Commun 66: 386–390. Available: http://www.pubmedcentral.nih.gov/articlerender.fcgi?artid=2852327&tool=pmcentrez&rendertype=abstract. Accessed 18 May 2014.

# Acknowledgements.

En primer lugar me gustaría agradecer esta tesis a David, director de este trabajo y mi mentor. Él es como el maestro artesano que comparte sus conocimientos con las generaciones futuras: de aprendiz en aprendiz. Gracias también por su esmero, talante, comprensión, crítica y dedicación personal a su trabajo que son y serán ejemplo para mí; y que sin ellas este trabajo hubiese sido pésimo.

Es imposible que yo hable de cristalografía y no mencione el Sincrotrón ALBA, la línea XALOC y, sobretodo, tres nombres propios: Jordi Benach, Jordi Juanhuix y Fernando. Gracias a todos ellos por su humanidad y ser mis maestros en la noche, en las noches de sincrotrón. Especialmente, quiero agradecer a Jordi Benach quién, sin exagerar, es mi segundo mentor y gran ejemplo; y a quien he echado mucho de menos este último año.

Por suerte la familia de la cristalografía en la UAB es grande y quiero agradecer a Ester Boix y Lionel sus ánimos de compartir. A Lionel le debo otras gracias por enseñarme a trabajar tan fino y tan bien detrás de la pantalla del ordenador.

Quiero agradecer esta tesis a otros grandes protagonistas, y aprendices como yo: Laura, Kamela, Yang, Sergi, Bing, Nathalia, Jara y Albert. Ellos son pilares y soportes en esos días cruzados que todos tenemos, pero si te dedicas a estudiar lo incierto (científico) pues te dan doble ración. A mis compañeros de laboratorio del grupo de “folding” muchas gracias por aguantarme y acompañarme en este periplo de la vida que ha durado 5 años. En especial quiero agradecérselo a Ricardinho, Virginia, Alba, Ricardo, Patri y Susana.

Quiero dar las gracias a todo el personal de la torre, el IBB y el MRB por ayudarme tantísimo. En especial a todo el grupo de Enzimo, “el servei de Proteòmica” y más nombres propios: Laia, Saray, Pol, Txino, Julia, Javi, Olivia, Miguel, Fani, Carla, Jofre y Gisela.

Si no todos casi todos cuando el sol estaba en lo más alto de la cúpula salía al encuentro de mis compañeros de carrera. Y recargaba las baterías calóricas en compañía de: Olivia, Samir, Marc, Jofre, Tamara, “el nen” y “el niño”. Muchas gracias amigos por vuestra ayuda, compañía, ánimos, charlas y “board games”. Y otro gracias Olivia por esos pitillos, cafés y más: ayuda,

compañía, ánimos y charlas; para cuando el sol ya estaba en lo más bajo.

También quiero agradecérselo a mis amigos de “tota la vida”: Chema, Javi, Pol, Mario, Enric, Sebas y en especial a Ricardo. Otros que no son de hace tanto tiempo pero cómo si lo fuera: Jesús, Marc Catalan, Chefo, Juanmi, MARCOS, Fricky, Javi, Sergio, Alba, Silvia, Carlos, Humbert y a “El Consejo”.

Ángel Jesús, Sandra y Ángel muchas gracias por vuestro amor. También gracias a Alan, Germán, mis tíos y primos. Y muchos besos a Belén, Miquel y Ester he de visitaros más. Gracias a Laia por elegirme a tu lado y ayudarme tanto con la tesis como con el futuro

Finalmente quiero agradecérselo, como todo lo que hice, hago y haré, a la familia: papá, mamá y María. Dicen que es muy difícil que te toque una vez la lotería, yo no juego porque que te toque dos veces es ya imposible.